Order of Magnitude Scaling of Complex Engineering Problems, and its Application to High Productivity Arc Welding

by

Patricio Fernando Mendez

Mechanical Engineer, 1992
University of Buenos Aires, Argentina

S.M., Materials Science and Engineering, 1995
Massachusetts Institute of Technology

Submitted to the Department of Materials Science and Engineering
in partial fulfillment of the requirements for the degree of

Doctor of Philosophy in Materials Engineering

at the

MASSACHUSETTS INSTITUTE OF TECHNOLOGY

June 1999

Author .....
Department of Materials Science and Engineering
April 30, 1999

Certified by .....
Thomas W. Eagar
POSCO Professor of Materials Engineering
Thesis Supervisor

Accepted by .....
Linn W. Hobbs
John F. Elliott Professor of Materials
Chairman, Departmental Committee on Graduate Students

Order of Magnitude Scaling of Complex Engineering Problems, and its Application to High Productivity Arc Welding

by

Patricio Fernando Mendez

Submitted to the Department of Materials Science and Engineering
on April 30, 1999, in partial fulfillment of the
requirements for the degree of
Doctor of Philosophy in Materials Engineering

Abstract

This thesis presents the Order of Magnitude Scaling methodology and uses it to determine the configuration and dominant forces in the weld pool during high productivity arc welding. This methodology was developed to consistently address problems for which experimental and mathematical treatment is difficult, yet the governing equations and some general characteristics are known. The results generated by this methodology can be grouped into two sets. One of these consists of estimations of the unknowns of the problem in the form of power laws. The other is a set of dimensionless groups that indicates the relative importance of the driving forces. It is not necessary to solve the original differential equations, because they are transformed into a significantly simpler set of algebraic equations. This transformation is possible through the combination of dimensional analysis and asymptotic considerations. A new condition is introduced for normalization: that the dimensionless functions vary smoothly. This essential condition was not considered in previous research. Matrix algebra is used to provide a systematic treatment for problems involving many parameters. The application of this technique to high productivity arc welding determined for the first time that the dominant force acting on a very depressed weld pool is the arc drag force. Experimental work in 304 stainless steel was performed to analyze the effect of the large depression on defect formation. It was found that higher welding speeds (20% or more) are possible with lower sulfur content (6 ppm vs. 230 ppm). Differences in the size and stability of the weld pool depression are proposed here as the explanation for this difference. Steels with lower sulfur content show a weld pool geometry that tends to decrease the size of the gouging region (the most depressed part of the weld pool). In higher sulfur steels, the gouging region tends to extend beyond the hot region of the arc. In this situation the gouging region freezes prematurely and defects such as humping or a split bead are generated.

Thesis Supervisor: Thomas W. Eagar
Title: POSCO Professor of Materials Engineering

Acknowledgments

And then Prof. Eagar said:

> "We have the funding, now go do something good."[1]

Such is the atmosphere of freedom and openness that Prof. Eagar set from the beginning, creating a fertile land for new ideas. I believe that this thesis would not have been possible under any advisor but him. He also provided ideas when the land was not so fertile, and never showed frustration nor impatience when this freedom would take me to dead ends (and I visited a lot of those). In all doctoral work, a student finds his or her own answers to an unsolved problem. Prof. Eagar went much further than that by encouraging me to find my own answers *in my own style*. I have been incredibly fortunate to have been his student.

When at one point too many dead ends became overwhelming, Prof. Scott had the patience and human qualities to listen openly and honestly. I am very grateful for that. Prof. Scott and Prof. Sonin constituted my thesis committee, together with Prof. Eagar. My discussions with them have been stimulating, fruitful, and friendly, especially those about dimensional analysis with Prof. Sonin, and about polymer fiber retraction with Prof. Scott.

The beginnings of my involvement with welding were under Prof. Szekely's guidance. He and I agreed on the importance of asymptotic solutions and dimensionless groups as a means to fully understand a problem. He helped and encouraged me to develop my own approach to problems. He was confident that we were headed in the right direction. His passing away in December of 1995 was a terrible loss for me and all of those close to him. I hope that this work would have pleased him. Perhaps some day I will know.

Prof. Rosales and Prof. Jerison of the Department of Mathematics gave me good feedback when I was developing the Order of Magnitude Scaling Method. Prof. Clark

[1]This work was sponsored mostly by the U. S. Department of Energy, Office of Basic Energy Sciences

of the Department of Materials gave me advise and material regarding the economics of welding. Dr. Stan David of Oak Ridge National Laboratory helped me with my first welding experiments, which were performed at his lab. Dr. Gerardo Trápaga, of the Department of Materials, also contributed useful insight during all of my research. Marco Ramirez provided me with important literature and data regarding the welding arc.

When the time for experiments arrived, Don Galler made them possible by building the test rig and discussing practical issues. Krista Niece joined the group as a UROP to help me carry out the experiments, and soon it was clear that she could take over many more tasks than we originally expected (she could also do them better than I could). Working with Don and Krista made the weld time "fun time."

But not all was work during these last few years, and I consider myself blessed with the friendship of some truly terrific people such as Jason Clevenger, beermeister, laser guru, and the only one who time after time could rebuild my computer after my disastrous attempts at "improving" it. Matías Zaldarriaga and Pablo García, party friends extraordinaire, were always together with me through the good, the not-so-good times, and an infinity of lunches at Walker. I cannot believe that I will not see them around that often anymore. Chris Rice, semi-solid connoisseur and my "English teacher," is one of the most outstanding engineers I ever worked with. Daniel Ciriello and I learned together the secrets of machine design at the University of Buenos Aires, where we created the so-called "método lineal" to save time in our projects. We never imagined that it would end up being part of a thesis!. My friends in Argentina have always cared about me despite the distance. I am so indebted to them: Carlos, Valeria, Martín, Alejandro, Adrián, María, Verónica, and many more. Many other fine people have also enriched my life during my time at M.I.T., a few of whom I mention: Kristin Lynch, Jesse Figueiredo, Hilary Sheldon, the members of the Joining Group, Mark Cheshire, Gaël Gioux, Tim Davis, and the people of SST. I hope that moving ahead does not move us apart in the years to come.

I saved the best for last, and it is my family, which made me who I am. I cannot be grateful enough to them. My parents Fernando and Dora, and my sisters Eugenia and Ana have been with me through all of my life, and forever will be that way. I know that they and my brothers in law Gustavo and Pablo are as happy as I am on my graduation. This important moment is even more exciting because my godchildren Maxi and Tomy are sharing it with me. I love them more than I can say, and I will work hard to be a godfather they can be proud of. I hope that sharing the good feelings of this moment will also cheer up my grandmother Leonor and my aunt Graciela in the difficult moments they are going through.

My time at M.I.T. has been one of the most exciting times of my life, personally and professionally. I have been very fortunate and privileged for having had this opportunity. I hope that this work, and those to come in the future, will show that this was an opportunity well used.

Contents

List of Figures

List of Tables

Chapter 1

Introduction

Arc welding was the original motivation for this thesis. It will be shown later that even relatively small improvements in arc welding productivity can yield important returns. One of the objectives of this thesis is to provide an understanding of some of the limits to welding productivity in order to overcome them. The focus will be on the generation of defects in the weld pool at high current and velocity.

The study of arc welding, however, presents some particular problems:

- Direct experimental observation is difficult. The bright arc light requires special equipment for visual observations. These observations can only be superficial, due to the opacity of the molten metal. The high temperatures involved limit the possibilities of direct measurements.

- The mathematical treatment is difficult. The properties of the arc are fully coupled with those of the weld pool. At the weld pool many phenomena act simultaneously, and it is not known which forces must be taken into account and which can be neglected. The governing equations are non-linear. The boundary conditions include a free surface. At the limit of productivity, this free surface is very deformed.

- Dimensional analysis provides little simplification. The problem involves so many governing parameters that their reduction in number is not significant.

There is a very large number of possible dimensionless sets that can describe the process, and their choice is not unequivocal. Moreover, physically meaningful dimensionless groups such as the Reynolds number, require the use of characteristic values (e.g. velocity), which are unknown for this problem.

The problems mentioned above limited the understanding of high current and high speed welding mainly to basic experimental observations [1, 2, 3, 4, 5, 6, 7]. These basic observations provided some physical insight into the problem, such as the presence of a very thin liquid layer under the arc at high currents and velocities.

A second objective of this thesis, is to develop a methodology that overcomes the difficulties that prevented a better quantitative understanding of high productivity arc welding. This methodology (Order of Magnitude Scaling) is presented in detail in the first part of this thesis, and it is shown that it is helpful for a variety of problems beyond just welding. In this methodology, the differential equations and boundary conditions need to be known, as if they were to be solved. However, instead of attempting to solve the differential equations, they are transformed into a set of algebraic equations, of much simpler solution. The results obtained are order of magnitude approximations to the exact solution to the problem in the form of a power law. These estimations are valuable in many ways. In some problems, an estimation of the solution is sufficient for making a decision. Much time can be saved in this case by performing an order of magnitude scaling study instead of a numerical analysis. The estimations obtained can be used to determine the relative importance of the different driving forces and effects in a system. When dominant and negligible aspects are identified the equations can be simplified accordingly, and the size of an experimental matrix can be significantly reduced. The simple expression of the estimations makes them suitable for use in real-time control systems.

Dimensional analysis and asymptotic considerations are used simultaneously in order to transform the differential equations into algebraic equations. This approach is similar to that of Chen [8] and Rivas and Ostrach [9]. This thesis, however, introduces a new condition for a proper normalization, which is that the dimensionless second

derivatives must be of the order of one. This is an essential condition, because it guarantees that the first derivatives will also be of the order of one. Only when all the dimensionless functions and their derivatives are of the order of one the transformation into a set of algebraic equations is meaningful. This condition prevents the appearance of problems such as singular limits, in which terms of an equation are multiplied by arbitrarily small coefficients, but they cannot be neglected without violating the boundary conditions of the problem. Matrix algebra is frequently used in dimensional analysis [10, 11, 12, 13, 14, 15, 16], and it is also incorporated here in order to have a systematic treatment of problems with many parameters. This thesis expands its scope by defining new sets and set relations expressed as matrix operations.

In order to validate and illustrate the application of this methodology, a number of examples with known solutions are studied. These examples provide the correct order of magnitude estimations of the solutions through an approach much simpler and systematic than the original.

The second part of this thesis applies the methodology of order of magnitude scaling to the problem that motivated its creation: the study of the weld pool at high current and velocities. This problem involves many driving forces acting simultaneously, without an obvious indication of which of these forces are dominant. Previous studies of the weld pool indicated that up to moderate currents (of the order of 250 A for GTAW) Marangoni forces are dominant [17, 18, 19]. At higher currents, electromagnetic forces and aerodynamic drag on the free surface increase in importance [20, 21]. These numerical models always considered a weld pool with recirculating flows, which is not representative of the case of high current and speed welding. In this regime, the weld pool is so deformed that the region under the arc turns into a thin liquid layer (the "gouging region"), where recirculating flows cannot occur [1, 2, 4, 5, 6]. The order of magnitude scaling of this problem shows for the first time, quantitatively, that the aerodynamic drag of the arc over the free surface is the dominant force driving the flow in the gouging region. The estimated thickness of the thin liquid layer is in agreement with that measured by Yamamoto [5]. Previous

experimental work on defect formation associated defects such as humping and undercutting with the presence of a gouging region [3, 5, 6]. A series of bead-on-plate welds was performed to analyze the relationship between the gouging zone and defect formation. It was found that higher welding speeds (20% or more) are possible in 304 stainless steel with lower sulfur content (6 ppm vs. 230 ppm). Differences in the size and stability of the weld pool depression are proposed here as the explanation of this difference. Steels with lower sulfur content show a weld pool geometry that tends to decrease the size of the gouging region (the most depressed part of the weld pool). In higher sulfur steels, the gouging region tends to extend beyond the hot region of the arc. In this situation, the gouging region freezes prematurely and defects such as humping or a split bead are generated.

The remaining chapters of this thesis follow the outline below:

Chapter 2 presents a methodology for obtaining order of magnitude estimations in complex engineering problems.

Chapter 3 illustrates the methodology for order of magnitude scaling through a number of increasingly complex examples.

Chapter 4 describes the very large impact of productivity improvements in automatic welding.

Chapter 5 shows that at high currents and speeds, the weld pool turns into a thin liquid film under the arc, generating welding defects such as humping, undercutting or tunnelling.

Chapter 6 focuses on arc welding under high currents. Using the order of magnitude scaling methodology of Chapter 2, this chapter studies in detail the weld pool when it turns into a thin liquid film under the arc (gouging region).

Chapter 7 studies in detail the relation between the gouging region and the generation of defects such as humping or split beads.

Part I

Order of Magnitude Scaling of Complex Engineering Problems

Chapter 2

Order of Magnitude Scaling Methodology

An engineering system can be characterized by various properties such as velocity or temperature. These properties are represented by functions, for example in a cartesian coordinate frame the X-component of a velocity is represented by the function $U(X, Y, Z)$. This function gives the value of U for each point in space.

The functions that represent a system are usually unknown. The values of the functions at different points and its characteristic values can be obtained empirically or through calculations. These results can be generalized with the technique of dimensional analysis.

Empirical methods are naturally limited to those systems in which measurements are possible and reliable. In addition, generalizations through dimensional analysis can be ambiguous in complex problems, where there is a large number of possible dimensionless groups.

Knowledge of the fundamentals (fluid dynamics, heat transfer, etc.) permits one to calculate the descriptive functions by solving a system of differential equations, where known information at the edges of the system or about its initial state constitutes the boundary or initial conditions. For simple systems the solution of the differential equations can be exact. For complex problems the mathematical treatment becomes

more difficult, and numerical methods are necessary. Numerical methods require great skill and insight, and their convergence is specially difficult for systems that show non-linearities or large deformations. On some occasions, the problem can be intractable with the available tools, and the physics of the problem must be idealized by neglecting driving forces or geometric complications. One inconvenience of simplifying the physics of a problem is the risk of unintentionally discarding a dominant force or effect.

For many practical cases, the analysis of a problem is started with some degree of previous insight. This insight may come from the literature, experiments, or experience for similar cases. It may consist of an understanding of the different regions into which a system may be subdivided (for example, the existence of a boundary layer), or whether the functions vary smoothly, etc.

The characteristic values of the functions that describe a system (maximum temperature, maximum velocity, etc.) are frequently enough to understand its main features. This section describes a methodology to obtain an order of magnitude estimation of the characteristic values through scaling. It combines elements of dimensional analysis, asymptotic considerations, and previous physical insight.

The following sections contain an overview of the literature, mathematical definitions and properties, and a summary of the usual stages followed when using this order of magnitude estimation methodology.

2.1 Related Work

There is a significant amount of literature on dimensional analysis [12, 13, 14, 15, 16, 22, 23, 24, 25, 26, 27, 28, 29, 30, 31]. A large portion of this literature also focuses on the application of dimensional analysis to the normalization of differential equations. Some of the literature uses the differential equations in order to form dimensionless groups (this is called "inspectional analysis [32]). There is a much smaller fraction of the literature that describes how asymptotic considerations in the

differential equations improve dimensional analysis. A possible reason for this is that the use of asymptotic considerations to improve dimensional analysis is considered self-evident; some physicists and mathematicians use it intuitively. Nevertheless, engineering systems frequently involve complexities that make them very difficult to understand by intuition alone, especially when the number of possible dimensionless combinations becomes too large.

Two references stand out in attempting to explain systematically the use of asymptotic considerations to improve dimensional analysis. In one of them, Astarita [33], brings up eight "lessons to be learned" through a series of examples. These lessons are not always true. After describing each lesson, Astarita's approach and Order of Magnitude Scaling will be compared.

Lesson 1: *"In the estimation of orders of magnitude, the cruder the better."*

This lesson suggests one may neglect the numeric coefficients. This is acceptable for simple problems. For complex problems, in which many characteristic magnitudes must be combined simultaneously, this might lead to errors beyond the order of magnitude approximation. This thesis shows how to deal with complex problems using matrix algebra. Including the numeric coefficients in the set of parameters of the problem improves the estimations without significantly increasing the complexity of the analysis of the problem.

Lesson 2: *The dimensionless functions should be defined in such a way that as many of the dimensionless coefficients as possible in the differential equations are one.* This lesson is not always true. For example in the boundary layer example of Section 3.2, the dimensionless coefficients of pressure, dynamic force and viscous force is one, but for the analysis of a thin weld pool, the coefficient of the dynamic forces can be much smaller than one. The introduction of a set of estimations in this thesis allows one to systematically determine which coefficients should be one and which should not.

Lesson 3: *Selection of the reference units is not fixed; they may be chosen in the*

most convenient form for a given problem.

Lesson 4: *The best way to determine the appropriate dimensionless groups is through ratios of dominant terms.*

When this lesson is applied to a set of governing equations it is equivalent to the "dominant balance" technique described by Bender *et al.* [34]. Astarita does not mention a particular methodology for applying these lessons. Instead he relies on the intuition of the researcher.

Lesson 5: *The set of reference units can be expanded by considering length units in different directions as different physical magnitudes.*, i.e. the length unit in the X-direction can be considered as a different physical magnitude than the length unit in the Y direction.

This lesson refers to what is termed "directional analysis" in the literature of dimensional analysis. It is supposed to provide a better understanding of problems with geometries with different scales in different directions [12, 13, 30, 35] . It is a subject of much debate, because it sometimes leads to confusion [14]. It is difficult to justify that a meter in one direction is as different from a meter in another direction as it is from a kilogram. In the methodology proposed in this thesis many different length scales can be used, not just one for each direction. Thus there is no need to artificially expand the set of reference units. This is possible through definition of sets of parameters, estimations, and reference units.

Lesson 6: *For problems that do not present a characteristic dimension because the domain is infinite, a characteristic length can be found by judicious dimensional analysis.*

This lesson refers to problems that do not present a characteristic dimension because the domain is infinite. In the methodology presented in this thesis, the domain of scaling must be finite, and that introduces a characteristic length that can be known (e.g. length of the boundary layer) or unknown (e.g. thickness of the

boundary layer). This characteristic length will belong to the set of parameters in the first case, and to the set of estimations for the latter (see the viscous boundary layer example in Section 3.2). The methodology presented in this thesis also helps to study problems with unknown characteristic magnitudes other than length.

Lesson 7: *"Dimensional analysis, scaling, and order of magnitude analysis are intertwined with each other."*

Lesson 8: *" Some thermodynamic thinking about dissipation is very often useful."*

In this methodology, physical insight is necessary in general, not just concerning dissipation.

In another important reference, Chen [8] presents a very detailed study of the simultaneous use of order of magnitude estimates and asymptotic limits. He states the following rules as "self evident":

1. If a set of equations and its boundary conditions are properly normalized, then the coefficients of the dominant terms in the non-dimensional system and boundary conditions are approximately equal to one.

2. Of alternate forms of normalization, the one with the smallest number of parameters is preferred.

3. If the dominant terms of a set of differential equations and its boundary/initial conditions are approximately one, and other terms contain coefficients that are approximately one or less, then the solution and all of its derivatives are also approximately one.

Unfortunately Chen's treatment of the dimensionless functions erroneously assumes that if the first derivative is approximately equal to one, then all other derivatives are also approximately equal to one. This opens the possibility for "pathological cases", where Rule 3 fails. Rule 2 is also not generally true, because sometimes it is

convenient to use many parameters for the normalization, for example in a problem with many length scales.

Similarly to Chen's and Astarita's analysis, this work uses differential equations to improve the dimensional analysis. This thesis expands their conclusions by presenting a study of the non-dimensional functions and their properties. This work also introduces different sets of parameters, such as the set of order of magnitude estimations. These sets of parameters provide a framework for the systematic combination of dimensional analysis and asymptotic consideration, allowing for a consistent way of normalizing the equations and obtaining an order of magnitude estimation of their characteristic values. For the more complex problems, matrix algebra greatly simplifies calculation of the estimations.

In this thesis, Matrix algebra has been applied to dimensional analysis for the determination of the complete set of dimensionless groups. Some sophisticated techniques exist in the literature for the solution of complex problems, but none of them involves the simultaneous use of asymptotic considerations as employed herein.

Figure 2-1 summarizes the techniques related to Order of Magnitude Scaling. These techniques are mainly dimensional analysis and asymptotic considerations. Intermediate asymptotics, as described by Barenblatt [31] and Chen [8] are basically the application of the framework of dimensional analysis to asymptotic considerations. The use of characteristic values from limiting cases to form useful dimensionless groups is described by Denn [36]. The application of matrix algebra to dimensional analysis has been discussed by many authors, among them Szirtes [16], Chen [11], and Barr [14]. The main goal in these cases is to facilitate the election of the appropriate set of governing dimensionless groups, and to reduce the amount of repetitive work. The technique of dominant balance, described by Bender and Orszag [34] permits one to study the limiting cases of a system of differential equations. The Order of Magnitude Scaling methodology makes use of these techniques. Dimensional analysis is used during the normalization of the original differential equations. Dominant balance is used to determine the dominant forces for a particular regime of a prob-

lem. This thesis introduces the requirement that the normalized second derivatives must be of the order of one, and that leads to the transformation of the system of differential equations into an algebraic one. The dominant balance used here does not require that the asymptotic cases are solved. In order to find the dominant forces and effects it is only necessary to find the normalization for which the dimensionless coefficients of the equations are one or less. Once the system was properly scaled, the original dimensionless equations are written in dimensionless form, with coefficients indicating the relative importance of each term, and those coefficients depending only on the dimensionless governing groups.

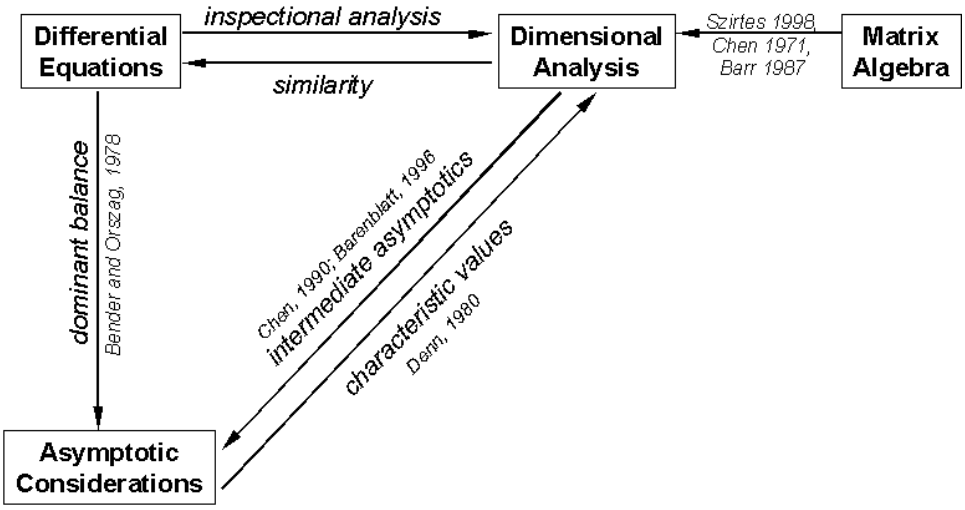

Figure 2-1: Techniques related to Order of Magnitude Scaling.

2.2 Mathematical Background

2.2.1 Definitions

It is necessary to define some concepts, because the terminology of dimensional analysis is not consistent with that of differential equations, and this work uses both techniques simultaneously. The physical quantities that determine a system, such as

viscosity, density, etc. will be called "parameters", and the argument of the functions included in the differential equations will be called "independent arguments" . The literature of dimensional analysis calls the former "independent variables," while the literature of differential equations uses that term for the latter.

The unknown functions that describe the properties of the system, such as a velocity $U(X, Y, Z)$, will be called "unknowns", and not "dependent variables" as the literature of dimensional analysis calls it. A comprehensive list of definitions of the concepts used in this chapter is included in Appendix A.

It is important to remark that the unknowns of a problem depend both on the independent arguments and the problem parameters. For example, in the viscous boundary layer the pressure function is $P(X, Y, \rho, \nu, U_\infty, L)$; however, for ease of notation when describing the dependence of a function, only the independent arguments will be stated explicitly as follows: $P(X, Y)$. Similarly, the dimensionless functions depend on the dimensionless independent arguments and the set of governing dimensionless groups, but only the dimensionless independent arguments will be explicitly stated. For example, the notation for the dimensionless pressure in the viscous boundary layer will be $p(x, y)$ instead of $p(x, y, \mathrm{Re})$. The characteristic values of a function (and their estimations) do not depend on the independent arguments, but they still depend on the parameters of the problem. In order to simplify the notation, this dependence will not be explicitly written in the equations. This way the characteristic value for the pressure in the viscous boundary layer will be written as P_C, and not as $P_C(\rho, \nu, U_\infty, L)$.

The notation "order of one" (O(1)) is a mathematical expression that means that the maximum of the absolute value is approximately one or less. The function can have any order of magnitude at any point, as long as that order of magnitude is smaller than one. The expression "order of magnitude of one" is an expression used in dimensional analysis that means that the maximum of the absolute value is approximately one, but not much less. The mathematical notation for this last definition is: $= \mathrm{O}(1), \neq \mathrm{o}(1)$, but in this thesis OM(1) will be used instead. The

expression "approximately equal to one" (≈ 1) applied to a function means that both the maximum and the minimum of the function have the same sign and are approximately one in absolute value. Figure 2-2 shows three different functions. The function $f_1(x)$ is of the order of one, but is neither of the order of magnitude of one nor approximately equal to one. The function $f_2(x)$ is of the order of one, and of the order of magnitude of one, but not approximately equal to one. The function $f_3(x)$ is of the order of one, of the order of magnitude of one, and approximately equal to one. From Figure 2-2 it can also be deduced that:

$$\begin{aligned} \text{approximately one} &\Rightarrow \text{order of magnitude of one} \\ \text{order of magnitude of one} &\Rightarrow \text{order of one} \end{aligned}$$

Throughout this thesis, functions and arguments with units are expressed in uppercase, and their dimensionless counterpart will be expressed in lowercase.

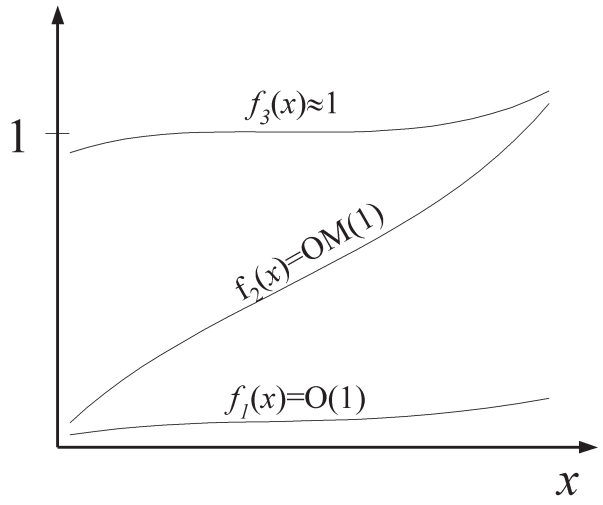

Figure 2-2: Functions showing different orders. The function $f_1(x)$ is of the order of one, but is neither of the order of magnitude of one nor approximately equal to one. The function $f_2(x)$ is of the order of one, and of the order of magnitude of one, but not approximately equal to one. The function $f_3(x)$ is of the order of one, of the order of magnitude of one, and approximately equal to one.

2.2.2 Non-Dimensional Functions and Their Properties

Let $F(X_1 \ldots X_i \ldots X_v)$ be a scalar function with units, defined over a domain D. The domain D over which the order of magnitude scaling will be performed is finite, defined by $A_i \leq X_i \leq B_i$, for $i = 1 \ldots v$, as shown in Figure 2-3.

The absolute value of $F(X_1 \ldots X_i \ldots X_v)$ over D will be minimum at point **A**, and maximum at point **B**. The actual location of points **A** and **B**, is not important; nor is it required that they are unique. When the dimensionless second derivatives are of the order of one, it can be shown that these points are not close to each other (see Appendix B).

Definition of the Non-Dimensional Functions and Independent Arguments

The non-dimensional form of the variable X_i is x_i, and that of $F(X_1 \ldots X_i \ldots X_v)$ is $f(x_1 \ldots x_i \ldots x_v)$. The definitions of these dimensionless expressions are:

$$x_i = \frac{X_i - A_i}{B_i - A_i} \tag{2.1}$$

$$f(x_1 \ldots x_i \ldots x_v) = \pm \frac{F(X_1 \ldots X_i \ldots X_v) - F(\mathbf{A})}{|F(\mathbf{B})| - |F(\mathbf{A})|} \tag{2.2}$$

The $\pm$ sign in equation 2.2 indicates that the sign of the dimensionless function f can be defined arbitrarily, in the way it is most convenient.

Definition of the Characteristic Values and Scaling Relationships

Equations 2.1 and 2.2 can be rewritten as:

$$X_i = A_i + X_{C_i} x_i \tag{2.3}$$

$$F(X_1 \ldots X_i \ldots X_v) = F(\mathbf{A}) \pm F_C f(x_1 \ldots x_i \ldots x_v) \tag{2.4}$$

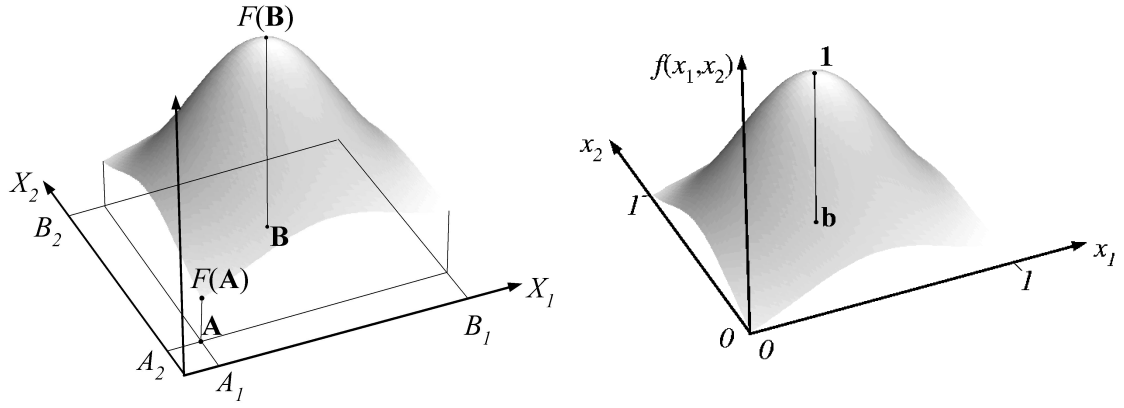

Figure 2-3: Dimensional and normalized functions. The figure on the left shows a 2D example of a dimensional function and its domain for scaling. The figure on the right shows the same function and domain in dimensionless form. In this example point **A** is at one corner of the domain, and point **B** is an interior point.

where:

$$X_{C_i} = B_i - A_i \tag{2.5}$$

$$F_C = |F(\mathbf{B})| - |F(\mathbf{A})| \tag{2.6}$$

When $F(\mathbf{A}) = 0$, F_C is the characteristic value of F. When $F(\mathbf{A}) \neq 0$, F_C is the characteristic value of the oscillation[1] of F. This concept applies similarly to the independent arguments. The characteristic values are defined positive, because when performing algebraic operations they might be raised to a non-integer power.

Definition of the Order of Magnitude Estimations

When the representative functions are unknown, the characteristic values need to be replaced by estimations, marked with a hat ($\widehat{\ }$). The relationship between the characteristic values and their estimations is:

$$X_{C_i} = \widehat{X}_{C_i} g_i(\Pi_1 \ldots \Pi_m) \tag{2.7}$$

[1]The oscillation of a function is the variation between its minimum and its maximum.

$$F_C \quad = \quad \widehat{F}_C g(\Pi_1 \ldots \Pi_m) \tag{2.8}$$

where $\Pi_1 \ldots \Pi_m$ constitute a complete set of dimensionless groups, with the unknown functions g and g_i approximately equal to one in the domain.

Properties of Non-Dimensional Functions

The dimensionless functions and their arguments defined above have important properties for order of magnitude scaling. One of these properties is that the non-dimensional independent arguments cover the zero to one interval:

$$0 \leq x_i \leq 1 \qquad\qquad i = 1 \ldots v \tag{2.9}$$

The dimensionless functions also have the property of being of the order of magnitude of one, because they have an absolute value lesser or equal to one, and exactly one at point **B**.

$$f(x_1 \ldots x_i \ldots x_v) = \mathrm{OM}(1) \tag{2.10}$$

The dimensionless functions possess additional properties under more restrictive conditions. Some of those conditions are particular to specific problems, and others are more general. For the more general case, if all the dimensionless second derivatives are of the order of one, the first derivative of the dimensionless function will also be of the order of one. The derivation of this property is included in Appendix B.

$$\frac{\partial^2 f}{\partial x_i x_j} = \mathrm{O}(1) \text{ for } j = 1 \ldots v \Rightarrow \frac{\partial f}{\partial x_i} = \mathrm{O}(1) \tag{2.11}$$

The above property determines an upper bound for the value of a first derivative, but not a lower bound. A lower bound can be established in some cases. One of those cases is when the maximum and the minimum of the original function have the same sign, and are located over a line parallel to a coordinate axis. In this case the first derivative in that direction will be exactly one at some point in the domain:

$\partial f/\partial x_i = \mathrm{OM}(1)$.

The property described in equation 2.11 is critical for a meaningful normalization because it allows one to determine the order of an unknown term without solving the equation. This property is useful for differential equations of second order or less, which constitute the majority of the differential equations in engineering. This methodology could be extended to include derivatives of order higher than two when those derivatives can be proven to be of the order of one. Those cases are not trivial, and the scope of this thesis will cover only derivatives of up to second order.

Order of Magnitude of an Unknown Term

The key of the methodology presented in this thesis is to be able to scale all known terms of an equation, and use this information to estimate the order of the unknown terms. By considering only the order of magnitude of the functions and their derivatives, an exact differential equation is converted into an approximate algebraic equation, which is significantly easier to solve. For example, the equation of conservation of mass in a two dimensional flow is:

$$\frac{\partial U}{\partial X} + \frac{\partial V}{\partial Y} = 0 \tag{2.12}$$

This equation can be normalized as:

$$\frac{\partial u}{\partial x} + N_1 \frac{\partial v}{\partial y} = 0 \tag{2.13}$$

where $N_1 = V_C X_C / U_C Y_C$. When $\partial u/\partial x$=OM(1), and $\partial v/\partial y$=OM(1) the dimensionless group N_1 must be approximately equal to one. If any physical magnitude in the definition of N_1 is an estimation, for example $N_1 = \widehat{V}_C X_C / U_C Y_C$, the estimation can be calculated by assigning $N_1 = 1$, and solving for $\widehat{V}_C$.

In general, a differential equation can be expressed as a sum of terms.

$$\sum_{i=1}^{w} a_i = 0 \tag{2.14}$$

where a_i are the terms of an equation, and w is the number of those terms. When all but one of the terms are of the order of one (for example $a_1 \ldots a_{\nu-1} = \mathrm{O}(1)$), an upper bound for the order of magnitude of the remaining term can be estimated:

$$a_w = -\sum_{i-1}^{w-1} a_i = (w-1)\mathrm{O}(1) \tag{2.15}$$

If the differential equation does not have many terms (five or less, for example), the unknown term will be of the order of one, but if the number of terms is large, equation 2.15 cannot guarantee that the unknown term will be of the order of one. The importance of equation 2.15 is that it provides information about functions involved in a differential equation, without actually solving it.

Estimation of the Order of Magnitude of the Second Derivatives

When the normalized second derivatives are of the order of one, much information can be obtained from a differential equation without solving it. Information about the second derivatives is frequently provided by previous physical insight even when the exact answer to the problem is unknown. The previous physical insight may be in the form of knowledge of previous experiments, models, etc., indicating whether the descriptive functions vary smoothly or not over a given domain. It is reasonable to assume that those functions that vary smoothly and with little curvature will have dimensionless second derivatives of the order of one.

For most problems where there is a sharp variation, the domain of interest can be split into smaller domains over which the functions vary smoothly, and order of magnitude scaling can be performed in each region using the methodology described here. For example, for analysis of the boundary layer, the semi-infinite domain can be

subdivided into two regions, one between the plate and the thickness of the boundary layer, and the other between the thickness of the boundary layer and infinity. In each of those regions the functions vary smoothly; therefore, the dimensionless functions and its two first derivatives are of the order of one (with the exception of the region close to the leading edge).

For functions of many arguments the estimation by examination of their cross second derivatives is more difficult. However, if the function can be represented by the product of single variable functions, the cross second derivative can be bounded by the product of the first derivatives and the single variable functions. A three variable example would be:

$$f(x,y,z) = f_1(x)f_2(y)f_3(z) \Rightarrow \frac{\partial^2 f}{\partial x \partial y} = \frac{df_1}{dx}\frac{df_2}{dy}f_3(z)$$

2.2.3 Algebraic Properties of Units, Parameters and Dimensionless Groups

Matrix algebra is not essential for appropriate order of magnitude determination; however, it is convenient when dealing with complex problems which involve many equations and parameters. The sets of derived units, dimensionless groups, and other combinations will be represented in the form of vectors or matrices, which contain exponents for each element of the combination. This is a very convenient notation that allows the use of matrix algebra to simplify the calculations and provides a consistent treatment of many different systems.

Relevant Sets Definitions

Table 2.1 shows a summary of the definitions of the different sets and their number of elements. Appendix A contains more precise definitions of these terms.

Table 2.1: Definitions of sets and matrices for order of magnitude scaling

set	number of elements	description
$\{I\}$	v	set of independent arguments
$\{U\}$	u	set of unknowns
$\{P\}$	n	complete set of parameters
$\{R\}$	t	set of reference units for $\{P\}$
$\{P_k\}$	k	set of reference parameters for $\{P\}$
$\{P_m\}$	m	elements of $\{P\}$ not included in $\{P_k\}$
$\{S\}$	q	set of estimations
$\{N\}$	p	set of dimensionless groups that appear in the dimensionless set of equations
$\{N_q\}$	q	subset of $\{N\}$ of known order of magnitude
$\{N_r\}$	r	elements of $\{N\}$ not included in $\{Nq\}$
$\{\Pi\}$	m	complete set of dimensionless groups
$\{\ldots\}$		set of elements such as units, parameters or groups
$[\ldots]$		matrix, or "units of"
$(\ldots)$		set of logarithms of parameters, units or groups
$(\ldots)_S$		set in which the estimations appear explicitly
$(\ldots)_\Pi$		set in which the elements are expressed as a function of the elements of $\{\Pi\}$
$[W]$	$(n+q)\times t$	matrix of dimensions
$[A]$	$(p+m)\times(n+q)$	matrix of dimensionless groups ($\{S\}$ explicit)
$[B]$	$(m+r)\times n$	matrix of dimensionless groups ($\{S\}$ implicit)
$[A_S]$	$q\times n$	matrix of estimations
$[B_N]$	$r\times m$	matrix of coefficients ($\{\Pi\}$ explicit)

Matrix Definitions

This section defines a number of matrices that express the relationships among the different sets. In order to simplify the notation, it is assumed that the set $\{P_k\}$ is the set of the first k elements of $\{P\}$, and that $\{N_q\}$ is the set of the first q elements of $\{N\}$.

The matrix of dimensions $[W]$ relates the problem parameters and estimations to the set of reference units. For convenience, matrix $[W]$ is subdivided into two submatrices $[U]$, and $[V]$, which assign the proper units to the complete set of parameters and the set of estimations respectively.

$$[W] = \begin{bmatrix} [U] \\ [V] \end{bmatrix} \tag{2.16}$$

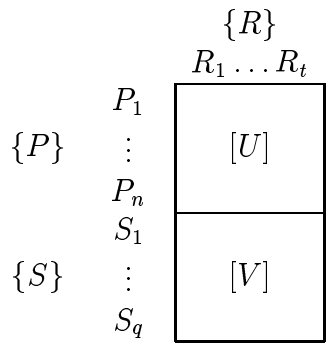

Figure 2-4: Construction of matrix $[W]$. It is subdivided into two submatrices, $[U]$, and $[V]$. In matrix $[U]$ the element U_{ij} is the exponent of R_j in the units of P_i, in matrix $[V]$ the element V_{ij} is the exponent of R_j in the units of S_i.

Matrix $[A]$ relates the dimensionless groups to the complete set of parameters and the set of estimations. For convenience, it is subdivided into submatrices $[A_{ij}]$.

$$[A] \quad = \quad \begin{bmatrix} [A_{11}] & [A_{12}] \\ [A_{21}] & [A_{22}] \\ [A_{31}] & [A_{32}] \end{bmatrix} \tag{2.17}$$

$$[A_1] = \begin{bmatrix} [A_{21}] \\ [A_{31}] \end{bmatrix} \tag{2.18}$$

$$[A_2] = \begin{bmatrix} [A_{22}] \\ [A_{32}] \end{bmatrix} \tag{2.19}$$

		$\{P\}$ $P_1 \dots P_n$	$\{S\}$ $S_1 \dots S_q$
	N_1		
$\{N_q\}_S$	$\vdots$	$[A_{11}]$	$[A_{12}]$
	N_q		
	Π_1		
$\{\Pi\}_S$	$\vdots$	$[A_{21}]$	$[A_{22}]$
	Π_m		
	N_{q+1}		
$\{N_r\}_S$	$\vdots$	$[A_{31}]$	$[A_{32}]$
	N_p		

Figure 2-5: Construction of matrix $[A]$. It is subdivided into submatrices $[A_{ij}]$. In matrix $[A_{12}]$ the element $A_{12_{ij}}$ is the exponent of S_j in N_i. The construction of the other submatrices follows an analogous process

Matrix $[B]$ relates the dimensionless groups which are not set to an arbitrary value to the parameters of the problem. For convenience it is divided into submatrices $[B_{ij}]$.

$$[B] = \begin{bmatrix} [B_{11}] & [B_{12}] \\ [B_{21}] & [B_{22}] \end{bmatrix} \tag{2.20}$$

		$\{P_k\}$ $P_1 \ldots P_k$	$\{P_m\}$ $P_{k+1} \ldots P_n$
$\{\Pi\}$	Π_1 $\vdots$ Π_m	$[B_{11}]$	$[B_{12}]$
$\{N_r\}$	N_{q+1} $\vdots$ N_p	$[B_{21}]$	$[B_{22}]$

Figure 2-6: Construction of matrix $[B]$. It is divided into submatrices $[B_{ij}]$. In matrix $[A_{12}]$ the element $B_{12_{ij}}$ is the exponent of P_{j+k} in Π_i. The construction of the other submatrices follows an analogous process.

Set and Matrix Relationships

The vectors and matrices defined are related through the following equations (Appendix B.2 contains a summary of the derivations):

$$\left\{ \begin{array}{c} ([P]) \\ ([S]) \end{array} \right\} = [W](R) \tag{2.21}$$

$$\left\{ \begin{array}{c} (N_q)_S \\ (\Pi)_S \\ (N_r)_S \end{array} \right\} = [A] \left\{ \begin{array}{c} (P) \\ (S) \end{array} \right\} \tag{2.22}$$

$$(S) = [A_S](P) \tag{2.23}$$

$$\left\{ \begin{array}{c} (\Pi) \\ (N_r) \end{array} \right\} = [B](P) \tag{2.24}$$

$$(N_r)_\Pi = [B_N](\Pi) \tag{2.25}$$

where:

$$[A_S] = -[A_{12}]^{-1}[A_{11}] \tag{2.26}$$

$$[B] = [A_1] + [A_2][A_S] \tag{2.27}$$

$$[B_N] = [B_{22}][B_{12}]^{-1} \tag{2.28}$$

Buckingham's theorem [37] determines that the number of elements of the set of governing dimensionless groups $\{\Pi\}$ is m, where:

$$m = n - k \tag{2.29}$$

The matrix of dimensions $[U]$ determines that the number of elements of the dimensionally independent set of parameters $\{P_k\}$ is k [24], where:

$$k = \text{rank } [U] \tag{2.30}$$

Modifications to the Complete Set of Parameters and Set of Reference Units

In some occasions not all the governing dimensionless groups are used in the differential equations. This brings additional insight into the physics of the problem. Two situations might cause this excess of dimensionless groups: The presence of parameters that represent temperatures, and the exclusion of a physical effect in the original system of equations.

Parameters that represent temperatures: When the scaling of a problem depends only on temperature differences, one of the temperature parameters can be disregarded for the purposes of dimensional analysis. This is equivalent to setting that temperature as the origin of the scale. In this case, the complete set of parameters is reduced by one element. The non-isothermal boundary layer example of Section 3.3 is done without disregarding any temperature to show that there is one

dimensionless group in excess, represented by a column of only zeros in matrix $[B_N]$.

Extension to the set of reference units: If the excess of dimensionless groups is not due to parameters that represent temperature, the other possible cause is that the original set of equations does not include an effect that is implicitly considered by the system of reference units. If the original set of equations is correct, then extending the set of reference units will simplify the problem. For example, neglecting frictional heating and expansion work in a flow, is equivalent to stating that thermal energy and mechanical energy do not interact with each other, thus splitting the law of conservation of energy into two more restrictive conservation laws. Because thermal and mechanical energy do not interact, they can be considered as different physical quantities, and assigned different units. The scaling of thermocapillary flows in Section 3.4 makes use of this type of extended set of reference units. If the extension is incorrect (a reference unit was added improperly) it is not possible to transform the original system of equations into its non-dimensional counterpart.

Verifications

The complete system of partial differential equations is correctly written only when there are as many equations as unknowns. The original system therefore consists of u equations with u unknowns.

The independence of the elements of the set of reference parameters can be verified by checking that the rank of the submatrix of $[U]$ that involves only the elements of $\{P_k\}$ has rank k.

The independence of the elements of $\{N_q\}$ can be verified by checking that the matrix $[A_{12}]$ is not singular. Similarly, the complete set of dimensionless groups $\{\Pi\}$ is independent when the matrix $[B_{12}]$ is not singular. A practical verification that the units used for the parameters are correct is to check that the multiplication $[A][W]$ yields a matrix with only zeros for elements.

The complete set of parameters $\{P\}$ and the set of reference units $\{R\}$ are optimal

when all of the of elements of $\{\Pi\}$ are included in the dimensionless equations. This condition can be generalized as:

$$\text{rank } [B_N] = m \tag{2.31}$$

If the rank is smaller than m, then a temperature parameter can be disregarded, or a new reference unit can be added. The choice of an optimum set of units has been addressed in the past (see Sedov's notes on the debate between Riabouchinsky and Rayleigh about the proper units to measure temperature [26, page 40]) this is the first time in which such a criterion is expressed mathematically.

2.3 Order of Magnitude Scaling Procedure

The properties of the dimensionless functions and sets defined above can be combined and used systematically to obtain order of magnitude estimations and scaling for a great variety of complex problems. When performing order of magnitude estimations and scaling of a problem, the following stages appear regularly:

1. Governing equations, boundary conditions, and domain for scaling.
2. Sets of parameters and units.
3. Scaling relationships, characteristic values, and order of magnitude estimations.
4. Dimensionless governing equations and boundary conditions.
5. Dimensionless groups of known order of magnitude.
6. Complete set of dimensionless groups.
7. Expression of the estimations.
8. Dimensionless governing equations and boundary conditions (in terms of the governing dimensionless groups).

This sequence cannot be considered as a fail-proof algorithm because every problem presents different aspects and new challenges, some of which could present unexpected exceptions. One of the goals of the Order of Magnitude Scaling method is to reduce the amount of intuition and effort required for estimation of a solution to the problem. The physical insight into a problem can be transformed into a consistent set of considerations, allowing engineers to systematically use powerful mathematical tools that would usually be avoided due to their complexity. The stages listed above are explained in more detail in the following subsections.

2.3.1 Governing Equations, Boundary Conditions, and Domain for Scaling

In this stage, the complete set of differential equations, boundary conditions and domain for scaling are determined.

All equations are simplified representations of reality, and in the choice of the governing equations for a system there is also a choice of the physics that are going to be considered. If a critical driving force or effect is omitted, then the scaling will be defective.

The domain for scaling is not necessarily the same domain over which the differential equations are defined. The domain for scaling must be finite, even when the differential equations are defined over an infinite domain. The viscous boundary layer example (Section 3.2) shows the importance of this difference.

2.3.2 Sets of Parameters and Units

The following sets are defined in this stage:

- The complete set of parameters $\{P\}$, which completely determine the problem.
- The set of reference units $\{R\}$.
- The matrix $[U]$ that relates the parameters to the reference units.

- A dimensionally independent subset $\{P_k\}$.

In this methodology, the set of parameters is determined from the equations and their boundary conditions. This makes the selection of parameters very clear and straightforward, eliminating any possibility of confusion. This is another advantage of using the governing equations to improve the dimensional analysis. When these equations are not used the choice of the complete set of parameters is not obvious (see for example Bridgman's discussion on gravitational attraction between two bodies [22]).

The set of reference units is determined from the units of the parameters, without the need to look at the unknowns or independent arguments for additional reference units[2]. This facilitates the verification of completeness and independence of some sets by using matrix algebra.

The complete set of parameters and the set of reference units can be modified using the concepts of Section 2.2.3.

2.3.3 Scaling Relationships, Characteristic Values, and Order of Magnitude Estimations

In this stage the scaling relationships, the characteristic values, and the order of magnitude estimations are determined. A set $\{S\}$ of q estimations is generated. Previous insight into the physics of the problem is necessary here, especially when the domain for scaling needs to be subdivided into smaller regions. This subdivision is necessary when the dimensionless second derivatives are not of the order of one, because the dimensionless functions cannot be guaranteed to have the special properties mentioned in Section 2.2.2. In this case, the domain of interest must be split along the transition into regions for which the second derivatives are of the order of one. For functions which present a sharp change in slope, (for example the boundary layer, Section 3.2)

[2]Although not proven in this work, I am not aware of any exception, and will leave it as a conjecture.

the subdivision into two smaller subdomains is simple and straightforward. For functions that have large second derivatives over all the domain, it is more difficult to make any particular choice for a subdivision. Many subdivisions can be necessary in some cases, to the detriment of the simplicity pursued by this methodology. A simple function that shows this problem is the exponential function:

$$Y = Y_0 e^{AX} \quad \text{with} \quad 0 \leq X \leq L, \quad Y_0 \leq Y \leq Y_L \tag{2.32}$$

Appendix B.3 shows that the dimensionless second derivative can be large when AL is large (i.e. when the end value is much larger than the starting value). In this case, the domain of interest should be split into smaller subdomains for which the second derivative is of the order of one. Appendix B.3 indicates that for $AL \gtrsim 1$, the size of the subdomains should be of the order of $1/A$, and their minimum number approximately $\ln(Y_L/Y_0)$. For example, for $Y_L/Y_0 \approx 7$, two subdomains are necessary. The larger the ratio between the end and starting values, the more subdomains are necessary.

In some cases the same variable is assigned more than one characteristic value because different driving forces or effects act over different ranges (for example the non-isothermal boundary layer (Section 3.3), uses two different characteristic thickness). In other cases the characteristic values such as the geometry of the problem are known beforehand; therefore, the number of estimations q does not necessarily equal the number of unknowns plus arguments $(u + v)$ in the problem.

2.3.4 Dimensionless Governing Equations and Boundary Conditions

In this stage the dimensional equations are normalized using the scaling relationships. There are many possible ways to normalize the equations. Each equation can be normalized by any of its terms. The normalizing procedure used in this methodology is the "dominant balance" technique, presented by Bender and Orszag [34]. It consists of

normalizing each equation by its dominant term (this requires physical understanding of the problem), this way the largest term (in absolute value) is one, and all the others are smaller. In this process a set $\{N\}$ of p dimensionless groups is generated, each group representing the ratio between a particular force and the dominant force in the equation. In these dimensionless groups, the estimations appear explicitly.

In standard dimensional analysis the governing equations are not used, and the choice of representative dimensionless groups is difficult and not unequivocal, especially for problems with a large number of parameters. For example Staicu [10] proposed the method of "minimum, integer, positive" exponents, based on the empirical observation of frequency of occurrence numeric exponents in a number of different problems [12, page 153].

2.3.5 Dimensionless Groups of Known Order of Magnitude

In this stage a subset $\{N_q\}$ of q elements from $\{N\}$ for which their order of magnitude is known is determined.

Since the dominant force and effect are used to normalize the equations, all ratios of forces will be smaller than one, because the dominant force is in the denominator. The same happens with the ratios of effects. Ratios between forces or effects larger than one indicate that the dominant factor was incorrectly chosen and the dimensional equations should be normalized again (this is the core of the dominant balance method).

In a system at equilibrium, the simultaneous action of all forces (for example electromagnetic, buoyancy, etc.) is balanced at every point by the counteraction of the effects (viscosity, acceleration, etc.); therefore, their ratio is one.

$$\frac{\sum \text{driving forces}}{\sum \text{effects}} = 1 \tag{2.33}$$

The ratio of just the dominant force and the dominant effect is not exactly one, but approximates one for the limiting cases when the secondary driving forces and

effects are negligible.

$$\frac{\text{dominant driving force}}{\text{dominant effect}} \rightarrow \frac{\sum \text{driving forces}}{\sum \text{effects}} = 1 \tag{2.34}$$

When analyzing a system, it is convenient to focus on the limiting cases. This way the ratios between dominant forces and effects are approximately one. The estimations will be more accurate for the limiting cases, which are the realistic representation for many systems (for example the weld pool under high currents, Section 6). Intermediate cases can be bound within the corresponding limiting cases.

The number of dimensionless groups of known order of magnitude is not necessarily the same as the number of equations; however, it must be the same as the number of estimations.

2.3.6 Complete Set of Dimensionless Groups

In this stage the governing dimensionless groups are defined, these are the Π groups anticipated by Buckingham's theorem [37]. The elements of this set can be chosen arbitrarily as long as they constitute a complete and independent set. The meaningful expression of relative importance of forces and effects is given by the coefficients in the dimensionless governing equations and boundary conditions.

2.3.7 Expression of the Estimations

In this stage the matrix of dimensionless groups $[A]$ is assembled, and the expression of the estimations is obtained by using equation 2.23 to solve the system of q equations $(N_1 \ldots N_q = 1)$ with q unknowns $(S_1 \ldots S_q)$.

2.3.8 Dimensionless Governing Equations and Boundary Conditions (in terms of the elements of the complete set of dimensionless groups)

In this stage the coefficients in the governing equations and boundary conditions are expressed in terms of the elements of the complete set of dimensionless groups $\{\Pi\}$ using equation 2.25. These coefficients are the meaningful expression of relative importance of forces and effects.

2.4 Comparison of Order of Magnitude Scaling with Dimensional Analysis

The methodology of order of magnitude scaling presented here overcomes some of the restrictions of dimensional analysis. Isaacson *et al.* describes these limitations as follows [12, page 190]:

1. The numerical constant entering into a physical equation has to be undetermined.

2. The nature of the functions, where there is more than one dimensionless product, must also be left undetermined.

The simple pendulum is a classic case of study in dimensional analysis, being analyzed in references [22, 25, 26, 29, 12, 31, 16] among others. All of these references obtain the following estimation of the period (using the notation of Section 3.1):

$$T = \sqrt{\frac{L}{g}} h(\Theta_0) \tag{2.35}$$

where the function h is undetermined; all that is known about it is that it depends only on Θ_0.[3] This function can be very large or very small, can have large variations or be approximately constant; dimensional analysis alone cannot provide any additional information.

The order of magnitude scaling of a pendulum presented in Section 3.1 yields additional information. The period of a pendulum is described as:

$$T = \begin{cases} 4\sqrt{\dfrac{L}{g}}\, g_I(\Theta_0) & \text{for small oscillations} \\ \\ 4\sqrt{\dfrac{L\Theta}{g}}\, g_{II}(\Theta_0) & \text{for large oscillations} \end{cases} \tag{2.36}$$

where the functions $g_I(\Theta_0)$ and $g_{II}(\Theta_0)$ are approximately one, therefore the correct order of magnitude for the period is obtained even when these functions are disregarded.

In general, dimensional analysis will yield results of the type:

$$Q_C = \prod_{i=1}^{k} P_i^{a_i} h(\Pi_1 \ldots \Pi_m) \tag{2.37}$$

where Q_C is any characteristic physical quantity of the problem, P_i are the reference parameters (elements of $\{P_k\}$), each of which raised to a power a_i. The function of this power product is to produce the units corresponding to Q_C. The function h depends only on the governing dimensionless groups Π_j, but nothing else is known about it. There is no obvious way either of determining the relative importance of each of the governing dimensionless groups.

[3] This dependence is omitted in references [29, 31, 16], where it is assumed $h(\Theta_0) =$ constant, mistakenly omitting an important parameter of the problem.

The order of magnitude scaling technique yields results of the type:

$$Q_C = \prod_{i=1}^{n} P_i^{a_i} g(\Pi_1 \ldots \Pi_m) \tag{2.38}$$

where the function g is approximately one. In this case, all of the elements in the complete set of parameters are necessary, and the power product actually constitutes an estimation of Q_C:

$$\prod_{i=1}^{n} P_i^{a_i} = \widehat{Q}_C \tag{2.39}$$

In addition, the relative importance of the governing dimensionless groups can be determined using the coefficients of the dimensionless governing equations and boundary conditions.

2.5 Summary

The set of estimations acts as a bridge between dimensional analysis and asymptotic considerations, allowing one to benefit from both techniques simultaneously. This method helps to transform physical insight and intuition into a consistent set of mathematical considerations, which facilitates the algebraic treatment of a problem. Order of magnitude estimates can be obtained in a straightforward and systematic manner, without modifying the physics contained in the original equations. Numerical constants such as the numbers π or $\sqrt{2}$ can be factored into the analysis in a simple and meaningful way. These order of magnitude estimations can be refined by studying how the dimensionless groups affect the dimensionless functions. This improvement can be done by perturbation methods, experimentation or analysis of numerical results. When this methodology is properly applied, even a single experiment can significantly improve the accuracy of the predictions over a large range (see the pendulum example in Section 3.1).

The methodology presented in this chapter also presents some limitations. Perhaps the most severe is that the second derivatives of the dimensionless functions

must be of the order of one. For functions with large second derivatives over all of the domain (for example the exponential function with positive exponent) the domain for scaling must be subdivided into many subdomains, losing the simplicity pursued by this technique. Problems involving this type of functions, such as some stability studies are beyond the scope of this methodology. Another limitation is that when the number of arguments and terms in the equation is too large, it cannot be guaranteed that all of the derivatives are of the order of magnitude of one. Although there is no theoretical limitations to the coordinate frame used to write the governing equations, they need to be written in scalar form. The implementation of vector operators is beyond the scope of this work.

Instead of having an abstract discussion about the details of this methodology, a series of examples are included in Chapter 3. In these examples, order of magnitude estimations are performed on a number of well known systems such as the viscous boundary layer. The results obtained are compared to the known solutions to show that this methodology can successfully approximate the solutions of a problem while making the mathematical treatment much simpler.

Chapter 3

Testing Order of Magnitude Scaling Using Known Examples

This chapter illustrates the methodology of order of magnitude scaling through a number of increasingly complex examples for which the solutions are known. In this way, effort can be focused on the use of the order of magnitude scaling methodology instead of the problem itself. In these sample cases, order of magnitude scaling is performed in a systematic and relatively simple way, and the results are compared to those obtained previously by other methods. No new solutions to engineering problems are presented in this chapter, but it is shown that the order of magnitude scaling method developed herein provides the same (or better) results as those obtained previously by other methods.

The following examples are studied:

Simple pendulum: This example was chosen because it involves a very simple problem where the estimations can be obtained in a straightforward way without using matrix algebra. There is only one unknown function with only one independent argument. Many textbooks include the simple pendulum as a classic example of the application of dimensional analysis, facilitating a direct comparison of dimensional analysis with order of magnitude scaling.

Viscous boundary layer: This is a more complex problem than the simple pendulum because more unknown functions with many independent arguments are involved. The matrix properties that relate the different sets will be used here. This is another classic example used in the dimensional analysis textbooks.

Non-isothermal boundary layer: This presents the additional complexity of heat transfer depending on the fluid flow problem. This example shows the use of different characteristic values for the same magnitude. It also shows the convenience of disregarding one temperature parameter when the problem only involves temperature differences.

Low-Prandtl-number thermocapillary flows: This reviews the scaling results obtained by Rivas and Ostrach [9] for low-Prandtl-number thermocapillary flows. This example shows order of magnitude scaling when the fluid flow is fully coupled to the heat transfer. The complete set of parameters and the set of reference units are optimized. This analysis uses the physical insight from Rivas and Ostrach, and suggests ways to improve their results.

3.1 Simple Pendulum

By performing order of magnitude scaling of a simple pendulum, one can estimate the increase in the period with larger oscillation angles. Angles for which the mass is almost exactly above the axis ($\Theta \approx \pi$) in Figure 3-1) illustrate a limitation of this method. Figure 3-1a shows a schematic of the system and the evolution of the pendulum angle with time.

The differential equation that represents the problem is equation 3.1, with initial conditions in equations 3.2 and 3.3. Equation 3.1 already includes simplifications to the physics of the problem; for example, it does not consider damping forces or mass

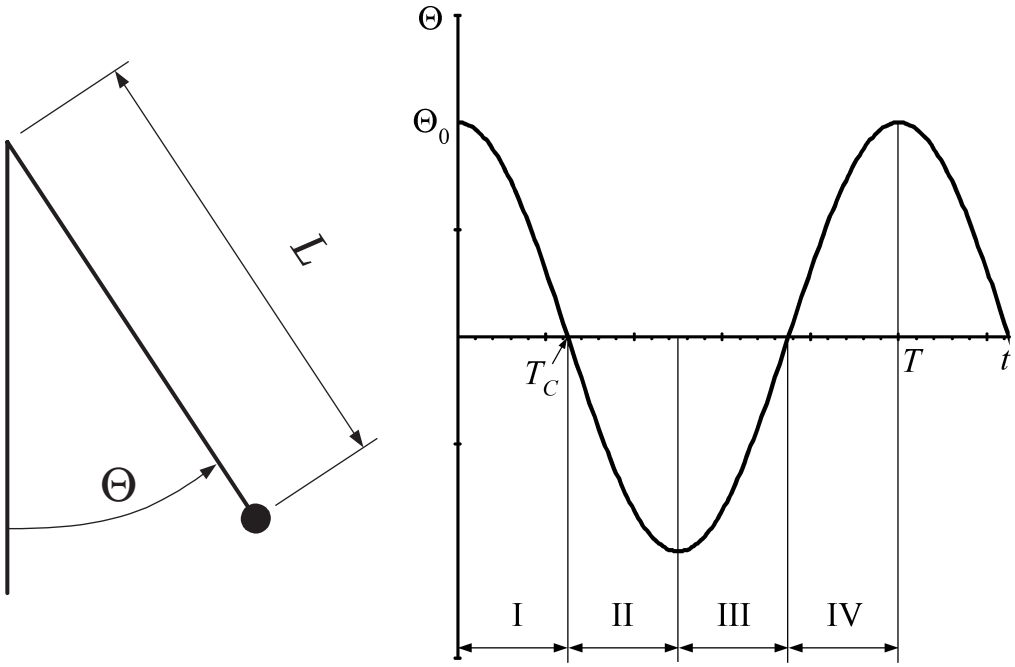

Figure 3-1: Schematic of the simple pendulum and its oscillations

in the link between the swinging mass and the axis.

$$L\ddot{\Theta} + g\sin\Theta = 0 \tag{3.1}$$

$$\Theta(0) = \Theta_0 > 0 \tag{3.2}$$

$$\dot{\Theta}(0) = 0 \tag{3.3}$$

The unknown in this system is the angle Θ, which depends only on the independent argument time (t). The parameters in this problem are the length of the link L, the acceleration of gravity g, and the initial angle Θ_0, therefore $\{P\} = \{L, g, \Theta\}$. The mass of the weight should not be included in $\{P\}$, because it never appears in the equation or in the initial conditions. The set of reference units is obtained by examination of the parameters. In SI units it is $\{R\} =\{\text{m, s}\}$. This set of reference units yields a set of two dimensionally independent parameters $\{P_k\} = \{L, g\}$. Using Buckingham's theorem it is possible to state that only one dimensionless group

is necessary to describe this problem, and the only possibility is the dimensionless parameter Θ_0.

In order to have second derivatives of the order of one, the period of the pendulum should be split into smaller components (see Section 2.3.3). A division into four equivalent components (I to IV in figure 3-1b) is reasonable for small and some large oscillations (see Section 2.2.2). It will be shown later that for oscillations in which the mass is almost exactly above the axis, the domain should be divided differently (Section 3.1.2). Considering segment I as the representative case, the domain for scaling is $0 \leq t \leq T_C$, with the angle varying in the range $0 \leq \Theta \leq \Theta_0$. The characteristic value for the oscillation angle is known (the parameter Θ_0). The characteristic value for the time necessary to complete a quarter of a period is T_C, which is unknown; its estimation is $\widehat{T}_C$. The set of estimations is $\{S\} = \{\widehat{T}_C\}$, and the corresponding scaling relationships are:

$$t = \widehat{T}_C \tau \tag{3.4}$$

$$\Theta(t) = \Theta_0 \theta(\tau) \tag{3.5}$$

where θ is the dimensionless angle and τ the dimensionless time. The dimensionless expression of the equation and its initial conditions is:

$$\theta'' + \frac{g\widehat{T}_C^2}{L\Theta_0} \sin(\Theta_0 \theta) = 0 \tag{3.6}$$

$$\theta(0) = 1 \tag{3.7}$$

$$\theta'(0) = 0 \tag{3.8}$$

Equation 3.6 has a particular feature. The second derivative in the first term must be of the order of magnitude of one; being of the order of one is not enough to determine the order of magnitude of the second term (see Section 2.2). The division of one period into four parts yields appropriate second derivatives. Equation 3.6 presents two different cases for the selection of the dimensionless group of known order of

magnitude.

Case I: The oscillation angle is small, therefore $\sin(\Theta_0\theta) \approx \Theta_0\theta$. For this case the dimensionless group of known order of magnitude is $g\widehat{T}_C^2/L$ which will be assigned the value of one. Therefore, the expression of $\widehat{T}_C$ is:

$$\widehat{T}_C = \sqrt{\frac{L}{g}} \tag{3.9}$$

The exact expression of T_C depends on the complete set of dimensionless groups, which in this case reduces to the parameter Θ_0:

$$T_C = \sqrt{\frac{L}{g}} g_I(\Theta_0) \tag{3.10}$$

where $g_I(\Theta_0)$ is an unknown function whose value is not very different from one. This function can be determined experimentally, or by solving the differential equation.

Case II: The oscillation angle is not small, therefore $\sin(\Theta_0\theta) = \mathrm{OM}(1)$. In this case, the dimensionless group of known order of magnitude is $g\widehat{T}_C^2/L\Theta_0 \approx 1$. The approximate expression of $\widehat{T}_C$ is:

$$\widehat{T}_C = \sqrt{\frac{L\Theta_0}{g}} \tag{3.11}$$

The exact expression of $\widehat{T}_C$ depends on the complete set of dimensionless groups.

$$T_C = \sqrt{\frac{L\Theta_0}{g}} g_{II}(\Theta_0) \tag{3.12}$$

where $g_{II}(\Theta_0)$ is an unknown function whose value is approximately equal to one. This function can be determined experimentally, or by solving the differential equation.

3.1.1 Comparison with Known Results

The exact length of the period is [25, 38]:

$$T = 4\sqrt{\frac{L}{g}}K\left(\sin\frac{\Theta_0}{2}\right) \tag{3.13}$$

where $K()$ is the complete elliptic integral of the first kind. Figure 3-2 shows the exact solution and the estimations from equations 3.9 and 3.11. The exact solution presents an asymptote for values close to π, when the pendulum oscillates to an almost vertical position above the axis. This situation will be analyzed later.

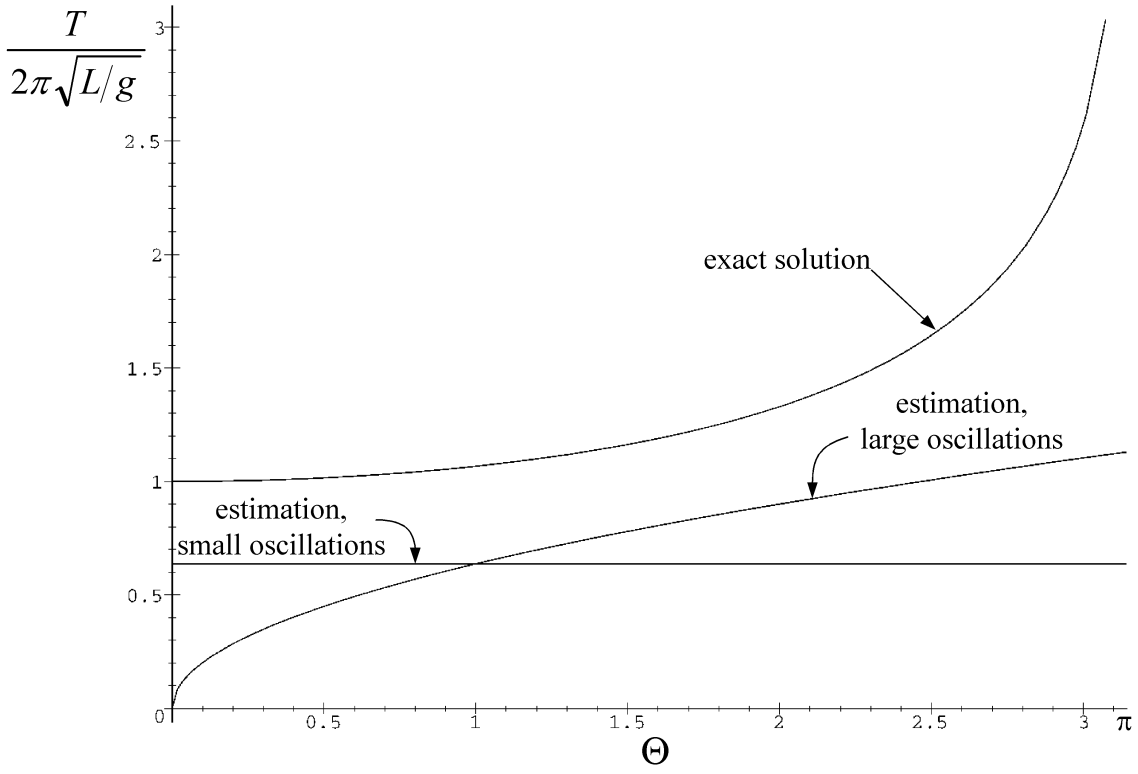

Figure 3-2: Exact and estimated period for the simple pendulum. The estimations are of the same order of magnitude of the exact solution.

The functions $g_I(\Theta_0)$ and $g_{II}(\Theta_0)$ relate the characteristic values of the exact solution to the estimations. Figure 3-3 shows that these functions are approximately

equal to one in their corresponding regions (small angles for g_I and large angles for g_{II}).

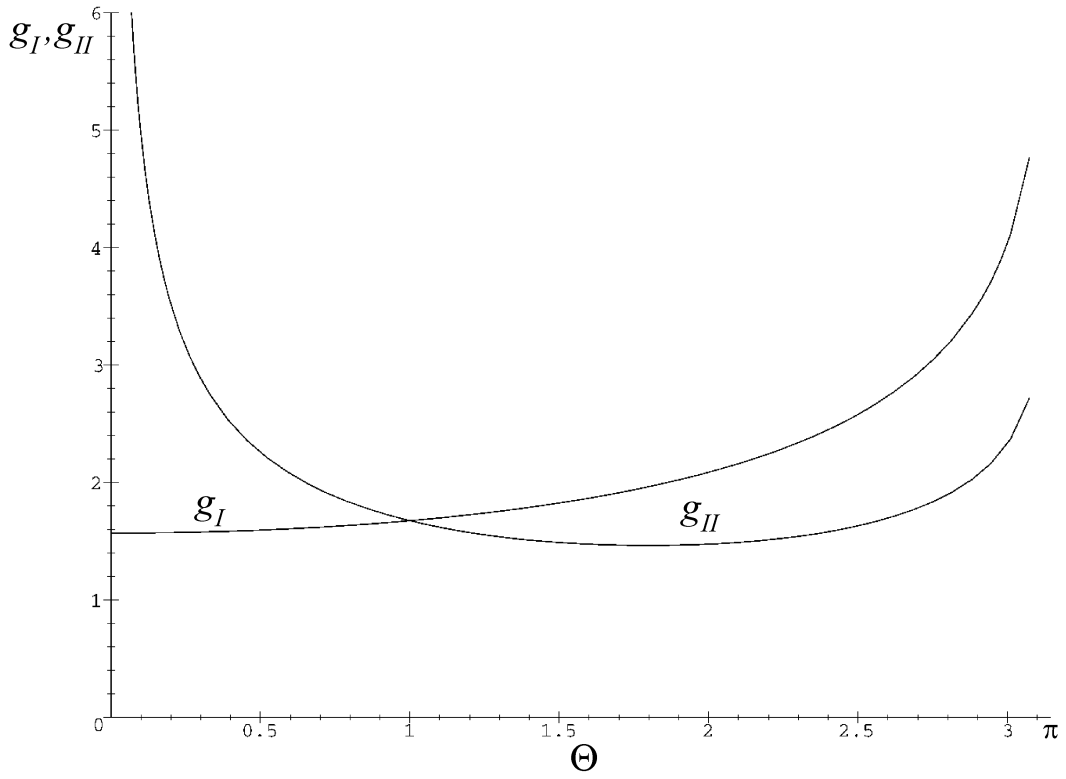

Figure 3-3: Dimensionless functions that relate the estimations to the exact solution. In their applicable range (small oscillations for g_I, large oscillations for g_{II}) these functions are approximately equal to one. Oscillation angles close to the vertical above the axis require special treatment (see Section 3.1.2).

The methodology presented here can only determine that the unknown functions g_I and g_{II} are approximately equal to one. Knowledge from experiments or previous results can help to estimate these functions with more accuracy. For example, knowing that the period of a pendulum at small angles is $T = 2\pi\sqrt{L/g}$, the function g_I can be approximated to $g_I \approx \pi/2$. It is also reasonable to approximate g_{II} by the same factor: $g_{II} \approx \pi/2$. This single point of information improves the accuracy of the predictions significantly, predicting the period of the pendulum with less than 10% error, as shown in Figure 3-4. This unexpectedly accurate result emphasizes the

importance of combining a deep analysis of a problem with previous knowledge. One of the goals of this methodology is to frame the analysis of a problem in such a way that previous insight can be readily used to improve accuracy.

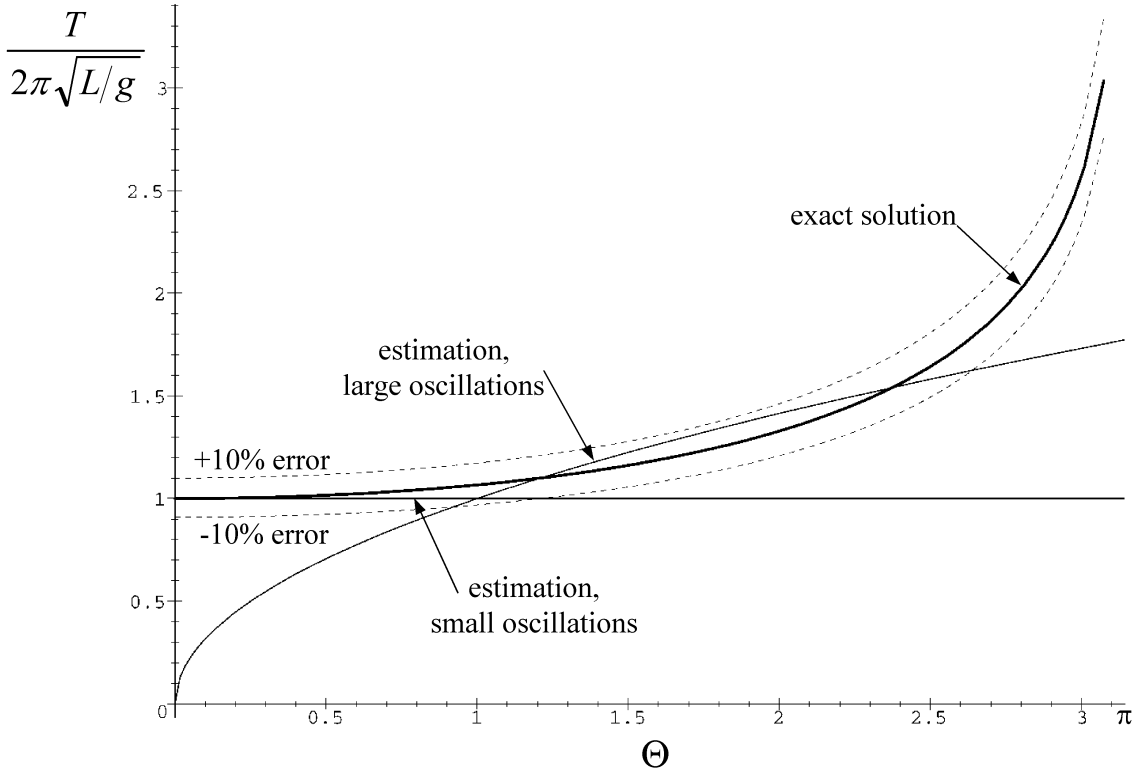

Figure 3-4: Estimated period of the simple pendulum corrected using known information. The predictions fall within a 10% error band. For oscillation angles close to π, the pendulum spends a large fraction of the period at the extreme angles, and special considerations are necessary

3.1.2 Almost Vertical Oscillations

For oscillations that involve angles close to the vertical over the axis, special considerations are necessary. In this situation the pendulum spends a large fraction of the period at the extreme angles, and the domain needs to be subdivided into fractions smaller than a quarter of a period. Figure 3-5 shows this type of oscillation.

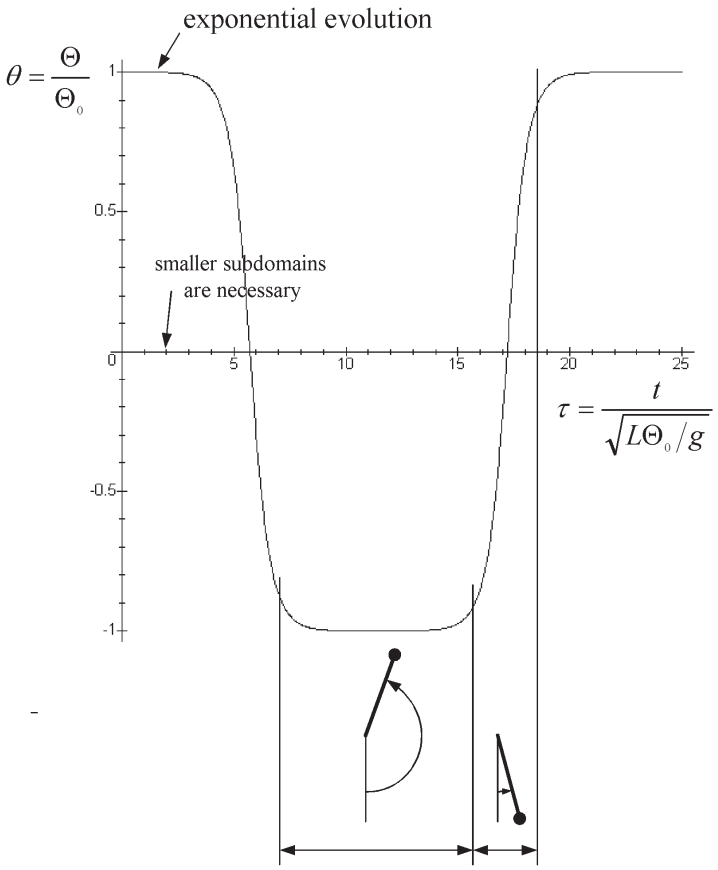

Figure 3-5: Oscillations of a simple pendulum at almost vertical angles (in this case $\Theta_0 = 0.9999\pi$). The pendulum spends most of the time close to the extreme angles. This portion of the period needs to be subdivided into smaller fractions, because the second derivative is too large.

At angles close to π the transformation $\Theta = \pi - \Phi$ is convenient. The scaling relationships for this case are:

$$t = \widehat{T}_C \tau \tag{3.14}$$

$$\Phi(t) = \Phi_0 + \Phi_C \phi(\tau) \tag{3.15}$$

where $\Phi_0 = \pi - \Theta_0$; and $\widehat{T}_C$, Φ_C are an estimation and a characteristic value respectively. The expression of $\widehat{T}_C$ is unknown, and Φ_C has to be determined in such a way that the domain subdivisions yield dimensionless functions with second derivatives approximately one. The dimensionless expression of the governing equation and its boundary conditions is:

$$\phi'' - \frac{g\widehat{T}_C^2}{L\Phi_C} \sin[\Phi_0 + \Phi_C \phi(\tau)] = 0 \tag{3.16}$$

$$\phi(0) = 0 \tag{3.17}$$

$$\phi'(0) = 0 \tag{3.18}$$

For almost vertical oscillations, the angle Φ is small, and equation 3.16 can be approximated to:

$$\phi'' - \frac{g\widehat{T}_C^2}{L}\phi = \frac{g\widehat{T}_C^2}{L}\frac{\Phi_0}{\Phi_C} \tag{3.19}$$

Equation 3.19 is a monotonically increasing function, with the derivatives proportional to the function; this indicates that this is a problem of the type analyzed in Section 2.3.3, indeed, the solution to this equation involves exponential functions, which require the subdivision of the domain into portions smaller than quarter periods (see Appendix B.3). In this case this methodology loses its simplicity, and other techniques may be more appropriate for the analysis of the asymptotic region at almost vertical angles.

3.2 Viscous Boundary Layer

In this section the viscous boundary layer is analyzed. It is assumed that the fluid is incompressible and isothermal, and no external pressure gradients are applied. Figure 3-6 illustrates the classical boundary layer representation.

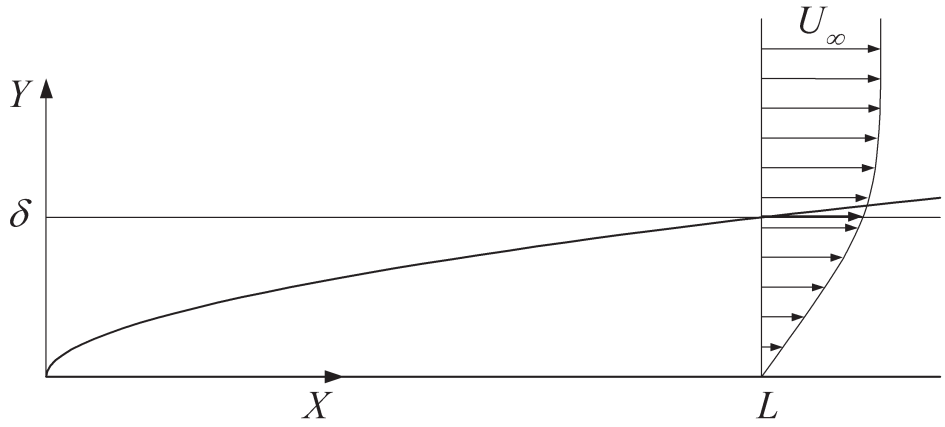

Figure 3-6: Schematic of the viscous boundary layer. The domain for scaling is the rectangle defined by $0 \leq X \leq L$, $0 \leq Y \leq \delta$.

3.2.1 Governing Equations, Boundary Conditions, and Domain for Scaling

The governing equations that represent this problem are the following:

$$\frac{\partial U}{\partial X} + \frac{\partial V}{\partial Y} = 0 \tag{3.20}$$

$$U\frac{\partial U}{\partial X} + V\frac{\partial U}{\partial Y} = -\frac{1}{\rho}\frac{\partial P}{\partial X} + \nu\left(\frac{\partial^2 U}{\partial X^2} + \frac{\partial^2 U}{\partial Y^2}\right) \tag{3.21}$$

$$U\frac{\partial V}{\partial X} + V\frac{\partial V}{\partial Y} = -\frac{1}{\rho}\frac{\partial P}{\partial Y} + \nu\left(\frac{\partial^2 V}{\partial X^2} + \frac{\partial^2 V}{\partial Y^2}\right) \tag{3.22}$$

where equation 3.20 is the equation of continuity, and equations 3.21 and 3.22 are the Navier-Stokes equations.

The boundary conditions are summarized in Table 3.1

Table 3.1: Boundary conditions for the viscous boundary layer (dimensional)

	U	V	P
$(X > 0, 0)$	0	0	
$(-\infty, Y)$	U_∞	0	
$(0, \infty)$			0

There are two independent arguments: X and Y. The equations are defined for an infinite domain over both independent arguments; however, a finite domain must be defined for the scaling. An arbitrary finite length L is defined as the domain limit in the X-direction. The domain in the Y-direction will be limited by the characteristic thickness of the boundary layer (δ). Because L is arbitrary, it is a known order of magnitude scaling factor, and belongs to the set $\{P\}$ of parameters that completely determine the problem. The thickness of the boundary layer is unknown, and its estimation $(\widehat{\delta})$ belongs to the set $\{S\}$ of estimations.

3.2.2 Sets of Parameters and Units

The set of parameters that completely determine the problem is obtained by inspection of the system of equations, its boundary conditions, and its domain, this way the complete set of parameters for this problem is:

$$\{P\}^T = \{\rho, \nu, U_\infty, L\} \qquad n = 4$$

A reasonable choice for the system of units is the SI. The set of reference units $\{R\}$ is obtained by expressing the units of each element of $\{P\}$ in the SI and inspecting the reference units involved:

$$\{R\}^T=\{\text{m, kg, s}\} \qquad t=3$$

The matrix of dimensions $[U]^T$ for this problem is shown in Figure 3-7. Its rank is 3; therefore, three dimensionally independent parameters constitute a set of reference parameters:

$$\{P_k\}^T = \{\rho, \nu, U_\infty\} \qquad k=3$$

	ρ	ν	U_∞	L
m	-3	2	1	1
kg	1			
s		-1	-1	

Figure 3-7: Matrix of dimensions $[U]^T$ for the viscous boundary layer. The submatrix on the left has rank 3

3.2.3 Scaling Relationships, Characteristic Values and Order of Magnitude Estimations

Scaling Relationships for the Independent Arguments

The domain for scaling is the rectangle $0 \leq X \leq L$, $0 \leq Y \leq \delta$, where L is the characteristic value for X, and δ the characteristic value for Y. Because δ is unknown, its estimation $\widehat{\delta}$ is used for the scaling relationships for the independent arguments:

$$X = Lx \tag{3.23}$$

$$Y = \widehat{\delta} y \tag{3.24}$$

Scaling Relationship for $U(X,Y)$

For laminar flow, the minimum value of U is 0, and the maximum is U_∞, therefore U_∞ is the characteristic value for U. Previous physical insight in this case comes from the well known solutions by Blasius [39]. Figure 3-8 shows that there are no

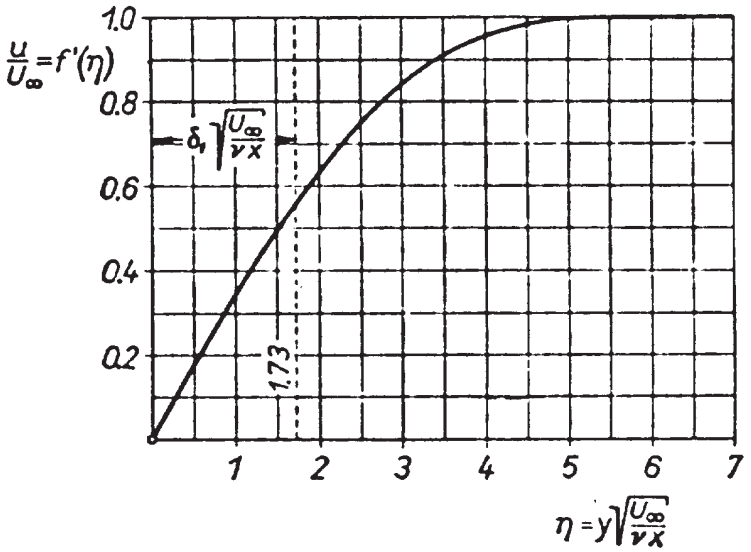

Figure 3-8: Parallel velocity distribution in the viscous boundary layer [39]. In the notation of this figure, symbols in small caps have units.

sharp changes in the slope of U inside the domain, therefore $u(x,y)$ and its first two derivatives are of the order of one. The scaling relationship for U then is:

$$U(X,Y) = U_\infty u(x,y) \tag{3.25}$$

Scaling Relationship for $V(X,Y)$

The transverse velocity V is 0 at the plate and upstream. Our previous physical insight from the known solution indicates that there are no sharp changes in the slope of V inside the domain, therefore $v(x,y)$ and its first two derivatives are of the order of one. The characteristic value of V is V_C, which is unknown; therefore, an

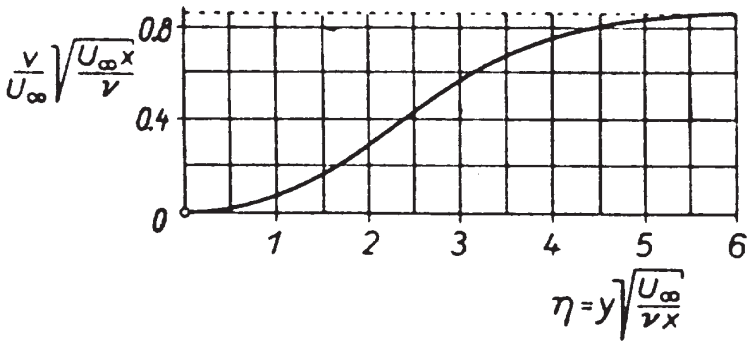

Figure 3-9: Transverse velocity distribution in the viscous boundary layer [39]. In the notation of this figure, symbols in small caps have units.

estimation will be used in the scaling relationship.

$$V(X,Y) = \widehat{V}_C v(x,y) \tag{3.26}$$

Scaling Relationship for $P(X,Y)$

The minimum value of P is 0 far from the plate, but its characteristic value P_C is unknown. It is estimated by $\widehat{P}_C$, and the scaling relationship is:

$$P(X,Y) = \widehat{P}_C p(x,y) \tag{3.27}$$

Based on the scaling relationships just established, the set of estimations $\{S\}$ is:

$$\{S\}^T = \{\widehat{\delta}, \widehat{V}_C, \widehat{P}_C\} \qquad q = 3$$

3.2.4 Dimensionless Governing Equations and Boundary Conditions

The original set of equations is normalized by using the scaling relationships. Equation 3.29 (conservation of momentum in the x-direction) was normalized with the

viscous forces. These viscous forces create pressures, which are the forces used to normalize equation 3.30 (conservation of momentum in the y-direction). The expression of the coefficients N_i appears in matrix [A] (Figure 3-10).

$$\frac{\partial u}{\partial x} + N_1 \frac{\partial v}{\partial y} = 0 \tag{3.28}$$

$$N_2 u \frac{\partial u}{\partial x} + N_3 v \frac{\partial u}{\partial y} = -N_4 \frac{\partial p}{\partial x} + \left(N_5 \frac{\partial^2 u}{\partial x^2} + \frac{\partial^2 u}{\partial y^2} \right) \tag{3.29}$$

$$N_6 u \frac{\partial u}{\partial x} + N_7 v \frac{\partial u}{\partial y} = -\frac{\partial p}{\partial y} + N_8 \left(N_5 \frac{\partial^2 v}{\partial x^2} + \frac{\partial^2 v}{\partial y^2} \right) \tag{3.30}$$

Table 3.2: Boundary conditions for the viscous boundary layer (dimensionless)

	u	v	p
$(x > 0, 0)$	0	0	
$(-\infty, y)$	1	0	
$(0, \infty)$			0

3.2.5 Dimensionless Groups of Known Order of Magnitude

The boundary layer is the region where the flow transitions from stagnant (at the wall) to free flow (far from the wall). Close to the wall the viscous forces are dominant, and far from the wall the inertial forces dominate. A practical and physically meaningful way to define the boundary layer (used by Rivas and Ostrach [9]) is the "region where the viscous forces are of the same order of magnitude as the inertial forces."

From inspection of the curves that describe the velocities (Figures 3-8 and 3-9) it can be seen that the second derivatives with respect to y are of the order of magnitude of one. The velocity U reaches its maximum and minimum values over a line X=constant, therefore $\partial u/\partial y$ is also of the order of magnitude of one. It can be established this way, that the dimensionless group N_3 in equation 3.29 is of the order of magnitude of one, and will be estimated as $N_3 = 1$.

The pressure variations inside the boundary layer are also of the order of the dynamic and viscous forces; therefore, estimating $N_4 = 1$ assigns $\partial p/\partial x$ in equation 3.29 the order of magnitude of one. Because the maximum and minimum values of U and V can be found over lines of Y=constant and X=constant, the terms $\partial u/\partial x$ and $\partial v/\partial y$ in equation 3.28 are of an order of magnitude of one; therefore, the dimensionless group N_1 can be estimated as equal to one.

3.2.6 Complete Set of Dimensionless Groups

From Buckingham's theorem it is known that this problem can be described completely by just one governing dimensionless group ($m = n - k = 1$). The Reynolds number is arbitrarily chosen to describe the problem:

$$\mathrm{Re} = \frac{U_\infty L}{\nu} \tag{3.31}$$

3.2.7 Expression of the Estimations

Matrix algebra will be used to illustrate its application in a simple case. This problem is simple enough however as to be solved by simple inspection. The matrix $[A]$ of dimensionless groups is shown in Figure 3-10.

The matrix of estimations $[A_S]$ is shown in Figure 3-11. It is obtained using equation 2.26.

The expression for the estimation of the boundary layer thickness is obtained from

	ρ	ν	U_∞	L	$\widehat{\delta}$	$\widehat{V}_C$	$\widehat{P}_C$
N_1			-1	1	-1	1	
N_3		-1			1	1	
N_4	-1	-1	-1	-1	2		1
Re		-1	1	1			
N_2		-1	1	-1	2		
N_5				-2	2		
N_6	1		1	-1	1	1	-1
N_7	1					2	-1
N_8	1	1			-1	1	-1

Figure 3-10: Matrix $[A]$ for the viscous boundary layer. The internal lines divide the submatrices $[A_{ij}]$

	ρ	ν	U_∞	L
$\widehat{\delta}$		1/2	-1/2	1/2
$\widehat{V}_C$		1/2	-1/2	-1/2
$\widehat{P}_C$	1		2	

Figure 3-11: Matrix $[A_S]$ for the viscous boundary layer

matrix $[A_S]$:

$$\widehat{\delta} = \sqrt{\frac{\nu L}{U_\infty}} \tag{3.32}$$

therefore, the characteristic value for the thickness is $\delta = \widehat{\delta} g(\mathrm{Re})$, where $g(\mathrm{Re})$ is approximately equal to one.

3.2.8 Dimensionless Governing Equations and Boundary Conditions (In Terms of the Reference Dimensionless Groups)

Even though an estimation of the characteristic value of the functions in the problem was already obtained, rewriting the equations in terms of the reference dimensionless groups is useful as a check of consistency and for added physical insight. The expression of the dimensionless coefficients of the equations as a function of the Π parameters is contained in matrix $[B_N]$ (Figure 3-12).

	Re
N_2	
N_5	-1
N_6	-1
N_7	-1
N_8	-1

Figure 3-12: Matrix $[B_N]$ for the viscous boundary layer.

$$\frac{\partial u}{\partial x} + \frac{\partial v}{\partial y} = 0 \tag{3.33}$$

$$u\frac{\partial u}{\partial x} + v\frac{\partial u}{\partial y} = -\frac{\partial p}{\partial x} + \left(\frac{1}{\mathrm{Re}}\frac{\partial^2 u}{\partial x^2} + \frac{\partial^2 u}{\partial y^2}\right) \tag{3.34}$$

$$\frac{1}{\mathrm{Re}}\left(u\frac{\partial u}{\partial x} + v\frac{\partial u}{\partial y}\right) = -\frac{\partial p}{\partial y} + \frac{1}{\mathrm{Re}}\left(\frac{1}{\mathrm{Re}}\frac{\partial^2 v}{\partial x^2} + \frac{\partial^2 v}{\partial y^2}\right) \tag{3.35}$$

(3.36)

The boundary conditions are the same as those of Table 3.2. The equations above are equivalent to their dimensional counterparts, no physical aspects have been neglected or modified. The boundary layer is commonly studied at large Reynolds numbers (but not so large as to be in the turbulent regime), because it is in that region when it can be considered thin and independent of Re. Inspecting the equations, it can be seen that at values of the Reynolds number larger than one, all terms are of the order of one. The term $\partial p/\partial y$ in equation 3.35 is very small ($O(Re^{-1})$), indicating that the pressure gradient is approximately parallel to the x axis.

3.2.9 Discussion

The expression of $g(\mathrm{Re})$ can be obtained by comparing the estimations with data from the literature, for example from Schlichting [39]. The function $g(\mathrm{Re})$ depends on the definition of boundary layer thickness being considered. The displacement thickness of the boundary layer is an integral definition that can be compared to the definition used here. For this definition, the dimensionless function is $g(\mathrm{Re})= 1.72$ (valid for high Reynolds numbers, but within the laminar regime). Another definition of the thickness of the boundary layer is where the parallel velocity is 99% of that of the free flow. In this case the dimensionless function would be $g(\mathrm{Re}) = 5$. It is not difficult to try to improve the order of magnitude estimations according to this definition. The thickness of the boundary layer could be estimated as the region where the inertial forces are 100 times larger than the viscous; this statement is translated into $N_2 = 100$, and the estimated boundary layer thickness is $\widehat{\delta} = 10\sqrt{\nu L/U_\infty}$, and the dimensionless function is $g(\mathrm{Re}) = 0.5$. Table 3.3 summarizes the comparison between known results and the order of magnitude estimations.

When performing order of magnitude scaling, the matrices involved are generally small, and the matrix operations relatively simple. The calculation process can be performed with basic software tools. Figure 3-13 shows the set up of the matrices in

Table 3.3: Comparison of estimated and exact thickness of the viscous boundary layer for different definitions. It can be observed that the dimensionless function $g(\mathrm{Re})$ is approximately equal to one for all cases.

Definition	Estimation	N_2	δ	$\widehat{\delta}$	$g(\mathrm{Re})$
displacement thickness	inertial forces$\approx$ viscous forces	1	$1.72\sqrt{\nu L/U_\infty}$	$\sqrt{\nu L/U_\infty}$	1.72
$99\%U_\infty$	inertial forces$\approx$ viscous forces	1	$5\sqrt{\nu L/U_\infty}$	$\sqrt{\nu L/U_\infty}$	5
$99\%U_\infty$	inertial forces$\approx$ $100\times$viscous forces	100	$5\sqrt{\nu L/U_\infty}$	$10\sqrt{\nu L/U_\infty}$	0.5

Microsoft Excel.

3.3 Non Isothermal Boundary Layer

The previous example—the viscous boundary layer, can be expanded into the non-isothermal case. In this case two regimes are possible, depending on which boundary layer (thermal or viscous) is thicker. Figures 3-14 and 3-15 show these two possible configurations. Neither frictional heating nor thermal expansion are included into the governing equations. The fluid is considered incompressible.

3.3.1 Governing Equations, Boundary Conditions, and Domain for Scaling

The governing equations that represent this problem are the following:

$$\frac{\partial U}{\partial X} + \frac{\partial V}{\partial Y} = 0 \tag{3.37}$$

	A	B	C	D	E	F	G	H	I	J	K	L	M
1		**MATRIX [W]**											
2		rho	nu	Uinf	L	delta	Vc	Pc					
3	m	-3	2	1	1	1	1	-1					
4	kg	1	0	0	0	0	0	1					
5	s	0	-1	-1	0	0	-1	-2					
6		**MATRIX [A]**								**$[A][W]^T$**			
7		rho	nu	Uinf	L	delta	Vc	Pc		m	kg	s	
8	N1	0	0	-1	1	-1	1	0		0	0	0	
9	N3	0	-1	0	0	1	1	0		0	0	0	
10	N4	-1	-1	-1	-1	2	0	1		0	0	0	
11	Re	0	-1	1	1	0	0	0		0	0	0	
12	N2	0	-1	1	-1	2	0	0		0	0	0	
13	N5	0	0	0	-2	2	0	0		0	0	0	
14	N6	1	0	1	-1	1	1	-1		0	0	0	
15	N7	1	0	0	0	0	2	-1		0	0	0	
16	N8	1	1	0	0	-1	1	-1		0	0	0	
17		**MATRIX [A_S]**											
18		rho	nu	Uinf	L								
19	delta	0	1/2	- 1/2	1/2								
20	Vc	0	1/2	1/2	- 1/2								
21	Pc	1	0	2	0								
22		**MATRIX [B]**											
23		rho	nu	Uinf	L								
24	Re	0	-1	1	1								
25	N2	0	0	0	0								
26	N5	0	1	-1	-1								
27	N6	0	1	-1	-1								
28	N7	0	1	-1	-1								
29	N8	0	1	-1	-1								
30					**MATRIX [B_N]**								
31					Re								
32	N2				0								
33	N5				-1								
34	N6				-1								
35	N7				-1								
36	N8				-1								
37													

Figure 3-13: Matrix set-up in Microsoft Excel

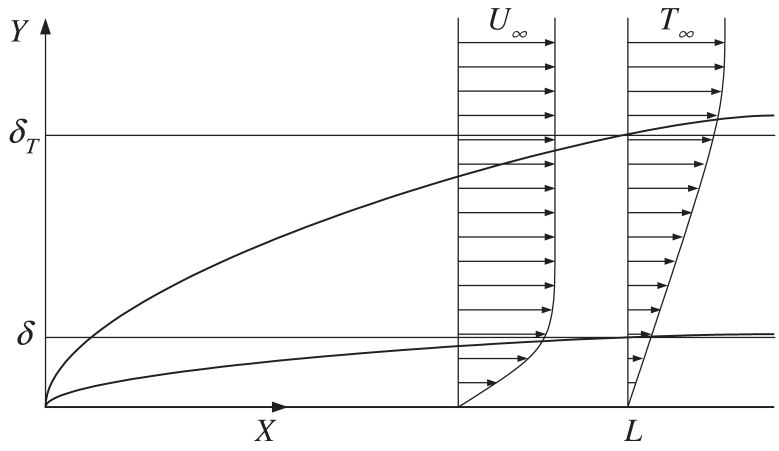

Figure 3-14: Regime I: Non isothermal boundary layer at low Pr. In this regime the thermal boundary layer is thicker than the viscous one, therefore the characteristic velocity in the thermal boundary layer is U_∞.

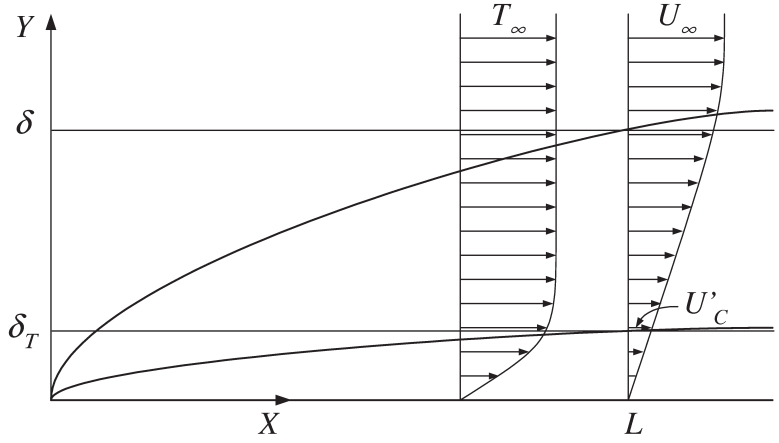

Figure 3-15: Regime II: Non isothermal boundary layer at high Pr. In this regime the thermal boundary layer is much thinner than the viscous one, therefore the characteristic velocity in the thermal boundary layer is $U'_C < U_\infty$.

$$U\frac{\partial U}{\partial X} + V\frac{\partial U}{\partial Y} = -\frac{1}{\rho}\frac{\partial P}{\partial X} + \nu\left(\frac{\partial^2 U}{\partial X^2} + \frac{\partial^2 U}{\partial Y^2}\right) \tag{3.38}$$

$$U\frac{\partial V}{\partial X} + V\frac{\partial V}{\partial Y} = -\frac{1}{\rho}\frac{\partial P}{\partial Y} + \nu\left(\frac{\partial^2 V}{\partial X^2} + \frac{\partial^2 V}{\partial Y^2}\right) \tag{3.39}$$

$$U\frac{\partial T}{\partial X} + V\frac{\partial T}{\partial Y} = \alpha\left(\frac{\partial^2 T}{\partial X^2} + \frac{\partial^2 T}{\partial Y^2}\right) \tag{3.40}$$

where equation 3.37 is the equation of continuity, equations 3.38 and 3.39 are the Navier-Stokes equations, and equation 3.40 is the equation of conservation of energy. The boundary conditions are summarized in Table 3.4.

The domain for scaling needs to be split into subdomains, which are presented in detail in Section 3.3.3.

3.3.2 Sets of Parameters and Units

The set of parameters that completely define the problem in this case is:

$$\{P\}^T = \{\rho, \nu, U_\infty, T_\infty, L, \alpha, T_0\} \qquad n = 7$$

Table 3.4: Boundary conditions for the non-isothermal boundary layer (dimensional)

	U	V	P	T
$(X > 0, 0)$	0	0		T_0
$(-\infty, Y)$	U_∞	0		T_∞
$(0, \infty)$			0	

Choosing the SI as the reference system of units, the set of reference units is the following:

$$\{R\}^T = \{\text{m, kg, s, K}\} \qquad t = 4$$

Table 3-16 shows the matrix $[U]^T$ for the non-isothermal boundary layer. Its rank is 4, and the chosen set of reference parameters is:

$$\{P_k\}^T = \{\rho, \nu, U_\infty, T_\infty\} \qquad k = 4$$

	ρ	ν	U_∞	T_∞	L	α	T_0
m	-3	2	1		1	2	
kg	1						
s		-1	-1			-1	
K				1			1

Figure 3-16: Matrix $[U]^T$ for the non-isothermal boundary layer. The submatrix on the left has rank 4

3.3.3 Scaling Relationships, Characteristic Values, and Order of Magnitude Estimations

Two boundary layers, one viscous and the other thermal, have different thickness and divide the domain for scaling into three parts:

- viscous boundary layer
- thermal boundary layer
- free flow

Each boundary layer defines a subdomain for scaling, indicated in Table 3.5. Two regimes are originated from the combination of the thickness of these two boundary layers:

Regime I: Shown in Figure 3-14. The thermal boundary layer is thicker than the viscous boundary layer, this way the characteristics of the flow are the same for both.

Regime II: Shown in Figure 3-15. The thermal boundary layer is much thinner than the viscous boundary layer, this way the characteristic parallel velocity in the thermal boundary layer is smaller than that of the viscous boundary layer, and convection is less important.

Table 3.5: Subdomains of the non-isothermal boundary layer for the different regimes. In the X-direction the domain is $0 \leq X \leq L$ for all cases.

	viscous boundary layer	thermal boundary layer
Regime I	$0 \leq Y \leq \delta$	$\delta \leq Y \leq \delta_T$
Regime II	$0 \leq Y \leq \delta$	$0 \leq Y \leq \delta_T$

In this section not all of the unknown characteristic values are estimated, because the focus of this example is on the thickness of the boundary layers. Some of the characteristic values that are not estimated are the temperature jump in the viscous boundary layer in regime I, and the characteristic pressure in the thermal boundary layer in regime II. These characteristic values are not necessary for the calculation of the characteristic thickness.

Scaling Relationships, Characteristic Values, and Order of Magnitude Estimations for Regime I

Viscous boundary layer: The behavior of the fluid flow is unaffected by the thermal effects; therefore, the scaling of the flow equations (equations 3.37 to 3.39) is the same as that of the viscous boundary layer.

$$X = Lx \tag{3.41}$$

$$Y = \widehat{\delta} y \tag{3.42}$$

$$U(X,Y) = U_\infty u(x,y) \tag{3.43}$$

$$V(X,Y) = \widehat{V}_C v(x,y) \tag{3.44}$$

$$P(X,Y) = \widehat{P}_C p(x,y) \tag{3.45}$$

Thermal boundary layer: The scaling relationships for the thermal boundary layer are different because its thickness is different than that of the viscous boundary layer.

$$X = Lx \tag{3.46}$$

$$Y = \widehat{\delta}_T y' \tag{3.47}$$

$$U(X,Y) = U_\infty u'(x,y') \tag{3.48}$$

$$V(X,Y) = \widehat{V}_C v'(x,y') \tag{3.49}$$

$$T(X,Y) = T_0 + T_C \theta(x,y') \tag{3.50}$$

where:

$$T_C = T_\infty - T_0 \tag{3.51}$$

The corresponding set of estimations in this case is:

$$\{S\}^T = \{\widehat{\delta}, \widehat{V}_C, \widehat{P}_C, \widehat{\delta}_T\} \qquad q = 4$$

Scaling Relationships, Characteristic Values, and Order of Magnitude Estimations for Regime II

The characteristic velocities inside the thermal boundary layer are smaller because the thermal boundary layer covers only part of the velocity profile.

Viscous boundary layer: The scaling of the flow equations (equations 3.37 to 3.39 is the same as that of regime I and the viscous boundary layer because the behavior of the fluid flow is unaffected by the thermal effects.

Thermal boundary layer:

$$X = Lx \tag{3.52}$$

$$Y = \widehat{\delta}_T y' \tag{3.53}$$

$$U(X,Y) = \widehat{U}'_C u'(x,y') \tag{3.54}$$

$$V(X,Y) = \widehat{V}'_C v'(x,y') \tag{3.55}$$

$$T(X,Y) = T_0 + T_C \theta(x,y') \tag{3.56}$$

where $\widehat{U}'_C$, and $\widehat{V}'_C$ are the estimations of the characteristic values of the velocities inside the thermal boundary layer.

Since the parallel velocity profile inside the viscous boundary layer is approximately linear (see Figure 3-8), the characteristic velocity in the X-direction can be

approximated as:

$$\widehat{U}'_C = \frac{U_\infty}{\widehat{\delta}}\widehat{\delta}_T \tag{3.57}$$

The corresponding set of estimations in this case is:

$$\{S\}^T = \{\widehat{\delta}, \widehat{V}_C, \widehat{P}_C, \widehat{\delta}_T, \widehat{U}'_C, \widehat{V}'_C\} \qquad q = 6$$

3.3.4 Dimensionless Governing Equations and Boundary Conditions

Dimensionless Governing Equations and Boundary Conditions for Regime I

$$\frac{\partial u}{\partial x} + N_1\frac{\partial v}{\partial y} = 0 \tag{3.58}$$

$$N_2 u\frac{\partial u}{\partial x} + N_3 v\frac{\partial u}{\partial y} = -N_4\frac{\partial p}{\partial x} + \left(N_5\frac{\partial^2 u}{\partial x^2} + \frac{\partial^2 u}{\partial y^2}\right) \tag{3.59}$$

$$N_6 u\frac{\partial u}{\partial x} + N_7 v\frac{\partial u}{\partial y} = -\frac{\partial p}{\partial y} + N_8\left(N_5\frac{\partial^2 v}{\partial x^2} + \frac{\partial^2 v}{\partial y^2}\right) \tag{3.60}$$

$$N_9 u'\frac{\partial \theta}{\partial x} + N_{10} v'\frac{\partial \theta}{\partial y'} = N_{11}\frac{\partial^2 \theta}{\partial x^2} + \frac{\partial^2 \theta}{\partial y'^2} \tag{3.61}$$

The boundary conditions are indicated in Table 3.6. The coefficients N_i are determined by matrix $[A]$ for regime I (Figure 3-17).

Equation 3.59 was normalized with the viscous forces, equation 3.60 with the characteristic pressure determined from the former equation. Equation 3.61 was normalized with the conductive terms.

Dimensionless Governing Equations and Boundary Conditions for Regime II

Equations 3.58 to 3.61 also apply to regime II. Two more equations are necessary to describe this regime. One is the non-dimensional expression of the characteristic parallel velocity in the thermal boundary layer (equation 3.57):

$$N_{12} = 1 \tag{3.62}$$

The second additional equation is the expression of the equation of conservation of mass in the thermal boundary layer:

$$\frac{\partial u'}{\partial x} + N_{13}\frac{\partial v'}{\partial y'} = 0 \tag{3.63}$$

The boundary conditions are indicated in Table 3.6. The coefficients N_i are determined by matrix $[A]$ for regime II (Figure 3-19).

Table 3.6: Boundary conditions for the non-isothermal boundary layer (dimensionless)

					Regime I		Regime II	
	u	v	p	θ	u'	v'	u'	v'
$(x > 0, 0)$	0	0		0	0	0	0	0
$(-\infty, y)$	1	0		0	1	0	N_{14}	0
$(0, \infty)$			0					

3.3.5 Dimensionless Groups of Known Order of Magnitude

Regime I

The dimensionless group N_1 can be estimated as equal to one because it belongs to an equation with only two terms of the order of magnitude of one. In Section 3.2.5 the viscous boundary layer was defined as the region in which the viscous and inertial

effects were of the same order of magnitude, therefore the group N_3 will also be estimated as equal to one. The pressures generated are of the order of magnitude of the viscous and dynamic forces; therefore, $N_4 = 1$.

The thermal boundary layer can be defined as the region in which convective and conductive heat transfer are of the same order of magnitude. The left member of equation 3.61 represents convection, and the right member conduction. In the boundary layer, these two members should be of the same order of magnitude; therefore, the group N_9 is chosen as equal to one.

Regime II

For regime II there are two additional dimensionless groups of known order of magnitude. One of them, N_{12}, is unity by definition (equation 3.57). The other, N_{13}, is estimated as equal to one because it relates two dimensionless functions of the order of magnitude of one.

3.3.6 Complete Set of Dimensionless Groups

The application of Buckingham's theorem indicates that the problem is completely determined by three governing dimensionless groups ($m = n - k = 3$). The Reynolds and Prandtl numbers, and the ratio of temperatures are arbitrarily chosen.

$$\mathrm{Re} = \frac{U_\infty L}{\nu} \tag{3.64}$$

$$\mathrm{Pr} = \frac{\nu}{\alpha} \tag{3.65}$$

$$\Theta = \frac{T_0}{T_\infty} \tag{3.66}$$

3.3.7 Expression of the Estimations

The matrix relationships derived previously will be applied to obtain an expression of the estimations in this problem.

Regime I

The matrix of dimensionless groups $[A]$ and the matrix of estimations $[A_S]$ for regime I are shown in Figures 3-17 and 3-18 respectively.

	ρ	ν	U_∞	T_∞	L	α	T_0	$\widehat{\delta}$	$\widehat{V}_C$	$\widehat{P}_C$	$\widehat{\delta}_T$
N_1			-1		1			-1	1		
N_3		-1						1	1		
N_4	-1	-1	-1		-1			2		1	
N_9			1		-1	-1					2
Re		-1	1		1						
Pr		1				-1					
Θ				-1			1				
N_2		-1	1		-1			2			
N_5					-2			2			
N_6	1		1		-1			1	1	-1	
N_7	1								2	-1	
N_8	1	1						-1	1	-1	
N_{10}						-1			1		1
N_{11}					-2						2

Figure 3-17: Matrix $[A]$ for the non-isothermal boundary layer, Regime I

	ρ	ν	U_∞	T_∞	L	α	T_0
$\widehat{\delta}$		1/2	-1/2		1/2		
$\widehat{V}_C$		1/2	1/2		-1/2		
$\widehat{P}_C$	1		2				
$\widehat{\delta}_T$			-1/2		1/2	1/2	

Figure 3-18: Matrix $[A_S]$ for the non-isothermal boundary layer, Regime I

The characteristic thickness for both boundary layers is obtained from matrix $[A_S]$:

$$\widehat{\delta} = \sqrt{\frac{\nu L}{U_\infty}} \tag{3.67}$$

$$\widehat{\delta}_T = \sqrt{\frac{\alpha L}{U_\infty}} \tag{3.68}$$

It is observed that the expression of the thickness for the viscous boundary layer is the same as that for the isothermal boundary layer. The ratio of thicknesses in regime I is:

$$\frac{\widehat{\delta}_T}{\widehat{\delta}} = \mathrm{Pr}^{-1/2} \tag{3.69}$$

This agrees with the literature (for example Chen [8]). It indicates that the two regimes are determined by the Prandtl number, which is a property of the fluid only. Regime I corresponds to a low Prandtl number, and regime II to a high one.

Regime II

The matrix of dimensionless groups $[A]$ and the matrix of estimations $[A_S]$ for regime II are shown in Figures 3-19 and 3-20 respectively.

The characteristic thickness for both boundary layers is obtained from matrix $[A_S]$:

$$\widehat{\delta} = \sqrt{\frac{\nu L}{U_\infty}} \tag{3.70}$$

$$\widehat{\delta}_T = \left(\frac{\nu L^3 \alpha^2}{U_\infty^3}\right)^{1/6} \tag{3.71}$$

It is observed that the expression of the thickness for the viscous boundary layer is the same as that for the isothermal boundary layer. The ratio of thicknesses in regime II is:

$$\frac{\widehat{\delta}_T}{\widehat{\delta}} = \mathrm{Pr}^{-1/3} \tag{3.72}$$

	ρ	ν	U_∞	T_∞	L	α	T_0	$\widehat{\delta}$	$\widehat{V}_C$	$\widehat{P}_C$	$\widehat{\delta}_T$	$\widehat{U}'_C$	$\widehat{V}'_C$
N_1			-1		1			-1	1				
N_3		-1						1	1				
N_4	-1	-1	-1		-1			2		1			
N_{10}					-1	-1					2	1	
N_{14}			-1					1			-1	1	
N_{15}					1						-1	-1	1
Re		-1	1		1								
Pr		1				-1							
Θ				-1			1						
N_2		-1	1		-1			2					
N_5					-2			2					
N_6	1		1		-1			1	1	-1			
N_7	1								2	-1			
N_8	1	1						-1	1	-1			
N_9						-1					1		1
N_{11}					-2						2		
N_{14}			1									-1	

Figure 3-19: Matrix $[A]$ for the non-isothermal boundary layer, Regime II

	ρ	ν	U_∞	T_∞	L	α	T_0
$\widehat{\delta}$		1/2	-1/2		1/2		
$\widehat{V}_C$		1/2	1/2		-1/2		
$\widehat{P}_C$	1		2				
$\widehat{\delta}_T$		1/6	-1/2		1/2	1/3	
$\widehat{U}'_C$		-1/3	1			1/3	
$\widehat{V}'_C$		-1/6	1/2		-1/2	2/3	

Figure 3-20: Matrix $[A_S]$ for the non-isothermal boundary layer, Regime II

This agrees with the literature (for example Chen [8]). It is worth remarking that this result was obtained without having performed any kind of integration or interpolation, as it was done for example by Bird *et al.* [40].

3.3.8 Dimensionless Governing Equations and Boundary Conditions (In Terms of the Reference Dimensionless Groups)

Regime I

Matrix $[B_N]$ is necessary for expressing the dimensionless governing equations and boundary conditions as functions of the reference dimensionless groups. This matrix is shown in Figure 3-21.

	Re	Pr	Θ
N_2			
N_5	-1		
N_6	-1		
N_7	-1		
N_8	-1		
N_{10}		1/2	
N_{11}	-1	-1	

Figure 3-21: Matrix $[B_N]$ for the non-isothermal boundary layer, Regime I

$$\frac{\partial u}{\partial x} + \frac{\partial v}{\partial y} = 0 \tag{3.73}$$

$$u\frac{\partial u}{\partial x} + v\frac{\partial u}{\partial y} = -\frac{\partial p}{\partial x} + \left(\frac{1}{\mathrm{Re}}\frac{\partial^2 u}{\partial x^2} + \frac{\partial^2 u}{\partial y^2}\right) \tag{3.74}$$

$$\frac{1}{\mathrm{Re}}\left(u\frac{\partial u}{\partial x} + v\frac{\partial u}{\partial y}\right) = -\frac{\partial p}{\partial y} + \frac{1}{\mathrm{Re}}\left(\frac{1}{\mathrm{Re}}\frac{\partial^2 v}{\partial x^2} + \frac{\partial^2 v}{\partial y^2}\right) \tag{3.75}$$

$$u'\frac{\partial \theta}{\partial x} + \mathrm{Pr}^{1/2}v'\frac{\partial \theta}{\partial y'} = \frac{1}{\mathrm{Re}\,\mathrm{Pr}}\frac{\partial^2 \theta}{\partial x^2} + \frac{\partial^2 \theta}{\partial y'^2} \tag{3.76}$$

The boundary conditions are indicated in Table 3.6. All but one of the terms in these equations are automatically of the order of one at high Reynolds and low Prandtl numbers. The one exception is one of the terms for conduction in the equation of energy (equation 3.76). This term represents the thickness of the thermal boundary layer relative to its length; therefore, far from the leading edge the boundary layer is thin, and the term in question is also of the order of one.

Regime II

	Re	Pr	Θ
N_2			
N_5	-1		
N_6	-1		
N_7	-1		
N_8	-1		
N_{10}			
N_{11}	-1	-2/3	
N_{14}		1/3	

Figure 3-22: Matrix $[B_N]$ for the non-isothermal boundary layer, Regime II

$$\frac{\partial u}{\partial x} + \frac{\partial v}{\partial y} = 0 \tag{3.77}$$

$$u\frac{\partial u}{\partial x} + v\frac{\partial u}{\partial y} = -\frac{\partial p}{\partial x} + \left(\frac{1}{\mathrm{Re}}\frac{\partial^2 u}{\partial x^2} + \frac{\partial^2 u}{\partial y^2}\right) \tag{3.78}$$

$$\frac{1}{\mathrm{Re}}\left(u\frac{\partial u}{\partial x} + v\frac{\partial u}{\partial y}\right) = -\frac{\partial p}{\partial y} + \frac{1}{\mathrm{Re}}\left(\frac{1}{\mathrm{Re}}\frac{\partial^2 v}{\partial x^2} + \frac{\partial^2 v}{\partial y^2}\right) \tag{3.79}$$

$$u'\frac{\partial \theta}{\partial x} + v'\frac{\partial \theta}{\partial y'} = \frac{1}{\mathrm{Re}\,\mathrm{Pr}^{2/3}}\frac{\partial^2 \theta}{\partial x^2} + \frac{\partial^2 \theta}{\partial y'^2} \tag{3.80}$$

The boundary conditions are indicated in Table 3.6, where $N_{14} = \mathrm{Pr}^{1/3}$. All the terms in these equations are automatically of the order of one for large Reynolds and Prandtl numbers (the Reynolds number should not be so large as to be in the turbulent regime) . In the normalized equations there is one boundary condition larger than one: $u(x, \infty) = \mathrm{Pr}^{1/3}$. This is in apparent conflict with the dominant balance technique, that requires all of the coefficients of the dimensionless equations to be lesser or equal to one. The value of the coefficients should be evaluated within the domain for scaling, and at the edge of this domain $N_{14} = 1$, as required. The larger value is useful for the complete solution of the equations, but irrelevant for order of magnitude scaling.

3.3.9 Discussion

This example emphasizes the possibility of arriving at important conclusions in a simple and systematic way. The relative thickness of the thermal and viscous boundary layers for this example was previously known; however, the previous ways to arrive at that answer are more complicated and involve operations such as interpolations or integrations. These operations are acceptable for a problem that is very well known and documented such as the boundary layer, but might not be feasible or practical for more complex and less well understood problems.

3.4 Low-Prandtl-Number Thermocapillary Flows

3.4.1 Governing Equations, Boundary Conditions, and Domain for Scaling

The problem is formulated as two-dimensional, with a non-deformable free-surface, as depicted in Figure 3-23. Buoyancy, gas shear on the surface, frictional heating and electromagnetic effects are not considered. The domain for scaling is $0 \leq X \leq \mathcal{L}$ and $0 \leq Y \leq D$. This domain will be split into subdomains in some cases. The unknowns

in this problem are the velocities U and V, the pressure P, and the temperature T.

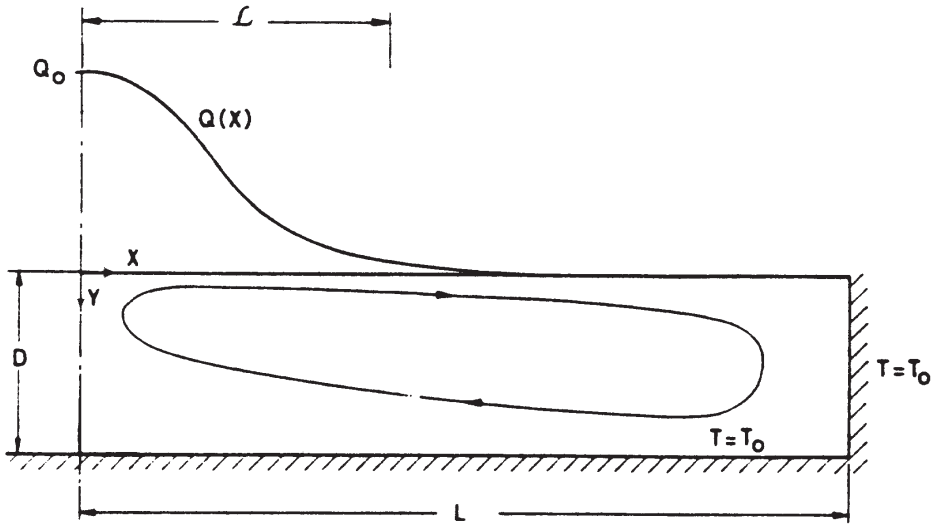

Figure 3-23: System coordinates and problem configuration for thermocapillary flows [9]. Only half the enclosure is shown

The governing equations that represent this problem are the following:

$$\frac{\partial U}{\partial X} + \frac{\partial V}{\partial Y} = 0 \tag{3.81}$$

$$U\frac{\partial U}{\partial X} + V\frac{\partial U}{\partial Y} = -\frac{1}{\rho}\frac{\partial P}{\partial X} + \nu\left(\frac{\partial^2 U}{\partial X^2} + \frac{\partial^2 U}{\partial Y^2}\right) \tag{3.82}$$

$$U\frac{\partial V}{\partial X} + V\frac{\partial V}{\partial Y} = -\frac{1}{\rho}\frac{\partial P}{\partial Y} + \nu\left(\frac{\partial^2 V}{\partial X^2} + \frac{\partial^2 V}{\partial Y^2}\right) \tag{3.83}$$

$$U\frac{\partial T}{\partial X} + V\frac{\partial T}{\partial Y} = \alpha\left(\frac{\partial^2 T}{\partial X^2} + \frac{\partial^2 T}{\partial Y^2}\right) \tag{3.84}$$

where equation 3.81 is the equation of continuity, equations 3.82 and 3.83 are the Navier-Stokes equations, and equation 3.84 is the equation of conservation of energy.

The boundary conditions are summarized in Table 3.7

Table 3.7: Boundary conditions for thermocapillary flows (dimensional)

	U	V	T	P
$(X,0)$	0	0	T_0	
$(0,Y)$	0	$\partial V/\partial X = 0$	$\partial T/\partial X = 0$	
(X,D)	Eq. 3.85	0	Eq. 3.86	
(L,Y)	0	0	T_0	
(L,D)				0

$$\rho\nu\frac{\partial U}{\partial Y} = \sigma_T\frac{\partial T}{\partial X} \tag{3.85}$$

$$k\frac{\partial T}{\partial Y} = -Q(X) \tag{3.86}$$

where equation 3.85 represents the Marangoni boundary condition, and equation 3.86 represents the heat input boundary condition at the free surface.

3.4.2 Sets of Parameters and Units

It was previously shown in Section 2.2.3 that when the scaling of the problem does not depend on any absolute temperature value, one of the temperature parameters can be disregarded for the purposes of dimensional analysis. In this case the disregarded temperature will be T_0; therefore, during the calculations it will not be included in the set $\{P\}$.

$$\{P\} = \{\mathcal{L}, \rho, \alpha, k, Q_0, \sigma_T, \nu, D, T_0 \text{ (not included)}\} \qquad n = 9 - 1 = 8$$

Section 2.2.3 also showed that when mechanical friction and heat generation are considered decoupled the thermal energy can be considered as a magnitude fundamentally different from mechanical energy, and it is assigned here the unit J="thermal Joule". This is equivalent of splitting the law of conservation of energy into two independent conservation laws—one for mechanical, and another for thermal energy. This addition of reference units to the SI is correct, otherwise it would not be possible to obtain a non-dimensional expression of the original equations. The set of reference units based on the SI is:

$$\{R\}^T = \{\text{m, kg, s, K, J}\} \qquad t = 5$$

The matrix $[U]^T$ for this problem shown in Figure 3-24. Its rank is 5, with the following set of reference parameters:

$$\{P_k\}^T = \{\mathcal{L}, \rho, \alpha, k, Q_0\} \qquad k = 5$$

Figure 3-24: Matrix of dimensions $[U]^T$ for thermocapillary flows. Thermal and mechanical energy are considered independent quantities, generating the unit J for thermal energy.

	$\mathcal{L}$	ρ	α	k	Q_0	σ_T	ν	D
m	1	-3	2	-1	-2		2	1
kg		1				1		
s			-1	-1	-1	-2	-1	
K				-1		-1		
J				1	1			

3.4.3 Scaling Relationships, Characteristic Values, and Order of Magnitude Estimations

Rivas and Ostrach identify three distinct regimes for this problem:

Regime I: Viscous forces dominate throughout the volume of the liquid. Since the Prandtl number is small, conduction also dominates in the volume.

Regime II: Inertial forces dominate the volume, but conduction is still the dominant heat transfer mechanism. Since the motion is induced by the Marangoni effect, viscous forces are still dominant near the surface. This creates a viscous boundary layer under the surface.

Regime III: Inertial forces dominate the volume, but velocities are so high that convection is now the dominant heat transfer mechanism. Since the temperature gradients are originated by a heat source at the free surface, conduction is still dominant there. In this case a thermal boundary layer appears simultaneously with the viscous one.

The dimensionless functions in the core region will be written in small caps (e.g. u), those in the viscous boundary layer will be primed (e.g. u'), and those in the thermal boundary layer will be double primed. (e.g. u''). The dimensionless functions and dimensionless groups for each regime are different, even though the same symbols are used. For the sake of keeping the notation consistent with Rivas and Ostrach, the estimations will not be marked with a hat in this case.

Scaling Relationships, Characteristic Values, and Order of Magnitude Estimations for Regime I

$$X = \mathcal{L}x \tag{3.87}$$

$$Y = Dy \tag{3.88}$$

$$U(X,Y) = U_R u(x,y) \tag{3.89}$$

$$V(X,Y) = V_R v(x,y) \tag{3.90}$$

$$P(X,Y) = P_R p(x,y) \tag{3.91}$$

$$T(X,Y) = T_0 + \Delta T \theta(x,y) \tag{3.92}$$

$$Q(X) = Q_0 q(x) \tag{3.93}$$

The set of estimations is:

$$\{S\} = \{U_R, V_R, P_R, \Delta T\} \qquad q = 4$$

Scaling relationships, Characteristic Values, and Order of Magnitude Estimations for Regime II

The presence of a viscous boundary layer divides the domain in two parts. A viscous boundary layer region and a core region. The thickness of the boundary layer is unknown.

All regions

$$X = \mathcal{L} x \tag{3.94}$$

$$Q(X) = Q_0 q(x) \tag{3.95}$$

Core region $(\delta_S \leq Y \leq D)$

$$Y = Dy \tag{3.96}$$

$$U(X,Y) = U_C u(x,y) \tag{3.97}$$

$$V(X,Y) = V_C v(x,y) \tag{3.98}$$

$$P(x,Y) = P_C p(x,y) \tag{3.99}$$

$$T(X,Y) = T_0 + \Delta T \theta(x,y) \tag{3.100}$$

(3.101)

Viscous boundary layer $(0 \leq Y \leq \delta_S)$

$$Y = \delta_S y' \tag{3.102}$$

$$U(X,Y) = U_S u'(x,y') \tag{3.103}$$

$$V(X,Y) = V_S v'(x,y') \tag{3.104}$$

$$P(X,Y) = P_S p'(x,y') \tag{3.105}$$

$$T(X,Y) = T_0 + \Delta T \theta'(x,y') \tag{3.106}$$

(3.107)

The set of estimations is:

$$\{S\} = \{U_C, V_C, P_C, \Delta T, \delta_S, U_S, V_S, P_S\} \qquad q = 8$$

Scaling Relationships, Characteristic Values, and Order of Magnitude Estimations for Regime III

The presence of viscous and thermal boundary layers divides the domain in three parts: a viscous boundary layer, a thermal boundary layer, and a core region. Because this example focuses on low-Prandtl-number fluids, the thermal boundary layer is thicker than the viscous one.

All regions

$$X = \mathcal{L}x \tag{3.108}$$

$$Q(X) = Q_0 q(x) \tag{3.109}$$

Core region ($\delta_S^* \leq Y \leq D$ for momentum, and $\delta_t \leq Y \leq D$ for thermal energy)

$$
\begin{aligned}
Y &= Dy && (3.110)\\
U(X,Y) &= U_C^* u(x,y) && (3.111)\\
V(X,Y) &= V_C^* v(x,y) && (3.112)\\
P(x,Y) &= P_C^* p(x,y) && (3.113)\\
T(X,Y) &= T_0 + \Delta T^* \theta(x,y) && (3.114)\\
& && (3.115)
\end{aligned}
$$

Viscous boundary layer ($0 \leq Y \leq \delta_S^*$)

$$
\begin{aligned}
Y &= \delta_S^* y' && (3.116)\\
U(X,Y) &= U_S^* u'(x,y') && (3.117)\\
V(X,Y) &= V_S^* v'(x,y') && (3.118)\\
P(X,Y) &= P_S^* p'(x,y') && (3.119)\\
T(X,Y) &= T_0 + \Delta T^* \theta'(x,y') && (3.120)\\
& && (3.121)
\end{aligned}
$$

Thermal boundary layer ($\delta_S^* \leq Y \leq \delta_t$)

$$
\begin{aligned}
Y &= \delta_t y'' && (3.122)\\
U(X,Y) &= U_t^* u''(x,y'') && (3.123)\\
V(X,Y) &= V_t^* v''(x,y'') && (3.124)\\
P(x,Y) &= P_t^* p''(x,y'') && (3.125)\\
T(X,Y) &= T_0 + \Delta T^* \theta''(x,y'') && (3.126)\\
& && (3.127)
\end{aligned}
$$

The set of estimations is:

$$\{S\} = \{U_C^*, V_C^*, P_C^*, \Delta T^*, \delta_S^*, U_S^*, V_S^*, P_S^*, \delta_t, U_t^*, V_t^*, P_t^*\} \qquad q = 12$$

3.4.4 Dimensionless Governing Equations and Boundary Conditions

The coefficients that appear in the dimensionless expressions represent dimensionless groups. The constitution of these groups is determined from the matrix $[A]$ corresponding to each regime.

Dimensionless Governing Equations and Boundary Conditions for Regime I

$$\frac{\partial u}{\partial x} + N_1 \frac{\partial v}{\partial y} = 0 \tag{3.128}$$

$$N_2 u \frac{\partial u}{\partial x} + N_3 v \frac{\partial u}{\partial y} = -N_4 \frac{\partial p}{\partial x} + N_5 \frac{\partial^2 u}{\partial x^2} + \frac{\partial^2 u}{\partial y^2} \tag{3.129}$$

$$N_6 u \frac{\partial v}{\partial x} + N_7 v \frac{\partial v}{\partial y} = -\frac{\partial p}{\partial y} + N_8 \left(N_5 \frac{\partial^2 u}{\partial x^2} + \frac{\partial^2 u}{\partial y^2} \right) \tag{3.130}$$

$$N_9 u \frac{\partial \theta}{\partial x} + N_{10} v \frac{\partial \theta}{\partial y} = N_5 \frac{\partial^2 \theta}{\partial x^2} + \frac{\partial^2 \theta}{\partial y^2} \tag{3.131}$$

Boundary conditions

$$\frac{\partial u}{\partial y} = N_{11} \frac{\partial \theta}{\partial x} \tag{3.132}$$

$$\frac{\partial \theta}{\partial y} = N_{12} q(x) \tag{3.133}$$

Dimensionless Governing Equations and Boundary Conditions for Regime II

Core region

$$\frac{\partial u}{\partial x} + N_1 \frac{\partial v}{\partial y} = 0 \tag{3.134}$$

$$u\frac{\partial u}{\partial x} + N_1 v\frac{\partial u}{\partial y} = -N_2\frac{\partial p}{\partial x} + N_3\left(N_4\frac{\partial^2 u}{\partial x^2} + \frac{\partial^2 u}{\partial y^2}\right) \tag{3.135}$$

$$N_5 u\frac{\partial v}{\partial x} + N_6 v\frac{\partial v}{\partial y} = -\frac{\partial p}{\partial y} + N_7\left(N_4\frac{\partial^2 u}{\partial x^2} + \frac{\partial^2 u}{\partial y^2}\right) \tag{3.136}$$

$$N_8 u\frac{\partial \theta}{\partial x} + N_9 v\frac{\partial \theta}{\partial y} = N_4\frac{\partial^2 \theta}{\partial x^2} + \frac{\partial^2 \theta}{\partial y^2} \tag{3.137}$$

Viscous boundary layer

$$\frac{\partial u'}{\partial x} + N_{10}\frac{\partial v'}{\partial y'} = 0 \tag{3.138}$$

$$u'\frac{\partial u'}{\partial x} + N_{10} v'\frac{\partial u'}{\partial y'} = -N_{11}\frac{\partial p'}{\partial x} + N_{12}\left(N_{13}\frac{\partial^2 u'}{\partial x^2} + \frac{\partial^2 u'}{\partial y'^2}\right) \tag{3.139}$$

$$N_{14} u'\frac{\partial v'}{\partial x} + N_{15} v'\frac{\partial v'}{\partial y'} = -\frac{\partial p'}{\partial y'} + N_{16}\left(N_{13}\frac{\partial^2 u'}{\partial x^2} + \frac{\partial^2 u'}{\partial y'^2}\right) \tag{3.140}$$

$$N_{17} u'\frac{\partial \theta'}{\partial x} + N_{18} v'\frac{\partial \theta'}{\partial y'} = N_{13}\frac{\partial^2 \theta'}{\partial x^2} + \frac{\partial^2 \theta'}{\partial y'^2} \tag{3.141}$$

Boundary conditions

$$\frac{\partial u'}{\partial y'} = N_{19}\frac{\partial \theta'}{\partial x} \tag{3.142}$$

$$\frac{\partial \theta}{\partial y} = N_{20} q(x) \tag{3.143}$$

Additional condition: The equation of continuity in its integral form can be applied to the region that divides the viscous boundary layer from the core region. A new equation is obtained this way, which states that the characteristic transverse velocity for the viscous boundary layer must be equal to that in the core region. Its dimensional expression is:

$$N_{21} = 1 \tag{3.144}$$

where $N_{21} = V_S/V_C$.

Dimensionless Governing Equations and Boundary Conditions for Regime III

Core region

$$\frac{\partial u}{\partial x} + N_1 \frac{\partial v}{\partial y} = 0 \tag{3.145}$$

$$u\frac{\partial u}{\partial x} + N_1 v\frac{\partial u}{\partial y} = -N_2\frac{\partial p}{\partial x} + N_3\left(N_4\frac{\partial^2 u}{\partial x^2} + \frac{\partial^2 u}{\partial y^2}\right) \tag{3.146}$$

$$N_5 u\frac{\partial v}{\partial x} + N_6 v\frac{\partial v}{\partial y} = -\frac{\partial p}{\partial y} + N_7\left(N_4\frac{\partial^2 u}{\partial x^2} + \frac{\partial^2 u}{\partial y^2}\right) \tag{3.147}$$

$$u\frac{\partial \theta}{\partial x} + N_1 v\frac{\partial \theta}{\partial y} = N_8\left(N_4\frac{\partial^2 \theta}{\partial x^2} + \frac{\partial^2 \theta}{\partial y^2}\right) \tag{3.148}$$

Viscous boundary layer

$$\frac{\partial u'}{\partial x} + N_9\frac{\partial v'}{\partial y'} = 0 \tag{3.149}$$

$$u'\frac{\partial u'}{\partial x} + N_9 v'\frac{\partial u'}{\partial y'} = -N_{10}\frac{\partial p'}{\partial x} + N_{11}\left(N_{12}\frac{\partial^2 u'}{\partial x^2} + \frac{\partial^2 u'}{\partial y'^2}\right) \tag{3.150}$$

$$N_{13}u'\frac{\partial v'}{\partial x} + N_{14}v'\frac{\partial v'}{\partial y'} = -\frac{\partial p'}{\partial y'} + N_{15}\left(N_{12}\frac{\partial^2 u'}{\partial x^2} + \frac{\partial^2 u'}{\partial y'^2}\right) \tag{3.151}$$

$$N_{16}u'\frac{\partial\theta'}{\partial x} + N_{17}v'\frac{\partial\theta'}{\partial y'} = N_{12}\frac{\partial^2\theta'}{\partial x^2} + \frac{\partial^2\theta'}{\partial y'^2} \quad (3.152)$$

Thermal boundary layer

$$\frac{\partial u''}{\partial x} + N_18\frac{\partial v''}{\partial y''} = 0 \quad (3.153)$$

$$u''\frac{\partial u''}{\partial x} + N_18v''\frac{\partial u''}{\partial y''} = -N_{19}\frac{\partial p''}{\partial x} + N_{20}\left(N_{21}\frac{\partial^2 u''}{\partial x^2} + \frac{\partial^2 u''}{\partial y''^2}\right) \quad (3.154)$$

$$N_{22}u''\frac{\partial v''}{\partial x} + N_{23}v''\frac{\partial v''}{\partial y''} = -\frac{\partial p''}{\partial y''} + N_{24}\left(N_{21}\frac{\partial^2 u''}{\partial x^2} + \frac{\partial^2 u''}{\partial y''^2}\right) \quad (3.155)$$

$$N_{25}u''\frac{\partial\theta''}{\partial x} + N_{26}v''\frac{\partial\theta''}{\partial y''} = N_{21}\frac{\partial^2\theta''}{\partial x^2} + \frac{\partial^2\theta''}{\partial y''^2} \quad (3.156)$$

Boundary conditions

$$\frac{\partial u'}{\partial y'} = N_{27}\frac{\partial\theta'}{\partial x} \quad (3.157)$$

$$\frac{\partial\theta''}{\partial y''} = N_{28}q(x) \quad (3.158)$$

Additional conditions: Equation 3.159 states that the characteristic transverse velocities for the core and the viscous boundary layer must be the same. This equation is equivalent to equation 3.144 for regime II.

Rivas and Ostrach also state that the transverse velocity of the thermal boundary layer equals that of the core flow (equation 3.160). This is not necessarily true, because in regime III the thermal boundary layer includes only a small part of the viscous boundary layer; therefore, the velocities of the former are smaller than those of the latter. For the sake of comparison, the relationship proposed by Rivas and Ostrach will be used here, and a more meaningful relationship will be proposed later.

$$N_{29} = 1 \quad (3.159)$$

$$N_{30} = 1 \tag{3.160}$$

3.4.5 Dimensionless Groups of Known Order of Magnitude

Regime I

Four dimensionless groups of known order of magnitude are necessary, because four estimates are necessary in Regime I. All of these groups will be estimated to be equal to unity. Three of them (N_1, N_{11}, and N_{12}) can be obtained immediately from the equations that contain only two terms (equations 3.128, 3.132, and 3.133). The remaining group (N_4) is obtained from the balance between the viscous forces and the pressure variations they generate (equation 3.129).

Regime II

Eight dimensionless groups will be estimated to be equal to unity in Regime II. The groups N_1, N_{10}, N_{19}, N_{20}, and N_{21} appear in equations with only two terms. The group N_2 relates the inertial forces in the core to the pressure variations they generate. The group N_{12} estimates that in the viscous boundary layer, the viscous forces are of the same order of magnitude as the dynamic forces (this is the definition of viscous boundary layer used in Section 3.2). The group N_{11} relates the viscous forces to the pressure variations generated by the inertial forces in the viscous boundary layer.

Regime III

Twelve dimensionless groups will be estimated to be equal to unity in Regime III. The groups N_1, N_9, N_{18}, N_{27}, N_{28}, N_{29}, and N_{30} appear in equations with only two terms. The group N_{11} estimates the viscous forces to be of the same order of magnitude as the dynamic forces in the viscous boundary layer. The group N_{25} estimates the convection to be of the same order of magnitude as conduction in the thermal boundary layer (this is the definition of thermal boundary layer used in Section 3.3). Groups N_2, N_{10}, and N_{19} relate the pressures to the dominant forces in their corresponding momentum

equations.

3.4.6 Complete Set of Dimensionless Groups

It was determined previously (Section 3.4.2) that this problem is completely described by eight parameters, of which five are dimensionally independent. Therefore, three dimensionless groups can completely describe the dimensionless formulation of this problem. The following are the groups used by Rivas and Ostrach:

$$\mathrm{Re}_\sigma = \frac{U_R \mathcal{L}}{\nu} \tag{3.161}$$

$$\mathrm{Pr} = \frac{\nu}{\alpha} \tag{3.162}$$

$$A = \frac{D}{\mathcal{L}} \tag{3.163}$$

The Reynolds number is based on the unknown characteristic velocity of the flow in regime I. The expression of this characteristic velocity as a function of the governing parameters will be determined later.

3.4.7 Expression of the Estimations

The matrix relationships derived previously will be applied to obtain an expression of the estimations in this problem.

Regime I

The matrix of dimensionless groups $[A]$ and the matrix of estimations $[A_S]$ for regime I are shown in Figures 3-25 and 3-26.

	$\mathcal{L}$	ρ	α	k	Q_0	σ_T	ν	D	U_R	V_R	P_R	ΔT
N_1	1							-1	-1	1		
N_4	-1	-1					-1	2	-1		1	
N_{11}	-1	-1				1	-1	1	-1			1
N_{12}				-1	1			1				-1
Re_σ	1						-1		1			
Pr			-1				1					
A	-1							1				
N_2	-1						-1	2	1			
N_3							-1	1		1		
N_5	-2							2				
N_6	-1	1						1	1	1		
N_7		1								2	-1	
N_8		1					1	-1		1	-1	
N_9	-1		-1					2	1		-1	
N_{10}			-1					1		1		

Figure 3-25: Matrix of dimensionless groups $[A]$ for thermocapillary flows in Regime I

	$\mathcal{L}$	ρ	α	k	Q_0	σ_T	ν	D
U_R	-1	-1		-1	1	1	-1	2
V_R	-2	-1		-1	1	1	-1	3
P_R				-1	1	1		
ΔT				-1	1			1

Figure 3-26: Matrix of estimations $[A_S]$ for thermocapillary flows in Regime I.

Regime II

The matrix of dimensionless groups $[A]$ and the matrix of estimations $[A_S]$ for regime II are shown in Figures 3-27 and 3-28.

	$\mathcal{L}$	ρ	α	k	Q_0	σ_T	ν	D	U_C	V_C	P_C	ΔT	δ_S	U_S	V_S	P_S
N_1	1							-1	-1	1						
N_2		-1							-2		1					
N_{10}	1												-1	-1	1	
N_{11}		-1												-2		1
N_{12}	1						1						-2	-1		
N_{19}	-1	-1				1	-1					1	1	-1		
N_{20}				-1	1			1				-1				
N_{21}										-1					1	
Re_σ		-1		-1	1	1	-2	2								
Pr			-1				1									
A	-1							1								
N_3	1						1	-2	-1							
N_4	-2							2								
N_5	-1	1						1	1	1	-1					
N_6		1								2	-1					
N_7		1					1	-1		1	-1					
N_8	-1		-1					2	1							
N_9			-1					1		1						
N_{13}	-2												2			
N_{14}	-1	1											1	1	1	-1
N_{15}		1													2	-1
N_{16}		1					1						-1		1	-1
N_{17}	-1		-1										2	1		
N_{18}			-1										1		1	

Figure 3-27: Matrix of dimensionless groups $[A]$ for thermocapillary flows in Regime II

Regime III

The matrix of dimensionless groups $[A]$ and the matrix of estimations $[A_S]$ for regime III are shown in Figures 3-29 and 3-30.

The ratio between the thermal and viscous boundary layers is Pr^{-1}, far from the expected ratio of $\mathrm{Pr}^{-1/2}$ for a non-isothermal boundary layer at low-Prandtl numbers.

	$\mathcal{L}$	ρ	α	k	Q_0	σ_T	ν	D
U_C	1/3	- 1/3		- 1/3	1/3	1/3	1/3	- 2/3
V_C	- 2/3	- 1/3		- 1/3	1/3	1/3	1/3	1/3
P_C	2/3	1/3		- 2/3	2/3	2/3	2/3	- 4/3
ΔT				-1	1			1
δ_S	2/3	1/3		1/3	- 1/3	- 1/3	2/3	- 1/3
U_S	- 1/3	- 2/3		- 2/3	2/3	2/3	- 1/3	2/3
V_S	- 2/3	- 1/3		- 1/3	1/3	1/3	1/3	1/3
P_S	- 2/3	- 1/3		-4/3	4/3	4/3	- 2/3	4/3

Figure 3-28: Matrix of estimations $[A_S]$ for thermocapillary flows in Regime II.

This is a consequence of having determined the transverse velocities of the thermal boundary layer and of the core as equal. It will be shown below that the more meaningful statement of equating the parallel velocities of the core and the thermal boundary layer leads to an improved estimation of the ratio between boundary layers.

3.4.8 Dimensionless Governing Equations and Boundary Conditions (In Terms of the Reference Dimensionless Groups)

The equations will not be re-written, but the expression of their coefficients is determined by the matrix $[B_N]$ corresponding to each regime. Using the same physical insight of Rivas and Ostrach their results are reproduced.

3.4.9 Discussion

Based on the fundamentals of the method of order of magnitude estimations proposed in this thesis, the accuracy of the estimations can be improved with little effort.

Because there are recirculatory flows, the predictions would improve if the characteristic distance in Y for the core region were considered as the one from the surface to the point at which the parallel velocity is zero.

Another possible improvement would be to replace the condition of equal transverse velocities for core and thermal boundary layer regions in regime III by the more

	$\mathcal{L}$	ρ	α	k	Q_0	σ_T	ν	D	U_C^*	V_C^*	P_C^*	ΔT	δ_S^*	U_S^*	V_S^*	P_S^*	δ_t	U_t^*	V_t^*	P_t^*
N_1	1							-1	-1	1										
N_2		-1							-2		1									
N_9	1												-1	-1	1					
N_{10}		-1												-2		1				
N_{11}	1						1						-2	-1						
N_{18}	1																-1	-1	1	
N_{19}		-1																-2		1
N_{25}	-1		-1														2	1		
N_{27}	-1	-1				1	-1					1	1	-1						
N_{28}				-1	1							-1					1			
N_{29}										-1					1					
N_{30}										-1									1	
Re_σ		-1		-1	1	1	-2	2												
Pr			-1				1													
A	-1							1												
N_3	1						1	-2	-1											
N_4	-2							2												
N_5	-1	1						1	1	1	-1									
N_6		1								2	-1									
N_7		1					1	-1		1	-1									
N_8	1		1					-2	-1											
N_{12}	-2												2							
N_{13}	-1	1											1	1	1	-1				
N_{14}		1												2	-1					
N_{15}		1					1						-1		1	-1				
N_{16}	-1		-1										2	1						
N_{17}			-1										1		1					
N_{20}	1		-1				1										-2	-1		
N_{21}	-2																2			
N_{22}	-1	1															1	1	1	-1
N_{23}		1																	2	-1
N_{24}		1					1										-1		1	-1
N_{26}			-1														1	1		

Figure 3-29: Matrix of dimensionless groups $[A]$ for thermocapillary flows in Regime III

	$\mathcal{L}$	ρ	α	k	Q_0	σ_T	ν	D
U_C^*	1/2	- 1/4	1/4	- 1/4	1/4	1/4	1/4	-1
V_C^*	- 1/2	- 1/4	1/4	- 1/4	1/4	1/4	1/4	
P_C^*	1	1/2	1/2	- 1/2	1/2	1/2	1/2	-2
ΔT^*	1/2	1/4	3/4	- 3/4	3/4	- 1/4	- 1/4	
δ_S^*		1/2	1/4	- 1/4	1/4	- 1/4	- 1/4	3/4
U_S^*		- 1/2	1/2	- 1/2	1/2	1/2	- 1/2	
V_S^*	- 1/2	- 1/4	1/4	- 1/4	1/4	1/4	1/4	
P_S^*			1	-1	1	1	-1	
δ_t		1/2	1/4	3/4	1/4	- 1/4	- 1/4	- 1/4
U_t^*			- 1/2	- 1/2	- 1/2	1/2	1/2	1/2
V_t^*	- 1/2	- 1/4	1/4	- 1/4	1/4	1/4	1/4	
P_t^*				-1	-1	1	1	1

Figure 3-30: Matrix of estimations $[A_S]$ for thermocapillary flows in Regime III.

	Re_σ	Pr	A
N_2	1		2
N_3	1		2
N_5			2
N_6	1		4
N_7	1		4
N_8			2
N_9	1	1	2
N_{10}	1	1	2

Figure 3-31: Matrix of dimensionless coefficients $[B_N]$ for thermocapillary flows in Regime I

	Re_σ	Pr	A
N_3	- 1/3		- 2/3
N_4			2
N_5			2
N_6			2
N_7	- 1/3		4/3
N_8	1/3	1	2/3
N_9	1/3	1	2/3
N_{13}	- 2/3		2/3
N_{14}	- 2/3		2/3
N_{15}	- 2/3		2/3
N_{16}	- 2/3		2/3
N_{17}		1	
N_{18}		1	

Figure 3-32: Matrix of dimensionless coefficients $[B_N]$ for thermocapillary flows in Regime II

	Re_σ	Pr	A
N_3	- 1/4	1/4	- 1/2
N_4			2
N_5			2
N_6			2
N_7	- 1/4	1/4	1 1/2
N_8	- 1/4	- 3/4	- 1/2
N_12	- 1/2	1/2	1
N_13	- 1/2	1/2	1
N_14	- 1/2	1/2	1
N_15	- 1/2	1/2	1
N_16		1	
N_17		1	
N_20		1	
N_21	- 1/2	-1 1/2	1
N_22	- 1/2	-1 1/2	1
N_23	- 1/2	-1 1/2	1
N_24	- 1/2	- 1/2	1
N_26			

Figure 3-33: Matrix of dimensionless coefficients $[B_N]$ for thermocapillary flows in Regime III

correct condition of equal parallel velocities for the core and boundary layer regions. If this is done, the ratio between the boundary layers is:

$$\frac{\delta_t}{\delta_S^*} = \mathrm{Re}^{1/7}\mathrm{Pr}^{-4/7}A^{2/7} \tag{3.164}$$

This ratio is much closer than the one expected for a non-isothermal boundary layer at low-Prandtl numbers ($\delta_t/\delta_S^* = \mathrm{Pr}^{-1/2}$). The reason they are different, is that in this problem there is no free flow outside the boundary layers; instead, the flow is affected by the shape of the cavity, and slightly, by the Reynolds number.

3.5 Summary

The known examples reviewed illustrate the practical implementation of the methodology of order of magnitude scaling and how the results obtained compare favorably to those obtained with other techniques.

The methodology presented here provides order of magnitude estimations of the characteristic values of a problem. It does so by transforming the original system of differential equations into a linear algebraic system. It is not necessary to perform any kind of integration or series expansion to obtain the order of magnitude estimations; however, if integration of the differential equations is necessary, the original system can be rewritten in a normalized form where the relative importance of each term is explicit, helping to systematically simplify the equations if necessary.

The example of the simple pendulum illustrates the main contribution of this methodology to traditional dimensional analysis: the scaling of the system involves dimensionless functions of known order of magnitude; thus, approximate estimations are obtained. The period of oscillation of a pendulum is estimated within a 60% error even at large oscillations. This estimation was done without integrating any equation or experimental observation. Including into the estimation only one additional piece of information—the known period of a pendulum for small oscillations; the estimations are refined to within 10% even at large oscillations (when $\Theta_0 \approx \pi$).

The viscous boundary layer example introduces the use of matrix algebra for the calculation of the estimations and dimensionless groups. The matrix operations are simple enough as to be performed with simple packages such as Microsoft Excel. The characteristic values are estimated without integrating the equations or using empirical data. The boundary layer thickness estimations are within a factor of two from the values used in the literature for the displacement thickness definition and the definition based on 99% of the remote velocity.

In the non-isothermal boundary layer problem the thickness of the viscous and thermal boundary layers are estimated by purely algebraic means, without the need of integrations or series expansions. The ratio of thickness obtained is the same reported in the literature, but this work uses much simpler means. In addition, this example illustrates that the set of parameters of a problem can be modified with unequivocal criteria to improve the dimensional analysis. Such unequivocal criteria are not always possible in standard dimensional analysis because the governing equations are not explicitly stated, so no additional information is available.

The example of thermocapillary flows at low-Prandtl-number shows that the methodology presented here can tackle very complex problems in a systematic way, and reproduce the results obtained by others through more tedious calculations. In addition, changes in physical insight are easy to implement, leading to more meaningful calculations.

Having verified that the order of magnitude scaling methodology provides correct estimations for known cases, in the second part of this thesis it will be applied to a new problem—the weld pool during high productivity arc welding. The order of magnitude scaling technique is especially suited for this complex problem for the following reasons: this is a case where it is very difficult to use analytical or numerical methods, order of magnitude estimations will provide new and useful information, and there is enough previous physical insight in the literature.

Part II

Application of Order of Magnitude Scaling to High Productivity Arc Welding

Chapter 4

Economic Impact of Welding

This chapter emphasizes the very large potential savings that can be achieved by welding process improvements. Since almost all manufactured products contain a weld, process improvements have a very large impact. For the particular case of automatic welding, welding speed has a direct impact on cost. Although precise data for the economics of welding is difficult to find, a simple analysis based on standard welding costing shows that an average increase of 10% in welding speed would result in worldwide savings of the order of several hundred million dollars.

4.1 Arc Welding Costs

According to references [41, 42, 43, 44, 45, 46], the cost of making a weld can be calculated as follows:

$$\text{welding cost} = \text{cost consumables} + \text{cost labor} + \text{cost overhead} \tag{4.1}$$

A more sophisticated model can be found in reference [47]. The consumables include the filler metal, the shielding (gas or flux), and the power. The cost of consumables is approximately constant on a *per length* basis. The filler metal is usually the dominant factor for the consumables, and the energy cost is usually negligible.

The cost of labor considers all the time an operator should be involved with a weld, not just arc time. These times include the time for joint preparation, assembly, positioning, welding, cleaning, and the like [43]. In automatic welding, the actual welding time ("arc time") is the dominant factor. The cost of labor on a *per length* basis is approximately inversely proportional to the welding speed.

The overhead cost is the cost of other business expenses. Its dominant aspect is the equipment cost (amortization). When the welding equipment is fully employed, faster welds mean lower equipment cost, because it is spread over more components. Figure 4-1 shows the variation in welding cost as a function of welding speed for the gas metal arc welding example of Table 4.1.

The cost calculations presented here assume a shop at full capacity, as in reference [47].

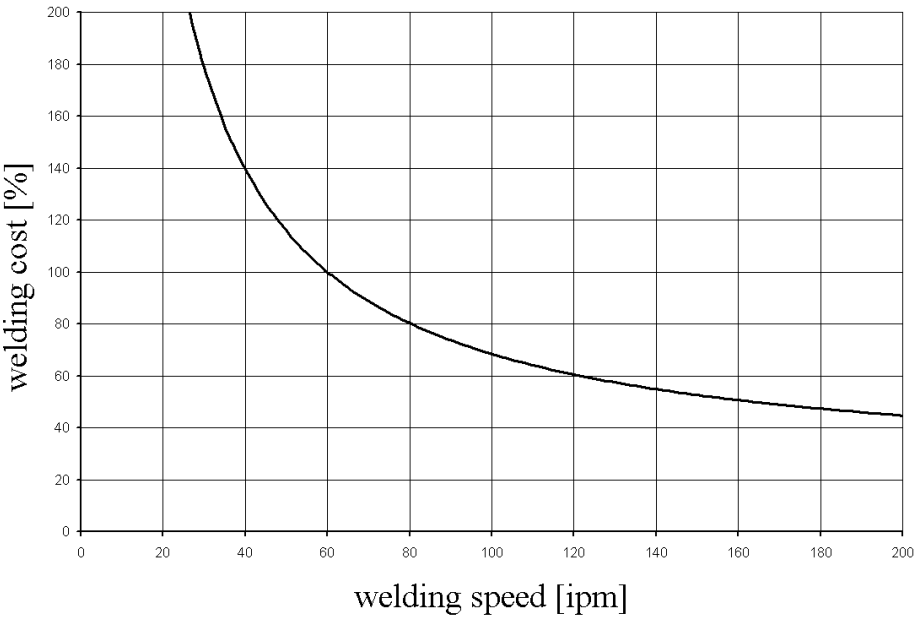

Figure 4-1: Welding cost as a function of welding speed for the GMAW example of Table 4.1. The nominal speed is 60 ipm (ipm=inches per minute).

Table 4.1 shows the cost distribution for a 10 ft long, full penetration square butt joint on 1/4" mild steel, from reference [46]. It considers two alternative processes:

submerged arc welding (SAW) and gas metal arc welding (GMAW).

Table 4.1: Typical cost distribution for arc welding [46]

		SAW	GMAW
consumables		21%	23%
	filler	48%	78%
	shielding	40%	17%
	power	12%	5%
labor+overhead		79%	77%
	labor	70%	68%
	overhead	30%	32%

Reference [45] analyzes costs for a wide variety of processes (gas tungsten arc welding, pulsed gas metal arc welding, plasma gas metal arc welding, and polyplasma[1]) and geometries (horizontal and vertical butt joints, external and internal corner). For the welding of 2 mm thick aluminum plate, the aggregated cost of labor and overhead lies between 92% and 95% of the total cost for all cases, while for a 10 mm thick aluminum plate, labor and overhead amount to 72% on average. This decrease in importance of the labor and overhead for thicker welds is to be expected because more filler material and other consumables are used for a given length.

Based on the data from the literature, it is reasonable to assume that a typical automatic weld would have a cost distribution of approximately 70% to 90% for labor and overhead, and 10% to 30% for consumables.

The ratio between consumable and equipment costs ranges between 0.36 and 1.81 for the welding of a 2mm aluminum plate, with an average value of 1.1 [45]. For the welding of a 10mm plate even this ratio is even higher. An analysis of welding costs in the Netherlands gives a ratio of 1.15. For the examples of Table 4.1 the ratio is

[1]Polyplasma is a process that uses a tungsten non-consumable electrode and two power sources in such a way that both the electrode and the workpiece have negative polarity. It is intended as an improvement of GTAW for the welding of thicker aluminum sheet.

0.9. It is reasonable to consider the expenditures in consumables and equipment are split in equal parts.

4.2 Potential Savings

Knowing that the cost of consumables is approximately constant for a given component, but the cost of labor and overhead decrease with welding speed, the potential savings can be calculated as:

$$\text{savings} = (\text{cost labor} + \text{cost overhead}) \left(\frac{V_{new} - V_{original}}{V_{original}} \right) \tag{4.2}$$

In equation 4.2 the savings and costs are in units of dollar per unit manufactured. The term $V_{original}$ refers to the original welding velocity used for costing, and V_{new} refers to a new velocity under consideration.

In the absence of precise information about the scale of expenditures in labor and overhead, they can be estimated from the expenditures in consumables. Approximately \$6 billion per year are spent on welding equipment and consumables in the world, of which approximately half are used in automatic welding [48]. Of this portion, half of it is consumables. For a 70%/30% distribution of labor plus overhead and consumables, the \$1.5 billion in consumables correspond to \$3.5 billion in labor and overhead. For a 90%/10%, labor and overhead amount to \$13.5 billion.

Equation 4.2 indicates that a 10% increase in the average welding speed for automatic welding implies expected worldwide savings between \$0.35 billion to \$1.35 billion. It is clear that the widespread utilization of welding greatly magnifies the effect of small improvements. Figure 4-2 shows the range of expected savings as a function of the increase in welding speed.

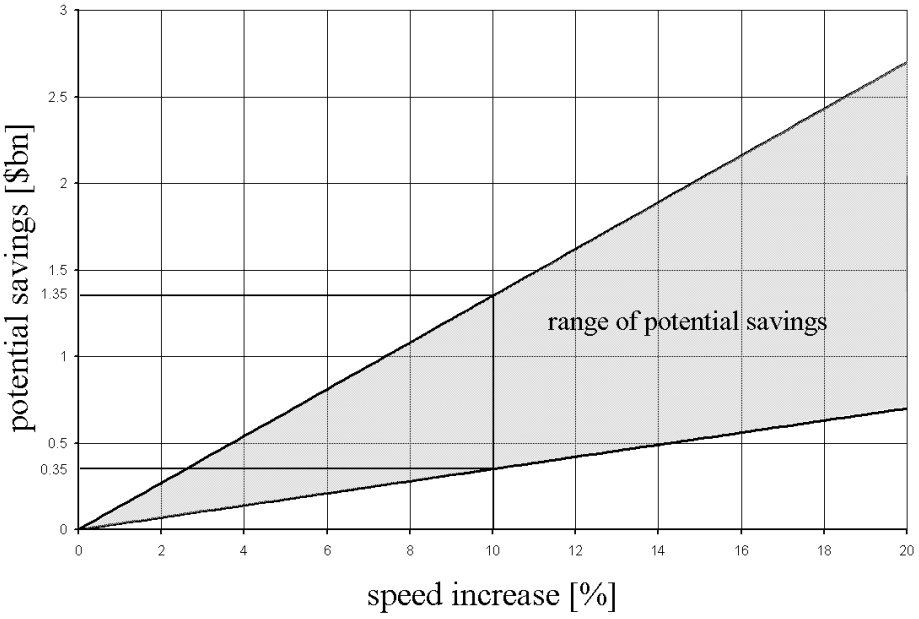

Figure 4-2: Potential welding savings as a function of welding speed. For a 10% speed increase the expected worldwide savings range between $0.35 billion and $1.35 billion.

Chapter 5

Defects in High Productivity Arc Welding

The previous chapter shows that even moderate improvements in the welding process translate into important savings. In particular, increases in the welding speed have direct impact in the productivity and cost. This chapter focuses on what limits the maximum welding speed.

5.1 Limits to the Welding Speed

Increases in speed have to be matched by increases in the heat input, otherwise the cross section of the weld would decrease, eventually not even reaching melting at any point. The heat input into the workpiece can be calculated as

$$\text{heat input} = \eta I V \tag{5.1}$$

where:

η = arc efficiency

I = welding current

V = arc voltage

The most practical way to increase the heat input is to increase the welding current, because the voltage and efficiency of the arc vary only moderately. The limit to a strategy of continuous increase in the welding speed and current is the appearance of defects such as humping, undercutting or tunnelling. Savage *et al.* [49] defined these defects as follows:

Humping: An irregular surface contour consisting of a series of bead-like protuberances separated by intervals of relatively uniform bead-surface contour (Figure 5-1).

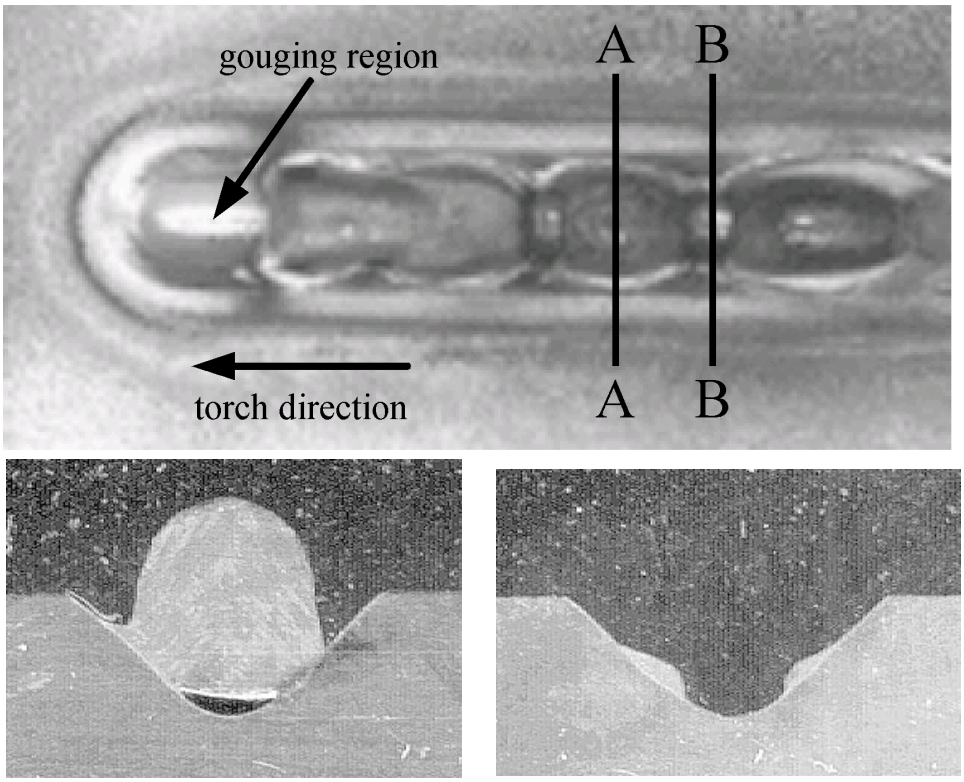

Figure 5-1: Humping in GTAW. The top figure is a top view of the humped weld seam, the bottom left picture is a cross section of the bead-like protuberance (cross section A-A), and the bottom right is a cross section of the void between beads (cross section B-B). This weld was made with a current of 305 A and a travel speed of 12 ipm; the shielding gas was 100% Ar

Undercutting: A groove, melted into the base metal adjacent to the fusion zone,

which is left unfilled with weld metal (Figure 5-2).

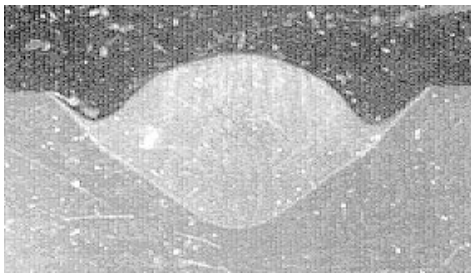

Figure 5-2: Undercutting in GTAW. Two unfilled grooves appear at the sides of the weld seam. This weld was made with a current of 300 A and a travel speed of 12 ipm; the shielding gas was 98% Ar, 2% O_2

Tunnelling: A special form of undercut in which an open channel, which remains unfilled with weld metal is formed at the root (Figure 5-3).

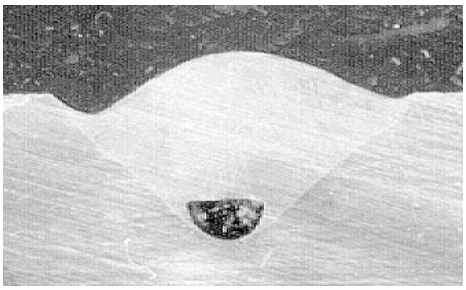

Figure 5-3: Tunnelling in GTAW. The cross section of the channel appears at the root of the weld. This weld was made with a current of 390 A and a travel speed of 12 ipm; the shielding gas was 98% Ar, 2% O_2

In addition to the types of defect observed by Savage *et al.*, other types of defects are observed during this research:

Split Bead: The weld seam is split into two independent parallel seams separated by an empty channel in between.

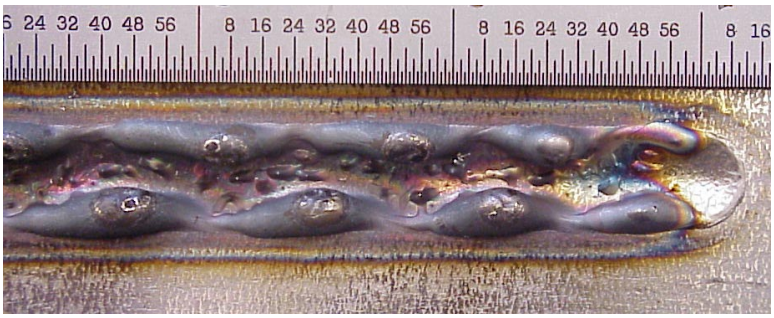

Figure 5-4: Parallel humping in GTAW. The two parallel humped beads can be seen on the sides of an empty groove. This weld was made with a current of 530 A and a travel speed of 35.4 ipm; the shielding gas was 100% Ar

Parallel Humping: Particular type of split bead in which the parallel seams are humped.

The appearance of these defects has been studied before and process maps have been developed for GTAW (see Figures 5-5 and 5-6). The two figures cannot be compared directly because many parameters are different, especially those that characterize the arc (for example arc length). However, the general trend of critical speed decreasing with current can be observed in both maps.

Both Savage and Shimada relate the appearance of defects to the presence of a "gouging region" in the weld pool. Observations by Bradstreet [3] for gas metal arc welding (GMAW) also show the same effect.

Yamamoto and Shimada [5] showed experimentally that at the gouging region, the molten metal turns into a thin liquid film of several tens of microns in thickness. Shimada *et al.*[6] concluded that this thin film is a consequence of the arc pressure, and that the onset of humping was determined by a hydraulic jump when the velocity in the film exceeded a critical value related to the hydrostatic pressure. It is shown in Chapter 6 that hydrostatic forces in the thin film are negligible compared to the gas shear force induced by the arc.

Some processes such as laser welding or deposition of microdroplets [50] show humping, but in these cases the liquid pool is long enough so as to generate capil-

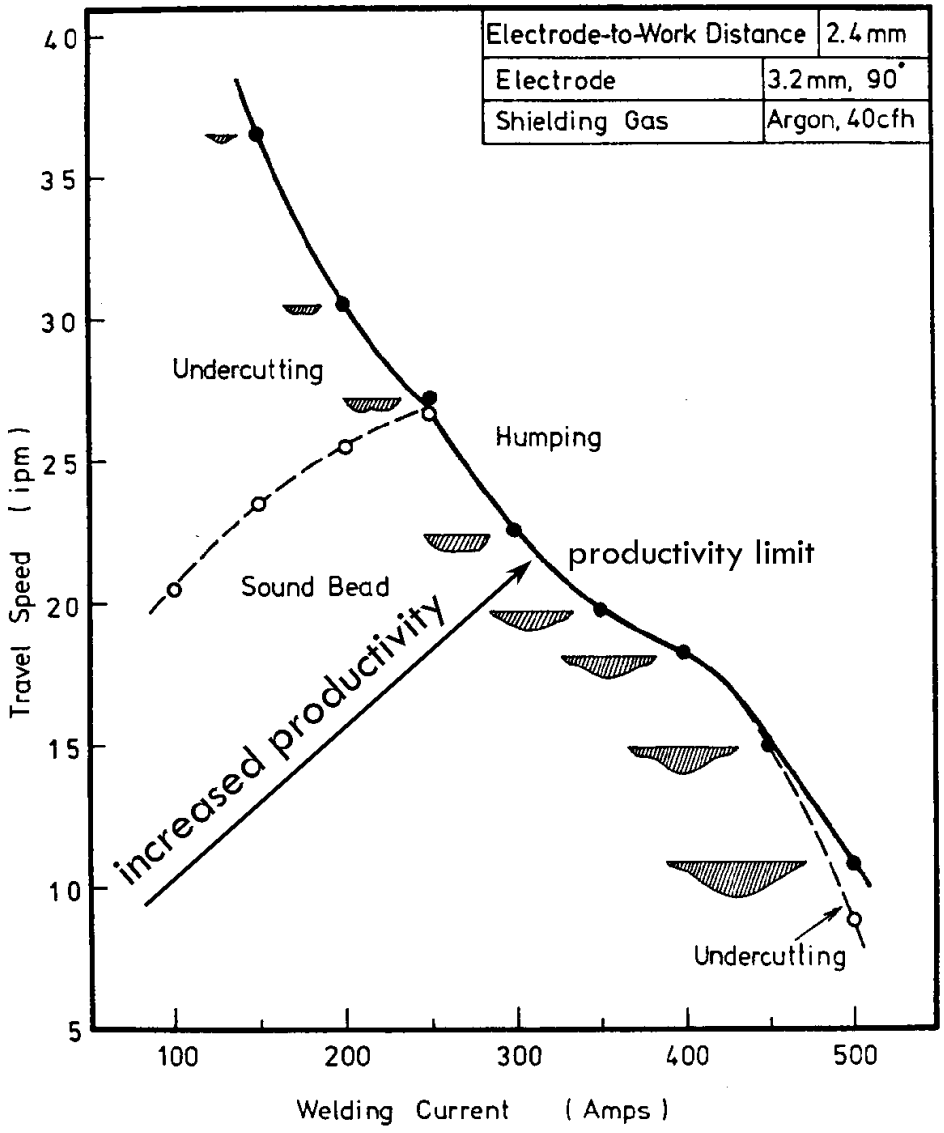

Figure 5-5: Process map for GTAW after Savage [49]. When the travel speed or welding current are too high, humping or undercutting occur. The weld cross section increases in size with the ratio current/speed. The initial arc length is 2.4 mm.

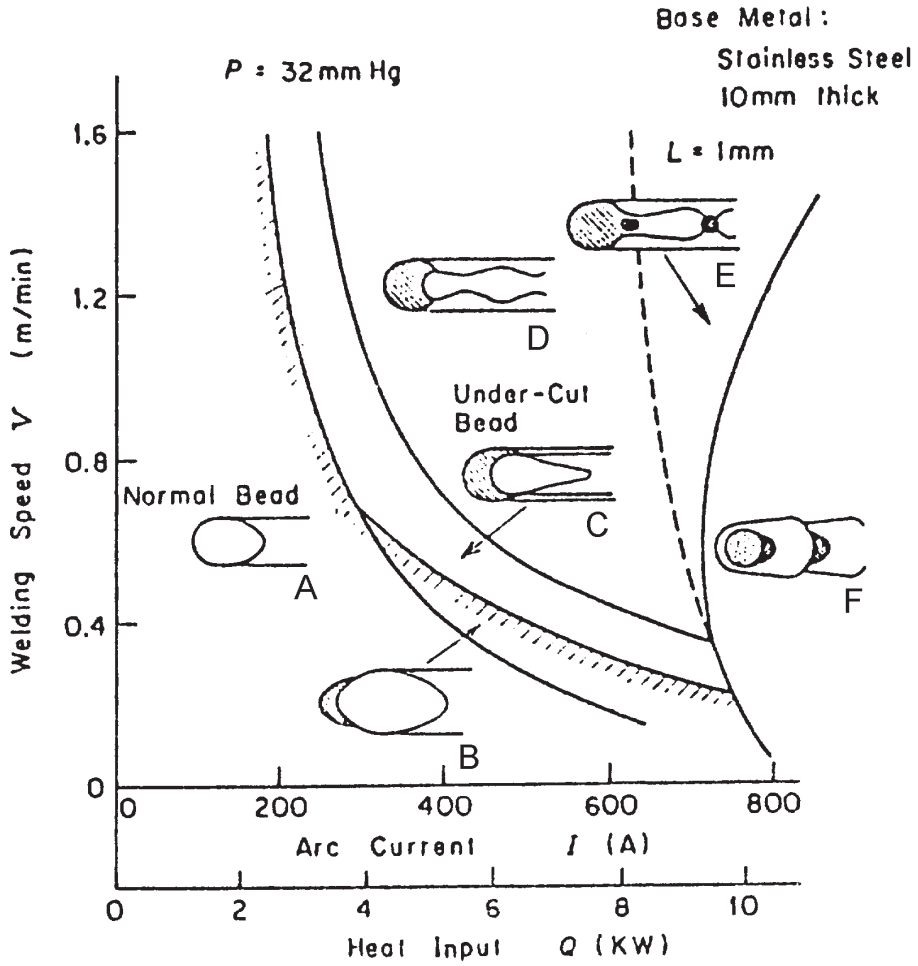

Figure 5-6: Process map for GTAW at low pressure after Shimada *et al.* [6]. The initial arc length is 1 mm. Each region contains a particular type of weld bead. Type A is a normal weld pool, with little surface depression. Type B is a sound weld, but the front of the weld pool is being "gouged". Type C has a more severe gouging and produces an undercut weld. Type D presents two parallel humped beads at the side of the welds, and a "dry" path in between them. Type E is similar to type D, but the parallel beads collapse into each other, sometimes leading to tunnelling. Type F presents "dry" spots in between protuberances.

lary instabilities. Gratzke *et al.* [51] concluded that humping cannot be due to the Marangoni effect, as suggested by Mills and Keene [52]. Although their observation is valid, their capillary instability calculations do not apply to most arc welding situations, where the weld pool geometry is very different from an elongated cylinder.

Undercutting and tunnelling are generally associated to the appearance of humping, and often appear simultaneously. They have been studied simultaneously with humping, although they are less well understood. Empirical evidence shows that undercutting in stainless steels is more pronounced in those steels with higher sulfur content, it increases with travel speed and slightly increases with arc length [52].

Table 5.1: Summary of relevant humping theories

Year	Author	Mechanism	Critical event	Ref.
1968	Bradstreet	capillary instability	(does not mention)	[3]
1975, 1982	Shimada *et al.*	hydraulic jump	velocity in thin weld pool exceeds critical value	[5, 6]
1990	Mills *et al.*	Marangoni forces	(does not mention)	[52]
1992	Gratzke *et al.*	capillary instability	weld pool length to width ratio exceeds critical value	[51]
1998	Mendez *et al.*	premature freezing	thin part of weld pool reaches cold region	[53]

5.2 Weld Pool Geometry at High Currents

Figure 5-7 shows a schematic of a weld pool at high current and traveling speed. Its most salient feature is the deep depression of the free surface. Its main elements are

a "gouging region" under the arc, a "rim" around it, and a bulk of molten metal at the rear of the weld pool. The gouging region is actually a very thin layer of liquid that copies the irregularities of the mushy zone, thus not reflecting light as a smooth surface. It will be shown in Chapter 6 that there are no recirculating flows in the thickness of the thin liquid layer. The "rim" around the gouging region is a thicker liquid portion that transports molten metal to the bulk of liquid at the rear. In different regimes these elements present changes, and these changes generate different defects such as humping, undercutting and tunnelling. It is observed experimentally that the transition line moves towards the rear as the current is increased [1, 6].

Because the appearance of defects is associated with the gouging region and a deep free surface depression, the understanding of this depression may yield information useful for the prevention of these defects. Many studies have been carried out trying to explain the large depression of the free surface. Most of these studies have been done on spot welds and a few on traveling welds. One of the difficulties in the study of deeply depressed weld pools at high currents is that the relative order of magnitude of the driving forces is unknown. With higher currents, the electromagnetic forces increase, but the weld pool geometry also changes. Thus, the relative effect of these forces is unknown.

The gouging region was studied by Ishizaki [1, 2]; in the former reference he experimentally studied the effect of the gas shear on the surface of the weld. He emptied the weld pool by hitting the weld in progress with a hammer, then filled up the void with water, and blasted air on the surface. He concluded that the air blast was responsible for the front gouging. Choo *et al.*[54] suggested that at high current levels the gas shear on the free surface could be as important as the Marangoni forces.

All of the studies suggest that the arc pressure alone is not enough to depress the free surface as much as it is observed experimentally for currents above 300A. Lin and Eagar [55, 56, 57, 58] and Rokhlin and Guu [59] measured the surface depression during spot GTA welds, and concluded that the actual depression is about five times larger than that calculated from arc pressure alone; therefore, additional driving forces

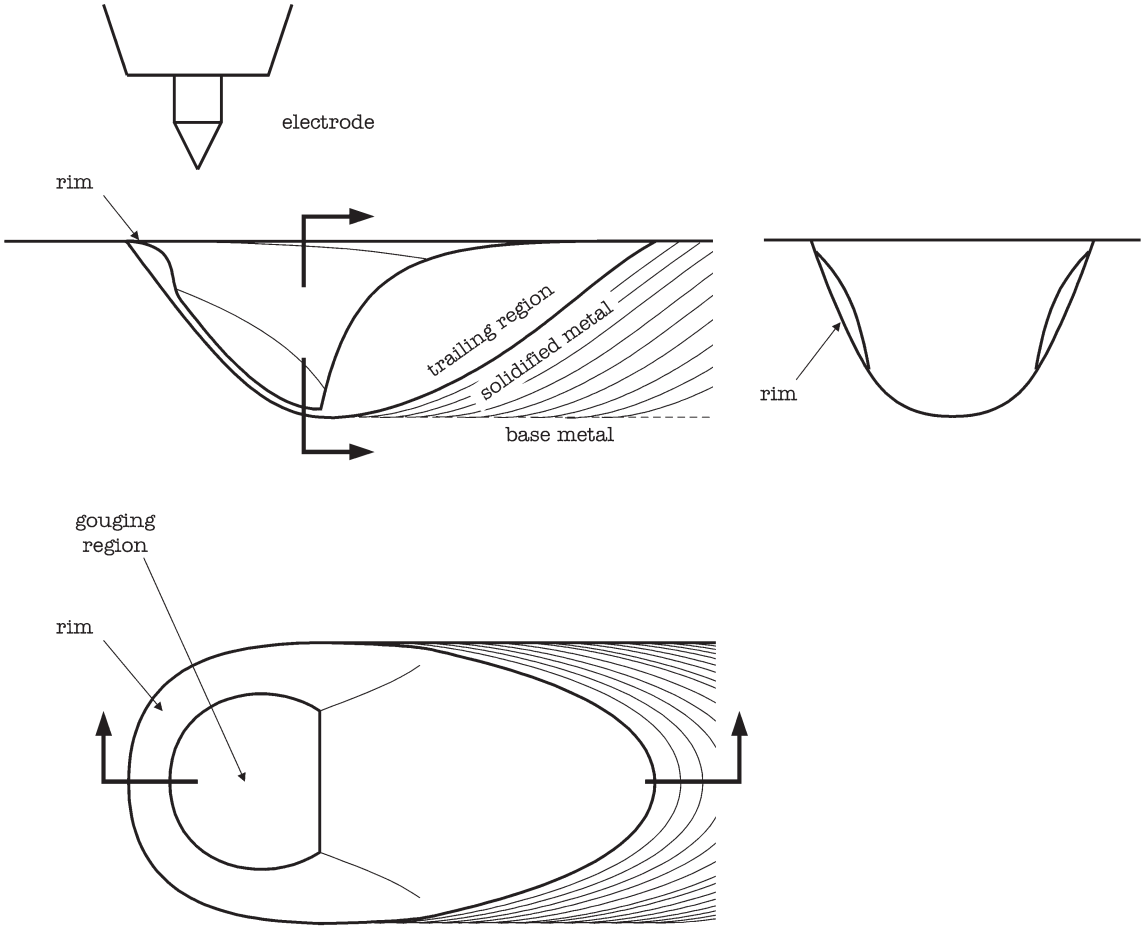

Figure 5-7: Schematic of the weld pool at high currents and speeds. The free surface is very depressed, turning into a thin liquid film under the arc. A thicker rim of liquid runs around the edge of the weld pool carrying molten metal to the bulk of liquid at the rear of the weld pool. The transition line marks the abrupt change from the thin liquid film into the bulk of liquid at the rear.

must be present.

Numerical analysis was performed on static and traveling welds. In all cases the free surface deformation is moderate or small, corresponding to currents below 300A. None of these numerical studies addresses the characteristic geometry typical of high current and speed (see Figure 5-7).

Table 5.2 summarizes the studies done on the deformation of the free surface of the weld pool. It shows that the early studies of weld pool depression were experimental, and included the major feature of the real weld pool at high currents: a gouging region. The analytical part of these works considers only arc pressure, capillary and hydrostatic forces, neglecting gas shear, Marangoni, and electromagnetic forces. As greater computer power became available in the late 70's, early 80's, researchers attempted to model the welding process including more complex driving forces. The earliest works on numerical modeling focused on spot GTA, perhaps the simplest welding process. It can be seen in the Table 5.2 that the maximum current considered in numerical models of GTAW seldom exceeds 150A. This is because the larger surface deformations caused by higher currents involves additional complexities and makes convergence very difficult. Na *et al.* consider a current of 300A in 1992, but his later work does not exceed 200A. The newest numerical models of GMAW reach higher current values, of the order of 300A, but still far from the values used in practice for high productivity welding ($\approx$ 600A). Weiss [60] also studied very depressed weld pools during vertical welding, focusing on the capillary forces and neglecting the fluid flow.

Another obstacle in the study of the weld pool is that the non-linear Navier-Stokes equations does not guarantee a unique solution (see Figure 5-8); this is especially important for large free surface deformations, where the shape of the free surface is unknown. Lin and Eagar [56] reported the existence of a hysteresis cycle in GTA in which two different values of penetration are possible for the same welding settings, depending upon whether the current was increasing or decreasing. Yamamoto and Shimada [5] also report a similar effect, where there are two different values for

Table 5.2: Summary of relevant studies on weld pool depression. X=experimental, A=analytical, N=numerical. GTA=gas tungsten arc, GMA=gas metal arc, SMA=shielded metal arc, SA=submerged arc

Year	Author	Type	Meth.	Amp. max.	Remarks	Reference
1962	Ishizaki	GTA, SMA, SA	X	1200	gouging, traveling	[1, 2]
1968	Bradstreet	GMA	X	570	gouging, traveling	[3]
1972	Demyantsevich	GTA	X	530	gouging, traveling	[4]
1975	Shimada *et al.*	GTA	X, A	800	gouging, traveling	[5, 6]
1979	Matsunawa *et al.*	GMA	X, A	350	gouging, traveling	[7]
1983	Lin *et al.*	GTA	X, A	600	spot weld	[55, 56, 57, 58]
1993	Rokhlin *et al.*	GTA	X, A	350	spot weld	[59]
1978	Friedman	GTA	N	125	spot weld	[61]
1989	Tsai *et al.*	GTA	N	≈150	spot weld	[62]
1989	Szekely *et al.*	GTA	N	150	spot weld	[63, 54, 64]
1991	Zacharia *et al.*	GTA	N	150	spot weld	[65, 66]
1992	Na *et al.*	GTA	N	300	spot weld	[21, 67, 68]
1988	Zacharia *et al.*	GTA	N	100	traveling weld	[19, 69]
1995	Kim *et al.*	GMA	N	300	traveling weld	[70]
1996	Weiss *et al.*	GMA	N	155	traveling weld	[60]
1997	Ushio *et al.*	GMA	N	250	traveling weld	[71]

penetration possible for the same welding velocity.

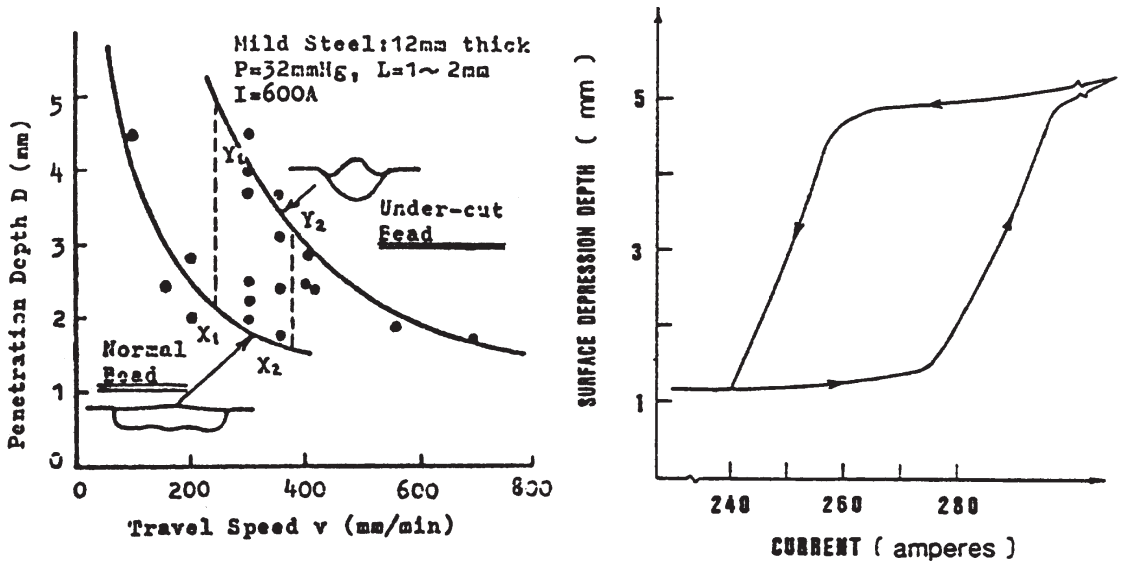

Figure 5-8: Unstable penetration regime. The figure on the left is from Yamamoto and Shimada [5] where they identify the unstable penetration region with the appearance of the gouging region. The figure on the right is from Lin and Eagar [56], where they identify the unstable region with a free surface depression much larger than what the arc pressure alone would provoke.

The next chapter presents a study of the gouging zone in the GTAW weld pool under high currents, including a detailed analysis of the driving forces acting on the molten metal.

Chapter 6

Order of Magnitude Scaling of a Thin Weld Pool

Chapter 4 shows the large and desirable impact of faster welding. Chapter 5 shows that the welding velocity is limited by the appearance of defects. These defects are associated with a "gouging region" at the front of the weld pool, where the weld pool turns into a thin liquid film. The gouging region has been studied experimentally; however, the analytical framework has been very simple, sometimes unknowingly omitting important driving forces. The most detailed numerical studies have so far concentrated exclusively on the region of lower currents, where the weld pool is thick. In this chapter, the methodology described of order of magnitude scaling in Chapter 2 is applied to the study of a thin weld pool (the gouging region) in GTAW. The appropriate differential equations include the various driving forces acting on the weld pool: gas shear, arc pressure, Marangoni, capillary, electromagnetic, gravity, and buoyancy. At high current and welding speed the shear force of the plasma on the free surface determines the flow of liquid metal under the arc, which acts almost directly over the melting interface, causing a deep weld penetration and a potentially unstable liquid film. Chapter 7 shows how the thin film at the gouging region can originate humping and other defects.

6.1 Overview of the Problem

Figure 6-1 presents the coordinate system and other important elements for the analysis. For a stationary torch the substrate moves to the right with velocity U_∞. If the substrate is considered as stationary the torch moves to the left, leaving behind a trail of solidifying metal. The weld pool has two characteristic regions, one is very thin and occurs under the arc (the gouging region), and a trailing region which is thicker. This analysis concentrates on the gouging region.

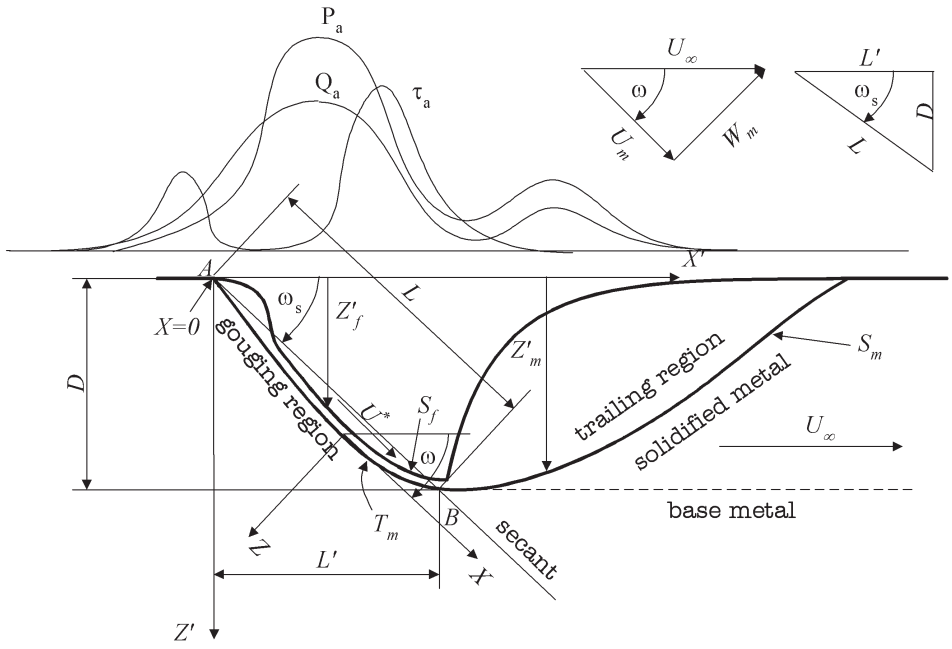

Figure 6-1: Coordinate system and other elements of a thin weld pool. The thickness of the thin liquid layer at point B is $\approx \delta^*$.

The curves labeled Q_a, P_a, and τ_a represent the heat input, arc pressure, and shear stress that the arc imposes on the free surface. S_f and S_m represent the free surface and the melting interface (assuming that the base metal has a sharp melting point). In this problem S_m is considered as prescribed, and S_f as an unknown to be determined.

For simplicity, a two-dimensional model is considered, neglecting transport phe-

nomena along the Y axis. The reference axes travel with the welding torch so that the problem can be solved as a pseudo-stationary one. The axes X and Z are tangential and normal to the melting interface (S_m), therefore their angle ω with the horizontal (X') changes along the melting front. The derivatives with respect to ω can be neglected when using the scaling relationships because the thickness of the liquid film is much smaller than the radius of curvature of the melting front. This approach is very similar to the one used by Wei and Giedt in their study of keyhole formation in electron beam welding [72]. The melting front angle ω_s is the angle of a secant to the melting front between the point of beginning of melting (point A in Figure 6-1) and the transition point where the trailing region begins (point B).

6.2 Two-dimensional Analysis of a Thin Weld Pool

6.2.1 Arc Behavior

No studies have been performed to determine the exact characteristics of the arc in deeply depressed weld pools. In the absence of specific data it is necessary to make some assumptions. The peak values Q_{max}, P_{max}, J_{max}, and τ_{max} are estimated as similar to the values for an arc on a flat surface; the first three need a correction for the larger area of the inclined front surface:

$$Q_{max} \approx Q_{max,flat}\cos(\omega_s) \tag{6.1}$$

$$P_{max} \approx P_{max,flat}\cos(\omega_s) \tag{6.2}$$

$$J_{max} \approx J_{max,flat}\cos(\omega_s) \tag{6.3}$$

$$\tau_{max} \approx \tau_{max,flat} \tag{6.4}$$

The arc length must also be corrected for the weld pool depression:

$$\text{arc length} \approx \text{arc length}_{flat} + D/2 \tag{6.5}$$

These approximations are conservative because they underestimate the importance of the dominant driving force and overestimate the magnitude of the other forces. The gas shear stress over the surface is expected to be larger than over a flat surface because of the slope of the melting front.

The data for an arc on a flat surface is interpolated from the measurements by Tsai [73] and modeling by Choo [64]. The heat distribution between the front and rear of the weld pool depends on the position of the transition line. As the current increases, the transition line moves towards the rear and less heat reaches the trailing region.

6.2.2 Governing Equations, Boundary Conditions, and Domain for Scaling

The fluid flow and heat transfer will be modeled as two-dimensional. This is a reasonable approach, because it yields an upper bound for the thickness of the thin liquid film. It will be shown later that the dominant force in this problem is the shear stress from the gas flow on the surface (also called aerodynamic drag). Due to the geometry of the weld pool, the region of maximum intensity of aerodynamic drag is near the plane of symmetry, where this flow is approximately parallel to that plane. The following driving forces are considered:

- Gas shear on the free surface
- Arc pressure
- Electromagnetic forces
- Hydrostatic pressure
- Capillary forces
- Marangoni forces
- Buoyancy forces

In this model the arc properties and the geometry of the melting interface are considered as known input. Therefore, the equations that completely describe the problem are the equations of conservation of mass (equation 6.6), the equations of conservation of momentum (Navier-Stokes, equations 6.7 and 6.8), the equation of conservation of energy (equation 6.9), Ohm's law (equations 6.10 and 6.11), the equation of conservation of charge (equation 6.12), and Ampère's law (equations 6.13 and 6.14). In this two-dimensional system, the magnetic flux vector is perpendicular to the page at all times. Among the boundary conditions, equation 6.17 includes the Marangoni effect and the gas shear due to the arc plasma, and equation 6.19 includes the arc pressure and the capillary forces. Equation 6.15 is an approximate integral expression of the mass conservation equation at the transition point (point B in Figure 6-1), which is located near the bottom of the weld pool, where the slope of the melting front (angle $\omega \approx 0$) is approximately horizontal. The integral equation of conservation of mass is redundant because mass conservation is already considered with a differential expression in equation 6.6; however, the integral expression will be useful later for the determination of the estimations. The effect of frictional and Joule heating is not included in these equations for the sake of simplicity. They are usually considered negligible in the literature. Other simplifications to the physics of the problem are the consideration of a material with constant thermophysical properties and a sharp melting point like a pure metal. The symbols used in this chapter are defined in Appendix C.

$$\frac{\partial U}{\partial X} + \frac{\partial W}{\partial Z} = 0 \tag{6.6}$$

$$\begin{aligned} U\frac{\partial U}{\partial X} + W\frac{\partial U}{\partial Z} = & -\frac{1}{\rho}\frac{\partial P}{\partial X} + \nu\left(\frac{\partial^2 U}{\partial X^2} + \frac{\partial^2 U}{\partial Z^2}\right) + g\sin(\omega) - \\ & -\frac{1}{\rho}J_Z B_Y - \beta g \sin(\omega)\,(T - T_m) \end{aligned} \tag{6.7}$$

$$U\frac{\partial W}{\partial X} + W\frac{\partial W}{\partial Z} = -\frac{1}{\rho}\frac{\partial P}{\partial Z} + \nu\left(\frac{\partial^2 W}{\partial X^2} + \frac{\partial^2 W}{\partial Z^2}\right) + g\cos(\omega) + \tag{6.8}$$

$$+\frac{1}{\rho}J_X B_Y - \beta g \cos(\omega)\,(T - T_m)$$

$$U\frac{\partial T}{\partial X} + W\frac{\partial T}{\partial Z} = \alpha\left(\frac{\partial^2 T}{\partial X^2} + \frac{\partial^2 T}{\partial Z^2}\right) \tag{6.9}$$

$$J_X = -\sigma_e \frac{\partial \Phi}{\partial X} \tag{6.10}$$

$$J_Z = -\sigma_e \frac{\partial \Phi}{\partial Z} \tag{6.11}$$

$$\frac{\partial^2 \Phi}{\partial X^2} + \frac{\partial^2 \Phi}{\partial Z^2} = 0 \tag{6.12}$$

$$\frac{\partial B_Y}{\partial Z} = -\mu_0 J_X \tag{6.13}$$

$$\frac{\partial B_Y}{\partial X} = \mu_0 J_Z \tag{6.14}$$

$$(U_\infty + C_1 U^*)\delta^* \approx U_\infty L \sin(\omega_s) \tag{6.15}$$

The expression of the constant C_1 in the integral equation of conservation of mass (equation 6.15) is:

$$C_1 = \frac{1}{U_C \delta_C}\int_0^{\delta_C} (U - U_\infty) dZ \tag{6.16}$$

where U_C and δ_C are the characteristic values of the velocity in $U(X,Y)$ and thickness of the thin liquid layer. Since these values are unknown, they are estimated by U^* and δ^*.

The constant C_1 represents the ratio between the average velocity and the free surface velocity for the liquid film at point B (Figure 6-1). For a flow dominated by viscous forces C_1 approaches 1/2, and for a flow dominated by inertial forces (uniform velocity profile) C_1 approaches 1. In this work the value $C_1 = 1/2$ will be used, because (as it will be shown later) in a thin weld pool the flow is dominated by

viscous forces.

Boundary conditions

Table 6.1: Boundary conditions for a thin weld pool (dimensional)

	U	W	P	T	Φ	δ	B_Y
S_f	Eq. 6.17, Eq. 6.18		Eq. 6.19	Eq. 6.20	Eq. 6.21		
S_m	U_m	W_m	Eq. 6.22	T_m			
$x = 0$						0	
$x' = \pm\infty$					0		0
$z' = +\infty$					0		0

$$\sigma_T \nabla T \cdot \mathbf{e}_t = -\tau_a - \rho\nu\nabla(\mathbf{U} \cdot \mathbf{e}_t) \cdot \mathbf{e}_n \tag{6.17}$$

$$\mathbf{U} \cdot \mathbf{e}_n = 0 \tag{6.18}$$

$$P = \frac{\sigma \frac{d^2 Z'_f}{dX'^2}}{\left(1 + \left(\frac{dZ'}{dX'}\right)^2\right)^{3/2}} + P_a \tag{6.19}$$

$$k\frac{\partial T}{\partial Z} = -Q_a \tag{6.20}$$

$$\sigma_e \frac{\partial \Phi}{\partial Z} = -J_a \tag{6.21}$$

$$P = \rho g Z'_m \tag{6.22}$$

where U_m and W_m are the velocity of the metal at the melting interface, $\mathbf{U}$ is the velocity vector and $\mathbf{e}_X$, $\mathbf{e}_Z$, $\mathbf{e}_t$ and $\mathbf{e}_n$ are the unit vectors for the X and Z directions, tangential and normal to the free surface, as shown in Figure 6-2. The domain for

scaling is $0 \leq X \leq L$ and $0 \leq Z \leq \delta^*$.

$$U_m = U_\infty \cos(\omega) \tag{6.23}$$

$$W_m = -U_\infty \sin(\omega) \tag{6.24}$$

$$\mathbf{U} = U\mathbf{e}_X + W\mathbf{e}_Z \tag{6.25}$$

$$\mathbf{e}_t = \cos(\gamma)\mathbf{e}_X - \sin(\gamma)\mathbf{e}_Z \tag{6.26}$$

$$\mathbf{e}_n = \sin(\gamma)\mathbf{e}_X + \cos(\gamma)\mathbf{e}_Z \tag{6.27}$$

$$\tan(\gamma) = \frac{d\delta}{dX} \tag{6.28}$$

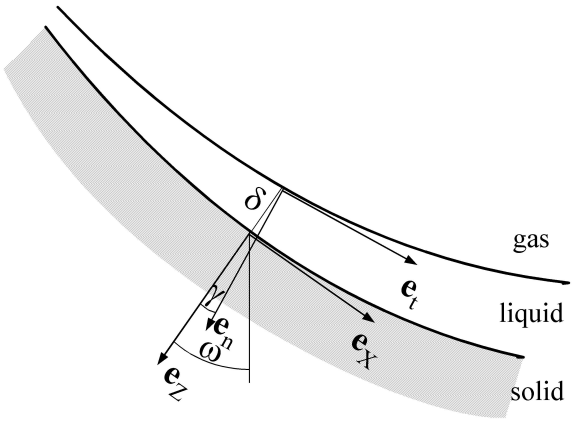

Figure 6-2: Coordinate vectors at the melting interface and free surface. The angle γ is small because the variations in thickness of the thin weld pool are smooth

6.2.3 Sets of Parameters and Units

Because this problem includes a large number of parameters, it is especially important to make careful considerations that simplify the use dimensional analysis.

In Section 2.2.3 it was shown that when the problem does not depend on any absolute value of a temperature, one of the temperature parameters can be disregarded for the purposes of dimensional analysis, in this case T_m. The problem also includes

the numerical constant C_1. The most practical way of dealing with numerical constants is to include them in the set of parameters that define the problem $\{P\}$. For practical reasons the numerical constant will be included as $C_1' = C_1/\sin(\omega_s)$. During the calculations the set $\{P\}$ will include the constant C_1', but not the temperature T_m.

$$\begin{aligned} \{P\}^T &= \{L, \rho, \alpha, k, Q_{max}, J_{max}, \sigma_e, g, \nu, \sigma_T, \sigma, C_1' \text{ (added)}, \\ &\quad P_{max}, \tau_{max}, U_\infty, \mu_0, \beta, \omega_s, T_m \text{ (not included)}\} \\ n &= 18 + 1 - 1 = 18 \end{aligned}$$

Section 2.2.3 also showed that when mechanical friction and heat generation are considered decoupled the thermal energy can be considered a fundamentally different magnitude than mechanical energy, and it is assigned here the unit J="thermal Joule". Similarly, the electric potential, which is considered decoupled from the thermal and mechanical energy will be assigned the unit V="Volt". This is equivalent of splitting the law of conservation of energy into three independent conservation laws, i.e. one for mechanical, one for thermal and a third one for electrical energy. This addition of reference units to the SI is correct, otherwise it would not be possible to obtain a non-dimensional expression of the original equations. The set of reference units based on the SI is:

$$\{R\}^T = \{\text{m, kg, s, K, A, J, V}\} \qquad t = 7$$

The matrix $[U]^T$ for this problem shown in Figure 6-3. Its rank is 7, with the following set of reference parameters:

$$\{P_k\}^T = \{L, \rho, \alpha, k, Q_{max}, J_{max}, \sigma_e\} \qquad k = 7$$

Figure 6-3: Matrix of dimensions $[U]^T$ for a thin weld pool. Thermal, electrical and mechanical energy are considered independent quantities, generating the units J for thermal energy and V for electric potential. In this matrix only σ_e contains the unit V. This unit is also used by Φ^*, the order of magnitude scaling factor for the electric potential, not shown in this matrix.

	L	ρ	α	k	Q_{max}	J_{max}	σ_e	g	ν	σ_T	σ	C_1'	P_{max}	τ_{max}	U_∞	μ_0	β	ω_s
m	1	-3	2	-1	-2	-2	-1	1	2				-1	-1	1	1		
kg		1								1	1		1	1		1		
s			-1	-1	-1			-2	-1	-2	-2		-2	-2	-1	-2		
K				-1						-1							-1	
A						1	1									-2		
J				1	1													
V							-1											

6.2.4 Scaling Relationships, Characteristic Values, and Order of Magnitude Estimations

The following equations constitute the set of scaling relationships:

$$X = Lx \tag{6.29}$$

$$X' = L'x' \tag{6.30}$$

$$Z = \delta^* z \tag{6.31}$$

$$\delta(X) = \delta^* \Delta(x) \tag{6.32}$$

$$U(X,Z) = U_m(\omega) + U^* u(x,z) \tag{6.33}$$

$$W(X,Z) = W_m(\omega) + W^* w(x,z) \tag{6.34}$$

$$P(X,Z) = P^* p(x,z) \tag{6.35}$$

$$T(X,Z) = T_m + T^* \theta(x,z) \tag{6.36}$$

$$Z_f'(X') = D z_f'(x') \tag{6.37}$$

$$Z_m'(X') = D z_m'(x') \tag{6.38}$$

$$Q_a(X) = Q_{max} q_a(x) \tag{6.39}$$

$$P_a(X) = P_{max} p_a(x) \tag{6.40}$$

$$\tau_a(X) = \tau_{max} t_a(x) \tag{6.41}$$

$$J_a(X) = J_{max} j_a(x) \tag{6.42}$$

$$J_X(X,Z) = J^* j_x(x,z) \tag{6.43}$$

$$J_Z(X,Z) = J_{max} j_z(x,z) \tag{6.44}$$

$$B_Y(X,Z) = B^* b(x,z) \tag{6.45}$$

$$\Phi(X,Z) = \Phi^* \phi(x,z) \tag{6.46}$$

The set of estimations is:

$$\{S\}^T = \{\delta^*, U^*, W^*, P^*, T^*, \Phi^*, J^*, B^*\} \qquad q = 8$$

6.2.5 Dimensionless Governing Equations and Boundary Conditions

A dominant balance was performed on the equations with the material properties of the typical case described in Section 6.2.10. It was found that the gas shear and the viscous forces are dominant in the typical system (see Figure 6-16). The dimensional equations were then normalized using these forces. Equation 6.49 was normalized with the pressure gradient, which is characterized by equation 6.48. The expression of the dimensionless groups N_i is contained in the matrix $[A]$, whose submatrices are shown in Figures 6-4 to 6-9.

$$\frac{\partial u}{\partial x} + N_1 \frac{\partial w}{\partial z} = 0 \tag{6.47}$$

$$N_2\left[(u_m+u)\frac{\partial u}{\partial x} + N_3(w_m+w)\frac{\partial u}{\partial z}\right] = -N_4\frac{\partial p}{\partial x} + N_5\frac{\partial^2 u}{\partial x^2} + \frac{\partial^2 u}{\partial z^2} - N_6\sin(\omega) - N_7 j_z b - N_8\sin(\omega) \tag{6.48}$$

$$N_9(u_m+u)\frac{\partial w}{\partial x} + N_{10}(w_m+w)\frac{\partial w}{\partial z} = -\frac{\partial p}{\partial z} + N_{11}\left(N_5\frac{\partial^2 w}{\partial x^2} + \frac{\partial^2 w}{\partial z^2}\right) + N_{12}\cos(\omega) + N_{13} j_x b - N_{14}\theta\cos(\omega) \tag{6.49}$$

$$N_{15}(u_m + u)\frac{\partial \theta}{\partial x} + N_16(w_m + w)\frac{\partial \theta}{\partial z} = N_5\frac{\partial^2 \theta}{\partial x^2} + \frac{\partial^2 \theta}{\partial z^2} \quad (6.50)$$

$$j_x = -N_{17}\frac{\partial \phi}{\partial x} \quad (6.51)$$

$$j_z = -N_{18}\frac{\partial \phi}{\partial z} \quad (6.52)$$

$$N_5\frac{\partial^2 \phi}{\partial x^2} + \frac{\partial^2 \phi}{\partial z^2} = 0 \quad (6.53)$$

$$\frac{\partial b}{\partial x} = -N_{20} j_z \quad (6.54)$$

$$\frac{N_{21}}{\sin(\omega_s)} + N_{22} \approx 1 \quad (6.55)$$

where:

$$u_m = N_{31}\cos(\omega) \quad (6.56)$$

$$w_m = -N_{32}\sin(\omega) \quad (6.57)$$

Boundary conditions

Table 6.2 presents the non-dimensional boundary conditions for this system. The conditions for the velocity at the surface have a complex mathematical expression, because the free surface is not necessarily parallel to the melting interface. Because the variation of film thickness over the length is smooth, equations 6.60 and 6.61 can contain the following simplifications:

$$\sin(\gamma) \approx \tan(\gamma) \quad (6.58)$$

$$\cos(\gamma) \approx 1 \quad (6.59)$$

Table 6.2: Boundary conditions for a thin weld pool (dimensionless)

	u	w	p	θ	ϕ	Δ	b
S_f	Eq. 6.60, Eq. 6.61		Eq. 6.62	Eq. 6.63	Eq. 6.64		
S_m	0	0	Eq. 6.65	0			
$x = 0$						0	
$x' = \pm\infty$					0		0
$z' = +\infty$					0		0

$$N_{23}\frac{\partial u}{\partial z} = -t_a - N_{24}\left(\frac{\partial \theta}{\partial x} + \frac{d\Delta}{dx}\frac{\partial \theta}{\partial z}\right) \tag{6.60}$$

$$w = N_{25}(u_m + u)\frac{d\Delta}{dx} - w_m \tag{6.61}$$

$$p = -N_{26}\frac{\sin(\omega_s)}{\cos^2(\omega_s)}\left(1 + \tan^2(\omega_s)\frac{dz'_f}{dx'}\right)^{-3/2}\frac{d^2 z'_f}{dx'^2} + N_{27}p_a \tag{6.62}$$

$$\frac{\partial \theta}{\partial z} = -N_{28}q_a \tag{6.63}$$

$$\frac{\partial \phi}{\partial z} = -N_{29}j_a \tag{6.64}$$

$$p = N_{30}z'_m \sin(\omega_s) \tag{6.65}$$

6.2.6 Dimensionless Groups of Known Order of Magnitude

For the equations that have only two terms it is easy to determine the dimensionless groups that can be approximated as equal to one. This way the following relationships are obtained:

$$N_1 = N_{17} = N_{18} = N_{20} = N_{28} \tag{6.66}$$

The main driving force (gas shear) acts mainly on the X direction. Therefore the momentum in X equation (equation 6.48) will be considered the most relevant of the two momentum equations. The characteristic pressure is obtained by defining $N_4 = 1$ in that equation. The dominant balance indicates that the gas shear at the surface is balanced by the viscous forces, therefore in equation 6.60 the group N_{23} should be set to one. For a thin liquid film the group N_{22} in the integral equation of conservation of mass (equation 6.55) dominates, and will be estimated as equal to one (this is valid only when the weld pool is very thin relative to its other dimensions).

6.2.7 Dimensionless Groups that Completely Describe the Problem

This formulation of the problem uses 18 meaningful parameters and 7 reference parameters; therefore, eleven dimensionless groups are necessary to describe the non-dimensional formulation of the problem. The selection of this parameters is arbitrary but for the analysis of the system in the conditions of the typical case these parameters can be chosen as:

$$\{\Pi\}=\{N_2,\, \omega_s,\, N_5,\, N_6,\, N_7,\, N_8,\, N_{15},\, N_{24},\, N_{26},\, N_{27},\, C_1'\} \qquad m = 11$$

The elements of $\{\Pi\}$ have a concrete physical meaning, and many can be associated with well known dimensionless groups, as shown in Table 6.3. The parameters N_6, N_7, N_8, N_{24}, N_{26}, and N_{27}, are ratios of driving forces for the flow. The groups N_2, N_5, and N_{15}, are ratios of effects. ω_s relates to the geometry. The element C_1' is a numerical constant that is included in the set only for practical reasons. The term "diffusivity" used to describe N_5 refers to diffusion-like processes such as heat conduction or momentum transfer.

One advantage of the governing dimensionless numbers used here is that the ratios mentioned actually describe the relative orders of magnitude of driving forces or effects

Table 6.3: Meaning of the governing dimensionless groups

	physical meaning	related group [74]
N_2	inertia/viscous	Reynolds
ω_s	melting front angle	see Figure 6-1
N_5	diffusivity in x/diffusivity in z	
N_6	gravity/viscous	Stokes
N_7	electromagnetic/viscous	Elsasser
N_8	buoyancy/viscous	Grashoff
N_{15}	convection/conduction	Peclet
N_{24}	Marangoni/gas shear	Marangoni
N_{26}	capillary/viscous	Capillary
N_{27}	arc pressure/viscous	Poiseuille

with more accuracy than the standard parameters. The reason for this is that they include information about the geometry and magnitudes of the problem that are not easily captured by the traditional formulation of the dimensionless groups.

6.2.8 Expression of the Order of Magnitude Estimations

Based on the sets defined so far, the elements of matrix $[A]$ ($[A_{11}]$, $[A_{21}]$, $[A_{31}]$, $[A_{12}]$, $[A_{22}]$, and $[A_{32}]$) can be constructed. These submatrices are shown in Figures 6-4 to 6-9.

	L	ρ	α	k	Q_{max}	J_{max}	σ_e	g	ν	σ_T	σ	C_1'	P_{max}	τ_{max}	U_∞	μ_0	β	ω_s
N_1	1																	
N_4	-1	-1							-1									
N_{17}	-1						1											
N_{18}						-1	1											
N_{20}	1					1										1		
N_{22}	-1											1			-1			
N_{23}		1							1					-1				
N_{28}				-1	1													

Figure 6-4: Matrix of dimensionless groups $[A_{11}]$ for a thin weld pool

The expression of the order of magnitude estimations is given by matrix $[A_S]$, shown in Figure 6-10. This matrix is obtained by substituting the matrices defined above into equation 2.26.

	δ^*	U^*	W^*	P^*	T^*	Φ^*	J^*	B^*
N_1	1	-1	1					
N_4	2	-1		1				
N_{17}						1	-1	
N_{18}	-1					1		
N_{20}								-1
N_{22}	1	1						
N_{23}	-1	1						
N_{28}	1				-1			

Figure 6-5: Matrix of dimensionless groups $[A_{12}]$ for a thin weld pool

	L	ρ	α	k	Q_{max}	J_{max}	σ_e	g	ν	σ_T	σ	C_1'	P_{max}	τ_{max}	U_∞	μ_0	β	ω_s
N_2	-1								-1									
ω_s																		1
N_5	-2																	
N_6								1	-1									
N_7		-1				1			-1									
N_8								1	-1								1	
N_{15}	-1		-1															
N_{24}	-1									1				-1				
N_{26}	-1										1							
N_{27}													1					
C_1'												1						

Figure 6-6: Matrix of dimensionless groups $[A_{21}]$ for a thin weld pool

	δ^*	U^*	W^*	P^*	T^*	Φ^*	J^*	B^*
N_2	2	1						
ω_s								
N_5	2							
N_6	2	-1						
N_7	2	-1						1
N_8	2	-1			1			
N_{15}	2	1						
N_{24}								
N_{26}				-1				
N_{27}				-1				
C_1'								

Figure 6-7: Matrix of dimensionless groups $[A_{22}]$ for a thin weld pool

	L	ρ	α	k	Q_{max}	J_{max}	σ_e	g	ν	σ_T	σ	C_1'	P_{max}	τ_{max}	U_∞	μ_0	β	ω_s
N_{32}															1			
N_9	-1	1																
N_{11}		1							1									
N_{12}		1						1										
N_{13}																		
N_{14}		1						1									1	
N_{19}																1		
N_{21}	-1																	
N_{29}						1	-1											
N_{30}	1	1						1										
N_{31}															1			
N_3									-1									
N_{10}		1																
N_{16}			-1															
N_{25}	-1																	

Figure 6-8: Matrix of dimensionless groups $[A_{31}]$ for a thin weld pool

	δ^*	U^*	W^*	P^*	T^*	Φ^*	J^*	B^*
N_{32}			-1					
N_9	1	1	1	-1				
N_{11}	-1		1	-1				
N_{12}	1			-1				
N_{13}	1			-1			1	1
N_{14}	1			-1	1			
N_{19}	1						1	-1
N_{21}	1							
N_{29}	1					-1		
N_{30}				-1				
N_{31}		-1						
N_3	1		1					
N_{10}			2	-1				
N_{16}	1		1					
N_{25}	1	1	-1					

Figure 6-9: Matrix of dimensionless groups $[A_{32}]$ for a thin weld pool

	L	ρ	α	k	Q_{max}	J_{max}	σ_e
δ^*	1/2	1/2					
U^*	1/2	-1/2					
W^*							
P^*	1/2	-1/2					
T^*	1/2	1/2		-1	1		
Φ^*	1/2	1/2				1	-1
J^*	-1/2	1/2				1	
B^*	1					1	

	g	ν	σ_T	σ	C_1'	P_{max}	τ_{max}	U_∞	μ_0	β	ω_s
δ^*		1/2			-1/2		-1/2	1/2			
U^*		-1/2			-1/2		1/2	1/2			
W^*					-1			1			
P^*		-1/2			1/2		3/2	-1/2			
T^*		1/2			-1/2		-1/2	1/2			
Φ^*		1/2			-1/2		-1/2	1/2			
J^*		1/2			-1/2		-1/2	1/2			
B^*									1		

Figure 6-10: Matrix of dimensionless groups $[A_S]$ for a thin weld pool. The matrix was split in two in this figure for reasons of space.

Having obtained the expression of the estimations, equation 2.27 provides matrix $[B]$, which contains the expression of the set of selected dimensionless groups $\{\Pi\}$ and the coefficients in the equations as a function of the problem parameters. The submatrices that constitute matrix $[B]$ are shown in Figures 6-11 to 6-14.

	L	ρ	α	k	Q_{max}	J_{max}	σ_e
N_2	1/2	1/2					
ω_s							
N_5	-1	1					
N_6	1/2	3/2					
N_7	3/2	1/2				2	
N_8	1	2		-1	1		
N_{15}	1/2	1/2	-1				
N_{24}	-1/2	1/2		-1	1		
N_{26}	-3/2	1/2					
N_{27}	-1/2	1/2					
C_1'							

Figure 6-11: Matrix of dimensionless groups $[B_{11}]$ for a thin weld pool

	g	ν	σ_T	σ	C_1'	P_{max}	τ_{max}	U_∞	μ_0	β	ω_s
N_2		-1/2			-3/2		-1/2	3/2			
ω_s											1
N_5		1			-1		-1	1			
N_6	1	1/2			-1/2		-3/2	1/2			
N_7		1/2			-1/2		-3/2	1/2	1		
N_8	1	1			-1		-2	1		1	
N_{15}		1/2			-3/2		-1/2	3/2			
N_{24}		1/2	1		-1/2		-3/2	1/2			
N_{26}		1/2		1	-1/2		-3/2	1/2			
N_{27}		1/2			-1/2	1	-3/2	1/2			
C_1'					1						

Figure 6-12: Matrix of dimensionless groups $[B_{12}]$ for a thin weld pool

	L	ρ	α	k	Q_{max}	J_{max}	σ_e
N_{32}							
N_9	-1/2	3/2					
N_{11}	-1	1					
N_{12}		2					
N_{13}	1/2	3/2				2	
N_{14}	1/2	5/2		-1	1		
N_{19}	-1	1					
N_{21}	-1/2	1/2					
N_{29}							
N_{30}	1/2	3/2					
N_{31}	-1/2	1/2					
N_3	1/2	1/2					
N_{10}	-1/2	3/2					
N_{16}	1/2	1/2	-1				
N_{25}							

Figure 6-13: Matrix of dimensionless groups $[B_{21}]$ for a thin weld pool

	g	ν	σ_T	σ	C_1'	P_{max}	τ_{max}	U_∞	μ_0	β	ω_s
N_{32}					1						
N_9		1/2			-5/2		-3/2	5/2			
N_{11}		1			-1		-1	1			
N_{12}	1	1			-1		-2	1			
N_{13}		3/2			-3/2		-5/2	3/2	1		
N_{14}	1	3/2			-3/2		-5/2	3/2		1	
N_{19}		1			-1		-1	1			
N_{21}		1/2			-1/2		-1/2	1/2			
N_{29}											
N_{30}	1	1/2			-1/2		-3/2	1/2			
N_{31}		1/2			1/2		-1/2	1/2			
N_3		-1/2			-3/2		-1/2	3/2			
N_{10}		1/2			-5/2		-3/2	5/2			
N_{16}		1/2			-3/2		-1/2	3/2			
N_{25}											

Figure 6-14: Matrix of dimensionless groups $[B_{22}]$ for a thin weld pool

6.2.9 Governing Equations in Terms of the Dimensionless Groups

Equation 2.28 provides matrix $[B_N]$ (shown in Figure 6-15). This matrix contains the expression (as a function of the governing dimensionless groups) of the coefficients used in the normalized equations.

	N_2	ω_s	N_5	N_6	N_7	N_8	N_{15}	N_{24}	N_{26}	N_{27}	C_1'
N_{32}											1
N_9	1		1								
N_{11}			1								
N_{12}			1/2	1							
N_{13}			1		1						
N_{14}			1/2			1					
N_{19}			1								
N_{21}			1/2								
N_{29}											
N_{30}				1							
N_{31}			1/2								1
N_3	1										
N_{10}	1		1								
N_{16}							1				
N_{25}											

Figure 6-15: Matrix of dimensionless groups $[B_N]$ for a thin weld pool

$$\frac{\partial u}{\partial x} + \frac{\partial w}{\partial z} = 0 \tag{6.67}$$

$$N_2\left[(u_m+u)\frac{\partial u}{\partial x} + (w_m+w)\frac{\partial u}{\partial z}\right] = -\frac{\partial p}{\partial x} + N_5\frac{\partial^2 u}{\partial x^2} + \frac{\partial^2 u}{\partial z^2} - \\ -N_6\sin(\omega) - N_7 j_z b - N_8\sin(\omega) \tag{6.68}$$

$$N_2 N_5\left[(u_m+u)\frac{\partial w}{\partial x} + (w_m+w)\right]\frac{\partial w}{\partial z} = -\frac{\partial p}{\partial z} + N_5\left(N_5\frac{\partial^2 w}{\partial x^2} + \frac{\partial^2 w}{\partial z^2}\right) + \\ +N_5^{1/2}N_6\cos(\omega) + N_5 N_7 j_x b - \tag{6.69}$$

$$-N_5^{1/2} N_8 \theta \cos(\omega)$$

$$N_{15}\left[(u_m+u)\frac{\partial\theta}{\partial x}+(w_m+w)\frac{\partial\theta}{\partial z}\right] = N_5\frac{\partial^2\theta}{\partial x^2}+\frac{\partial^2\theta}{\partial z^2} \tag{6.70}$$

$$j_x = -\frac{\partial\phi}{\partial x} \tag{6.71}$$

$$j_z = -\frac{\partial\phi}{\partial z} \tag{6.72}$$

$$N_5\frac{\partial^2\phi}{\partial x^2}+\frac{\partial^2\phi}{\partial z^2} = 0 \tag{6.73}$$

$$\frac{\partial b}{\partial x} = -j_z \tag{6.74}$$

$$\frac{N_5^{1/2}}{\sin(\omega_s)}+1 \approx 1 \tag{6.75}$$

where:

$$u_m = N_5^{1/2} C_1' \cos(\omega) \tag{6.76}$$

$$w_m = -C_1' \sin(\omega) \tag{6.77}$$

Boundary conditions

Table 6.4: Boundary conditions for a thin weld pool (dimensionless; as a function of the governing dimensionless groups)

	u	w	p	θ	ϕ	Δ	b
S_f	Eq. 6.78, Eq. 6.79		Eq. 6.80	Eq. 6.81	Eq. 6.82		
S_m	0	0	Eq. 6.83	0			
$x = 0$						0	
$x' = \pm\infty$					0		0
$z' = +\infty$					0		0

$$\frac{\partial u}{\partial z} = -t_a - N_{24}\left(\frac{\partial \theta}{\partial +}x\frac{d\Delta}{dx}\frac{\partial \theta}{\partial z}\right) \tag{6.78}$$

$$w = (u_m + u)\frac{d\Delta}{dx} - w_m \tag{6.79}$$

$$p = -N_{26}\frac{\sin(\omega_s)}{\cos^2(\omega_s)}\left(1 + \tan^2(\omega_s)\frac{dz'_f}{dx'}\right)^{-3/2}\frac{d^2 z'_f}{dx'^2} + N_{27}p_a \tag{6.80}$$

$$\frac{\partial \theta}{\partial z} = -q_a \tag{6.81}$$

$$\frac{\partial \phi}{\partial z} = -j_a \tag{6.82}$$

$$p = N_6 z'_m \sin(\omega_s) \tag{6.83}$$

Equations 6.67-6.83 completely describe the problem, and are a function of ten governing dimensionless groups in the set $\{\Pi\}$. For the two-dimensional system of equations presented above, the only mathematical simplifications made are to neglect the derivatives with respect to ω, and to neglect some terms in the expression of the velocity boundary conditions at the free surface. In physical terms, the first of these simplifications implies the liquid film thickness is much smaller than the radius of curvature of the melting front, thus the angle ω can be considered constant point by point. The second simplification means that the liquid film thickness varies slowly and smoothly, so the terms associated with this variation are very small.

6.2.10 Values for a typical case

The exact relative importance of the driving forces depends on each particular case; however, the analysis of a typical case with a deeply depressed surface is enough to characterize the thin weld pool at the gouging region by similarity. The particular

case analyzed is that of Figure 5-1, with its main welding parameters and physical properties shown in Tables 6.5 and 6.6 respectively. The measured weld penetration and its location are:

$$\begin{aligned} D &= 3.2 \text{ mm} \\ L' &= 4.15 \text{ mm} \\ \omega_s &= 0.657 \text{ rad} \end{aligned}$$

Table 6.5: Welding parameters for weld of Figure 5-1

base material	AISI 304 (50 ppm S)
current	305 A
voltage	14.5 V
speed	12 ipm (5.08 mm/s)
arc length$_{flat}$	3.175 mm
shielding gas	100% Ar

With these settings, the estimated parameters for the arc are:

$$\begin{aligned} Q_{max} &= 3.34 \times 10^7 \, \mathrm{W/m^2} \\ P_{max} &= 713 \, \mathrm{Pa} \\ J_{max} &= 4.29 \times 10^6 \, \mathrm{A/m^2} \\ \tau_{max} &= 92.1 \, \mathrm{Pa} \end{aligned}$$

6.3 Results

The estimations obtained are presented in Table 6.7. The characteristic thickness for the liquid film is on the order of tens of microns, which is orders of magnitude smaller than the thickness for a weld pool with recirculation (of the order of millimeters). On

Table 6.6: Physical properties for AISI 304 with 50 ppm S. This data is based on references [66, 68, 75, 76, 77, 78].

ρ	6907	kg/m^3	ν	8.32×10^{-7}	m^2/s
α	3.30×10^{-6}	m^2/s	σ_T	1.50×10^{-4}	N/mK
k	18.0	W/mK	σ	1.56	N/m
σ_e	7.7×10^{5}	A/Vm	β	9.79×10^{-5}	1/K
T_s	1523	K	T_l	1723	K

such a thin weld pool, the characteristic temperature variation is of the order of 10^2 K, much smaller than that for weld pools with recirculation (of the order of 10^3 K). This smaller temperature jump makes Marangoni forces less relevant. Thus, variations in the sulfur content are expected to have a much smaller influence on penetration than in thicker weld pools. The values for the Π parameters are represented in Figure

Table 6.7: Typical values for the estimations in a thin weld pool

δ^*	4.51×10^{-5}	m	T^*	83.8	K
U^*	0.722	m/s	Φ^*	2.51×10^{-4}	V
W^*	6.20×10^{-3}	m/s	J^*	3.69×10^{4}	A/m^2
P^*	1.07×10^{4}	Pa	B^*	2.83×10^{-2}	Wb/m^2

6-16. The value 1 corresponds to the ratio between the viscous forces and the gas shear force (dominant). An analysis of the groups related to the driving forces shows that their influence is smaller than 10% of the dominant force. Group $N_2 \approx 0.34$ is the ratio between two effects (viscous and dynamic), and does not involve ratios of driving forces. Its value indicates, however, that inertial forces should be taken into account in more accurate calculations. The very small value of Π_3 indicates that in the X-direction thermal conduction and viscous effects are negligible. Convection (Π_7) is very small, but inertial forces (Π_1) could be of importance.

The thickness of the mushy zone can be estimated as:

$$\text{thickness mushy zone} \approx kT_{sl}/Q_{max} = 1.07 \times 10^{-4}\,\text{m} \tag{6.84}$$

The film thickness is only a half of this, and will capture the irregularities in the melting of the base metal, thus giving the impression of a "dry" surface.

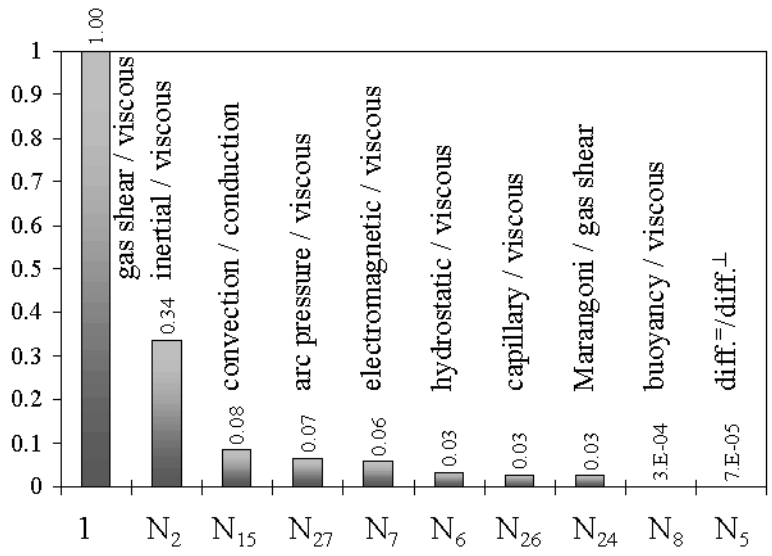

Figure 6-16: Typical value of the governing dimensional groups for a thin weld pool. The gas shear on the free surface is the dominant driving force, and viscosity is the dominant resistance (effect). All other forces and effects are normalized by them. In the asymptotic case when all other forces and effects are negligible the ratio of the ratio gas shear/viscous effect is one. for the typical case presented, gas shear is an order of magnitude stronger than any other force. The viscous forces are the dominant resistance, but inertial effects are not negligible.

6.4 Experimental Verification

When the weld pool is thick and allows recirculating flows, Marangoni forces are important, affecting the penetration of the weld. The Marangoni forces are affected by surface active elements such as sulfur. To verify that in a thin weld pool the Marangoni forces are of little importance, a set of welds was performed in the same conditions on 304 stainless steel differing only on their sulfur content (6 ppm vs. 230 ppm). The welding parameters were such that these welds had a gouging region. They were sectioned and etched, and penetration was measured. It was observed that

penetration was not affected by the sulfur content, indicating that the Marangoni flows were of little effect at these high current levels.

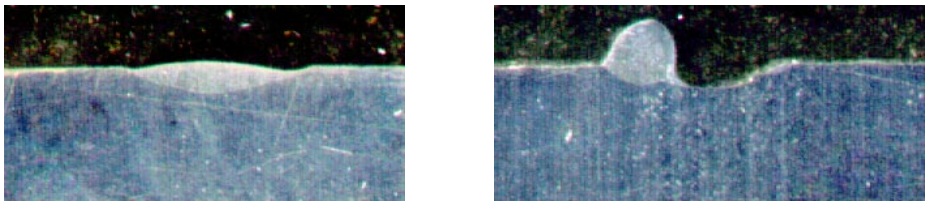

Figure 6-17: Comparison of penetration for high and low sulfur welds. The weld on the left has a sulfur content of 6 ppm and the one of the right 230 ppm. The penetration for both welds is 0.9 mm. The weld on the right showed a double humping defect, which appears as a bump.

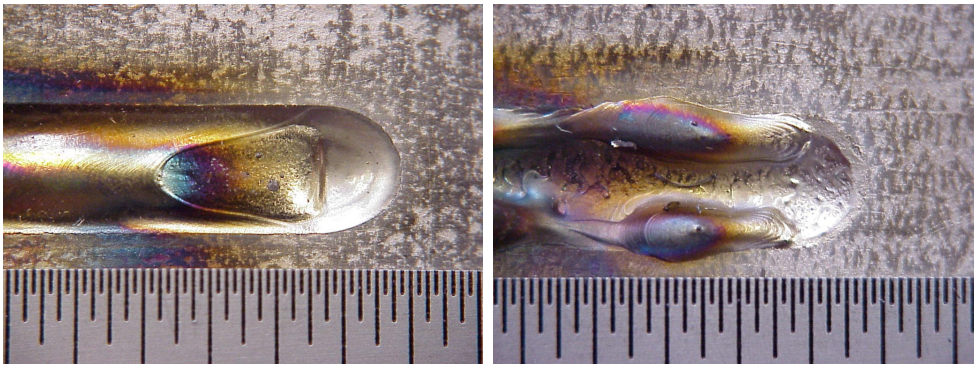

Figure 6-18: Gouging region for the welds of Figure 6-17. The one on the left corresponds to low sulfur and the one to the right to high sulfur. Both weld beads have the same size. A double humping defect is seen on the weld on the right.

6.5 Discussion

The non-dimensional system of equations 6.67-6.83 considers that the layer thickness is much smaller than the radius of curvature of the melting front, and that one of the terms in equation 6.75 is negligible. This assumptions are reasonable, in the light of the results obtained, since the thickness of the thin liquid film was estimated to

be of the order of magnitude of 10^{-5}m in a weld pool with characteristic dimensions of the order of 10^{-3}m. As mentioned above, the behavior of the arc in such a deeply depressed weld pool is not well known. It is difficult to estimate the tail end temperature and characteristics without knowledge of how much heat it receives. When the tail receives little energy, there is a risk of premature freezing of the thin film and humping with the mechanism described above. When the fraction of power reaching the tail is higher, temperature differences could be of the order of 10^3 K. In this case, Marangoni forces are dominant and would produce strong recirculating flows. Ishizaki [2] suggested that this hot metal widens the weld bead after the arc acted over the melting front ("primary" and "secondary" penetration in his terms). Finger-like penetration in GTA welding can then be explained as a combination of a deep penetration caused by the direct action of the arc on the melting front, and a widening of the bead at the surface by the hot liquid of the tail. For very fast welds, the tail can be very elongated and experience humping through a mechanism of capillary instabilities [51].

6.6 Summary

For thin weld pools under high current arcs, the gas shear stress is the main determinant of the motion of the liquid under the arc. Other factors such as Marangoni, electromagnetic and buoyancy have a much smaller effect.

The characteristic thickness, surface velocity and temperature under the arc can be evaluated with the following expressions (typical values are in parenthesis):

$$\delta^* = (2\mu U_\infty D/\tau_{max})^{1/2} \quad (\approx 50\,\mu\text{m}) \tag{6.85}$$

$$T^* = Q_{max}\delta^*/k \qquad (\approx 100\,\text{K}) \tag{6.86}$$

$$U^* = 2U_\infty D/\delta^* \qquad (\approx 1\,\text{m/s}) \tag{6.87}$$

The freezing time for the thin film is very small, and premature freezing can start a

humped bead.

The thickness of the weld pool is of the order of the mushy zone, therefore the free surface captures its irregularities and has the appearance of "dry" metal.

Finger-like penetration in GTA welding can be explained as a combination of the deep penetration caused by the direct action of the arc on the melting front, and a widening of the bead by the hot metal of the tail. Since the Marangoni forces are small relative to the aerodynamic drag, surface active elements such as sulfur have a negligible effect on penetration.

A more accurate estimation of the characteristics of the arc in deeply depressed weld pools is necessary. This is especially important if the melting front is also considered an unknown, because the arc acts almost directly over it.

Chapter 7

Mechanism of Generation of Defects

In the previous chapter it was shown that the weld pool at high currents turns into a thin film, and that the dominant driving force is the gas shear on the surface. In this chapter it will be shown how this characteristic can produce defects such as humping, undercutting and tunnelling.

7.1 Humping Threshold

Humping is always accompanied by a gouging region. If the gouging region extends to a position where there is not enough heating from the arc, it will freeze, producing a void in the weld seam. The time scale for freezing is very short. It can be estimated by balancing the rate of heat extraction at the solid-liquid interface, and the heat capacity of the thin layer:

$$\text{time scale for freezing} = \left(\frac{1}{2}\frac{kT^*}{\alpha} + \rho\Delta H_{sl}\right)\frac{\delta^*}{Q_m ax} \approx 2.8 \times 10^{-3}\,\text{s} \qquad (7.1)$$

where ΔH_{sl} is the latent heat of melting. Such fast freezing indicates that for all practical purposes, the gouging region will freeze immediately if it reaches a cold

part, and the humping process will start, as shown schematically in Figure 7-1. The location of the transition point is therefore critical. Humping will start when the transition point is pushed far enough towards the rear of the weld pool, to where the heat from the arc decreases.

7.2 Location of the Transition Point

7.2.1 Forces Acting on the Transition Point

The location of the transition point is determined by a balance of the forces acting on it. These forces are:

- Hydrostatic
- Capillary
- Arc Pressure
- Other forces (Marangoni, electromagnetic, etc.)

Hydrostatic forces: These are originated by the pressure due to the column of metal (H) between the transition point and the highest point of the free surface. The expression is:

$$P_h = \rho g H \tag{7.2}$$

Capillary forces: The expression is:

$$P_c = \sigma \left(\frac{1}{R_1} + \frac{1}{R_2} \right) \tag{7.3}$$

The simple appearance of this equation is misleading, because the principal curvatures of the free surface are very difficult to obtain or predict, and they could be positive or negative.

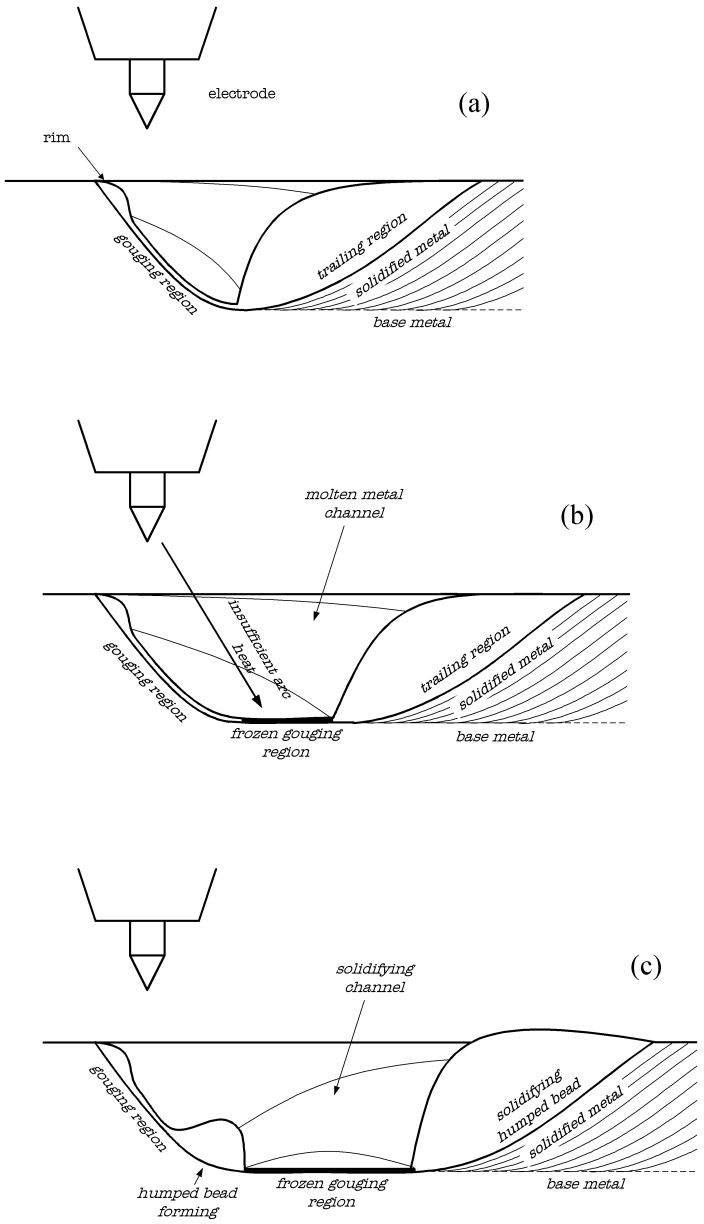

Figure 7-1: Schematic of humping formation in GTAW. Figure (a) illustrates a weld pool in which the gouging region does not extend far from the arc, therefore the thin liquid layer feeds the trailing region, and humping does not happen. Figure (b) represents a weld pool in which the trailing region starts far from the arc. In this case, the further portion of the trailing region does not receive enough heat from the arc an freezes almost instantly. The trailing region is fed by two molten metal channels, one on each side of the weld, surrounding the gouging region with a rim of molten metal. Figure (c) shows the evolution of the weld of Figure (b). The side channels start to solidify, and stop feeding the trailing region, which also begins to solidify. With no possibility of transferring molten metal to the rear of the weld pool a new humped bead starts to form.

Arc pressure and gas shear This is the pressure and shear due to the impingement of the plasma on the free surface. For a flat surface the arc pressure has symmetry of revolution, with a distribution profile resembling that of a gaussian distribution. Very little is known about the behavior of a welding arc on very irregular geometries such those encountered on very depressed weld pools in traveling welds. In those cases, the symmetry of revolution is broken, and the arc force is expected to increase with the deformation [79]. For relatively slow welds, the weld pool is located directly below the arc, and its depression resembles that of static welds. For faster welds, the distance traveled before melting starts is longer; therefore, the weld pool shifts towards the rear of the arc. In this situation the arc force acts on the front of the weld pool, facilitating the creation of the gouging region, and pushing the transition point towards the rear.

The arc pressure and gas shear affect all of the free surface, but its influence decreases towards the rear, being negligible when the rear of the weld pool extends too far.

On the verge of humping, the transition point is at the edge of the arc with the trailing region behind; therefore, very little action from the arc on the trailing region is expected in welds on the verge of humping.

The arc pressure scales with the square of the current, therefore, at higher currents, the arc pressure will push the transition point to the rear.

Other forces Many other forces act on the trailing region, such as Marangoni, electromagnetic and buoyancy. These forces are induced by the action of the arc, which is very weak over the trailing region on the verge of humping. These forces are expected to be of little importance for influencing the onset of humping.

7.2.2 Force Balance at the Transition Point

The location of the transition point can be determined by a force balance at that point. The forces involved are the arc pressure (P_a), which tends to expand the size

of the gouging region, pushing the transition point to the rear, and the hydrostatic and capillary forces (P_h and P_c respectively), which push the transition point to the front, thus decreasing the size of the gouging region.

$$P_a = P_h + P_c \tag{7.4}$$

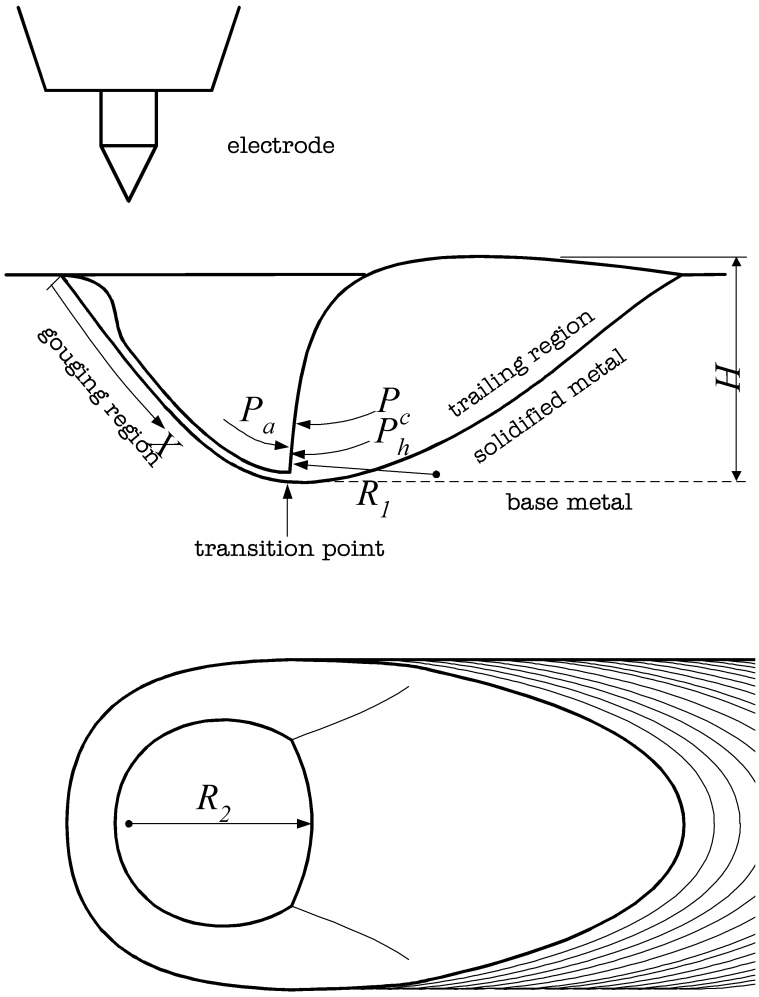

Figure 7-2: Forces acting at the transition point

The force balance can be expressed in a non-dimensional form using the following

scaling relationships:

$$X = X_C x \tag{7.5}$$

$$R_1 = H r_1 \tag{7.6}$$

$$R_2 = X_C r_2 x \tag{7.7}$$

$$P(X) = P_{max} p(x) \tag{7.8}$$

where X_C is the estimated distance of influence of the arc, beyond which the arc pressure becomes very small relative to its maximum value, and the radii of curvature are scaled with the hydrostatic head H and the distance of influence of the arc. The dimensionless functions obtained are expected to be of the order of magnitude of one for welds pools larger than the distance of influence of the arc.

The force balance at the transition point can be expressed with the following non-dimensional relationship:

$$p(x) = \frac{\sigma}{X_C P_{max}} \left[\frac{1}{r_2} + \frac{X_C}{H} \left(\frac{\rho g H^2}{\sigma} - \frac{1}{r_1 x} \right) \right] \tag{7.9}$$

For flat surfaces the arc pressure $P(X)$ is commonly approximated by a Gaussian distribution. The actual shape of the function differs when the weld pool presents a large depression, but no studies have been performed so far in that situation. In this study the numerical values by Choo [64] and experimental values quoted by Lin [56] for flat surfaces will be used.

The expression for the maximum pressure can be correlated from Choo's numerical examples:

$$P_{max} = 5.616 \times 10^{-3} I^{1.956} h^{-0.216} \tag{7.10}$$

where P_{max} is measured in Pascals, I in Ampères and h in millimeters.

The estimated distance of influence of the arc X_C, stays approximately constant at approximately 1.9 mm for arc lengths ranging between 1 and 5 mm and currents up to 300 A.

The radius r_1 is of the order of magnitude of the depth from top of the free surface in the trailing region to the bottom of the gouging region (metallostatic head). This radius is influenced by the "contact angle" of the trailing region at the transition point. A wetting angle yields a lower curvature than a non-wetting angle. Experiments showed that 304 stainless steel with 6 ppm of sulfur has a more wetting contact angle than with 230 ppm (Figure 7-3)

The position of the transition point is determined by solving equation 7.10 for x.

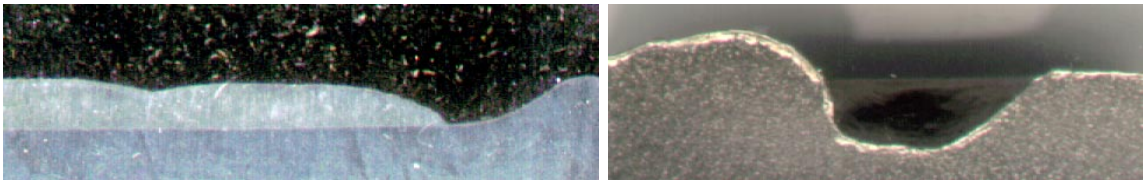

Figure 7-3: Contact angle for low and high sulfur. The sulfur content of the base metal is 6 ppm for the picture on the left, and 230 ppm for that on the right. It can be observed that the trailing region with higher sulfur content has a less wetting contact angle at the end of the gouging region.

7.2.3 Stability of the Gouging Region

Equation 7.10 can be represented graphically as in Figure 7-4. The left member of equation 7.10 shows the normalized arc pressure, represented by p_a. The other three curves represent combined normalized hydrostatic and capillary pressures (metal pressure) for three possible situations.

When these combined pressures are higher than the arc pressure at all times, there is no gouging region.

When the metal pressure crosses the pressure curve twice, there are two equilibrium points for the forces. One of them is unstable, because any fluctuation which increases the size of the gouging region will increase the relative force of the arc, expanding the gouging region even further, until it reaches the stable point. A fluctuation that decreases the size of the gouging region will create a force balance favorable

to the metal pressure, closing the gouging region. At the stable point, a fluctuation that increases the gouging region also increases the closing forces (metal pressure minus arc pressure), and a fluctuation that tends to decrease the gouging region increases the opening forces (arc pressure minus metal pressure).

The third possible case is when the metal pressure crosses the arc pressure curve only once. The crossing point is unstable, and the arc effect creates a gouging region which is larger than the unstable equilibrium position. The arc pressure is always larger than the metal pressure, and the trailing end of the weld pool breaks into two parallel streams. Increases in welding current with a constant metallostatic head, decrease the metal pressure curve by approximately a constant factor (only P_{max} is significantly affected). Increases in the metallostatic head shifts the metal pressure curve up in a parallel way (only D is significantly affected). When the metal pressure decreases, the transition point moves towards the rear, therefore an increase in current or a decrease in penetration will expand the gouging region.

Figure 7-5 shows both members of equation 7.9 with the data from Savage *et al.* [49], and estimating $r_1 = 1$ and $r_2 = 1$. These curves correspond to the arc and metal forces at the onset of humping. They metal curves intersect the arc force curve at about the same point ($x \approx 1.25$). This is exactly what was expected, that at the onset of humping all forces balance at about equal distance from the center of the arc, and that is the location where the gouging region freezes. That location is of the order of magnitude of one in dimensionless terms, indicating that the gouging region freezes at the edge of the arc.

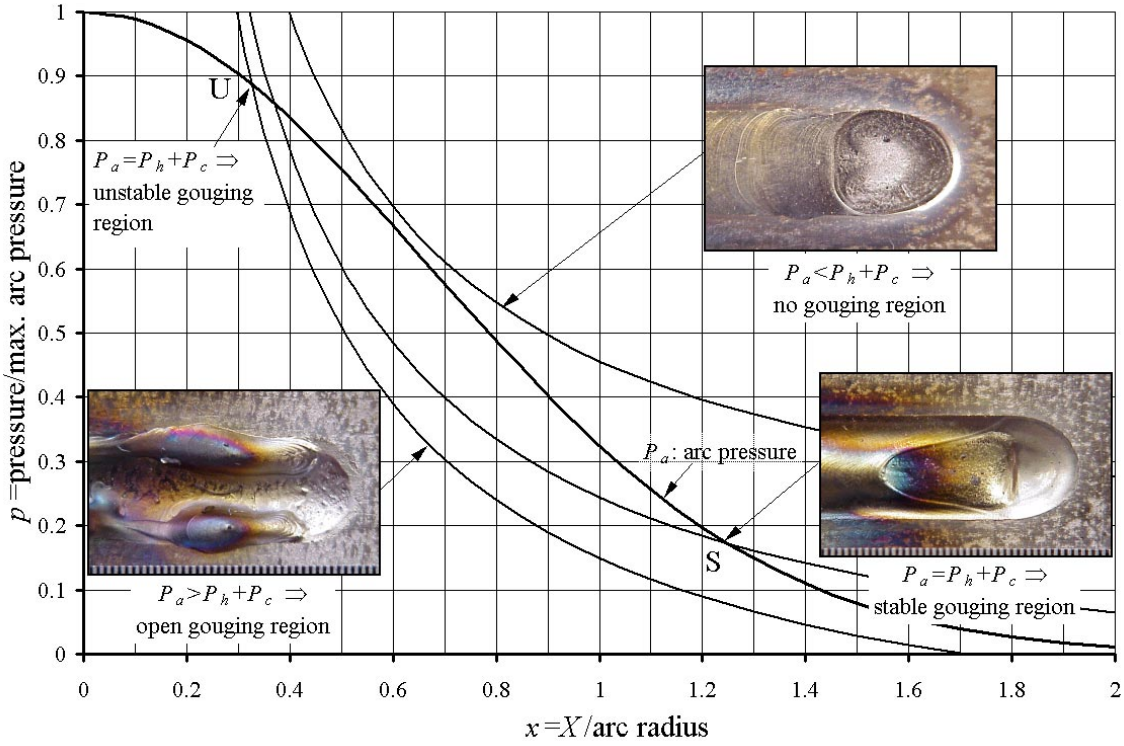

Figure 7-4: Stability of the gouging region. The bell-shaped curve represents the arc pressure. The other three curves represent the combination of hydrostatic and capillary forces at the transition point. The top curve corresponds to the case when the hydrostatic and capillary forces are larger than the arc pressure, therefore there is no gouging region. The intermediate curve intersects the arc pressure at two points, U (unstable equilibrium), and S (stable equilibrium). Point S determines the extension of the gouging region. If the gouging region extends beyond point S, the hydrostatic and capillary forces become stronger than the arc pressure, decreasing the size of the gouging region. The bottom curve intersects the arc pressure point at an unstable point, and for larger distances the arc pressure dominates over the hydrostatic and capillary forces. The gouging region in this case is open, generating a split bead

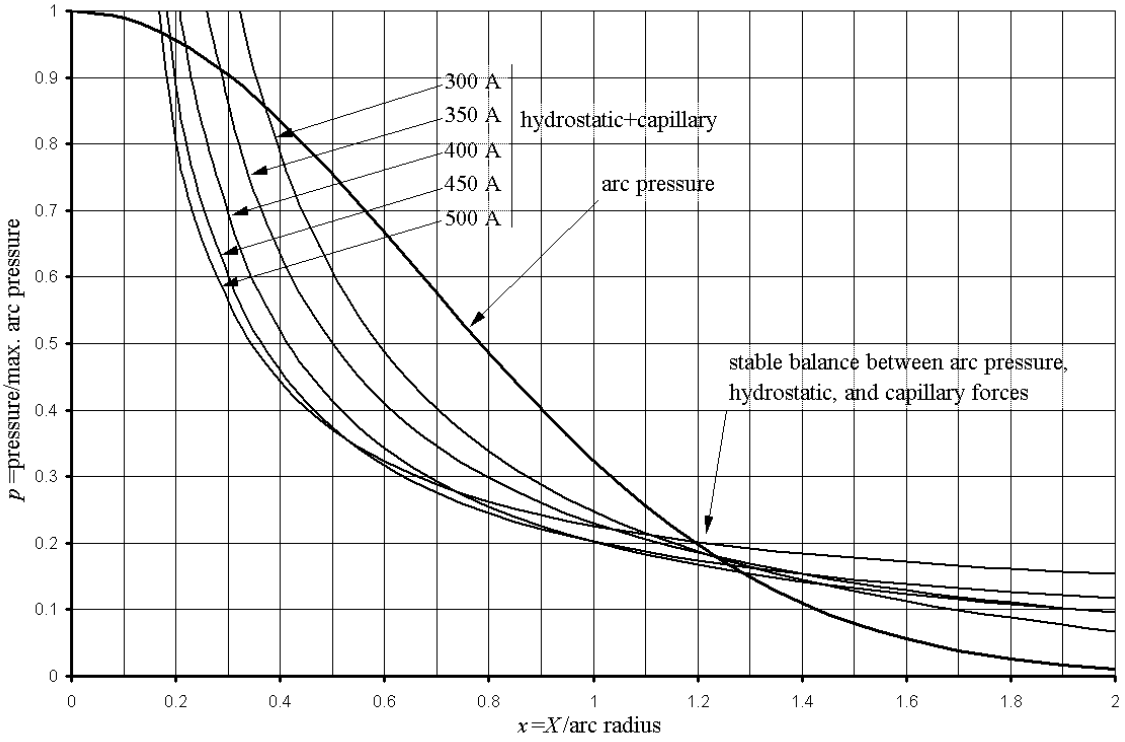

Figure 7-5: Force balance at the transition point at the onset of humping. These curves have been calculated using equation 7.9 and the experimental data by Savage [49] for weld pool geometry, and Choo [54] for the arc pressure. The extension of the gouging region is determined by the point where the arc pressure, hydrostatic and capillary forces have a stable balance. For a range of currents, and at the onset of humping, the gouging region extends slightly beyond the arc region (x=1.2 to 1.3). This fact supports the idea that in the conditions these welds were made, humping was determined by the freezing of the thin liquid layer that extended beyond the hot region of the arc.

Chapter 8

Conclusions

The methodology of Order of Magnitude Scaling was applied to the problem of high productivity welding, and it was shown quantitatively, for the first time, that the aerodynamic drag of the arc over the free surface is the dominant force driving the flow in the gouging region. Other factors such as Marangoni, electromagnetic, capillary and buoyancy forces have a much smaller effect.

At high current and velocity, the portion of the weld pool under the arc turns into a thin liquid film (the gouging region). For this thin film, the characteristic thickness, surface velocity and temperature under the arc can be evaluated with the following expressions (typical values are in parenthesis):

$$\delta^* = (2\mu U_\infty D/\tau_{max})^{1/2} \quad (\approx 50\,\mu\text{m}) \tag{8.1}$$

$$T^* = Q_{max}\delta^*/k \qquad (\approx 100\,\text{K}) \tag{8.2}$$

$$U^* = 2U_\infty D/\delta^* \qquad (\approx 1\,\text{m/s}) \tag{8.3}$$

The gouging region has a very fast time scale for freezing (of the order of milliseconds), and this can lead to defect formation if the gouging zone reaches regions with insufficient heat input.

The thickness of the weld pool is of the order of the mushy zone, therefore the free surface captures its irregularities and has the appearance of "dry" metal.

Finger-like penetration in GTA welding can be explained as a combination of the deep penetration caused by the direct action of the arc on the melting front, and a widening of the bead by the hot metal of the tail. Since the Marangoni forces are small relative to the aerodynamic drag, surface active elements such as sulfur have a negligible effect on penetration.

A more accurate estimation of the characteristics of the arc in deeply depressed weld pools is necessary. This is especially important if the melting front is also considered an unknown, because the arc acts almost directly over it.

It was found that higher welding speeds (20% or more) are possible in 304 stainless steel with lower sulfur content (6 ppm vs. 230 ppm). Differences in the size and stability of the weld pool depression are proposed here as the explanation for this difference. Steels with lower sulfur contents show a weld pool geometry that tends to decrease the size of the gouging region (the most depressed part of the weld pool). The gouging region tends to extend beyond the hot region of the arc in higher sulfur steels. In this situation the gouging region freezes prematurely and defects such as humping or a split bead are generated. The experiments also showed that in the high productivity regime, the sulfur content affects the generation of defects, but not the depth of penetration.

A new methodology was developed, Order of Magnitude Scaling, which permits one to obtain estimates of the solution for complex problems in a simple and systematic manner, even when the problem would be very difficult to study through experiments or by solving the governing equations. This methodology acts as a bridge between dimensional analysis and asymptotic considerations, allowing one to benefit from both techniques simultaneously. Physical insight and intuition are applied into a consistent set of mathematical considerations. The original set of differential equations is transformed into a set of algebraic equations, of much simpler solution. The results obtained are order of magnitude approximations to the exact solution to the problem in the form of power laws. These estimations are valuable in many ways. In some problems an estimation of the solution is sufficient for making a decision.

Much time can be saved in this case by performing an order of magnitude scaling study instead of a numerical analysis. The estimations obtained can be used to determine the relative importance of the different driving forces and effects in a system. When dominant and negligible aspects are identified the equations can be simplified accordingly, and the size of an experimental matrix can be significantly reduced. The simple expression of the estimations makes them suitable for use in real-time control systems.

Estimations of critical processing parameters can be obtained much faster than by other methods such as numerical calculations, because of the simplicity of this methodology. The simple expression of the estimations not only provides useful insight on the process behavior, but also makes them suitable for use in real-time control systems. This methodology also provides an estimation of the relative importance of the different driving forces and effects in a system. This ranking can be obtained even when the characteristic parameters of the system (such as velocity) are initially unknown. The procedure can reproduce the results obtained with other techniques, and even add physical insight that complements those results.

Order of magnitude estimates can be obtained in a straightforward and systematic manner, without modifying the physics contained in the original equations. Numerical constants such as the numbers π or $\sqrt{2}$ can be factored into the analysis in a simple and meaningful way. These order of magnitude estimations can be refined by studying how the dimensionless groups affect the dimensionless functions. This improvement can be done by perturbation methods, experimentation or analysis of numerical results. When this methodology is properly applied, even a single experiment can significantly improve the accuracy of the predictions over a large range. This technique was tested on four cases with a known solution, where correct order of magnitude estimations were obtained in all cases without integrating the differential equations.

Order of Magnitude Scaling also presents some limitations. Perhaps the most severe is that the second derivatives of the dimensionless functions must be of the

order of one. For functions with large second derivatives over all of the domain (for example the exponential function with positive exponent) the domain for scaling must be subdivided into many subdomains, losing the simplicity pursued by this technique. Problems involving this type of functions, such as some stability studies are beyond the scope of this methodology. Another limitation is that when the number of arguments and terms in the equation is too large, it cannot be guaranteed that the derivatives are of the order of magnitude of one. Although there is no theoretical limitations to the coordinate frame used to write the governing equations, they need to be written in scalar form. The implementation of vector operators is beyond the scope of this work.

8.1 Recommendations for Improving Welding Productivity

Productivity can be enhanced by using the forehand technique. In this technique the welding torch is tilted in such a way that the plasma jet has a velocity component in the direction of motion of the torch. The main effect of this is to lower the arc pressure that is pushing the transition point into the cold region. This beneficial effect of the forehand technique was observed by Bradstreet [3] and Shimada [6].

If the workpiece was inclined so that the welding direction is downwards, it is reasonable to expect that gravity forces (which push the transition point towards the hot region) would become more important, and the welding speed limit would be increased. Additional experiments would be necessary to test this hypothesis, since no studies about such a technique have been reported in the welding literature.

Other possibility for improving welding productivity would be to modify the arc behavior, in such a way that the arc pressure at the transition point decreases, but the hot region remains approximately the same. More knowledge of the welding arc is necessary for effectively implementing this. It is known, however, that blunt GTAW electrodes generate less pressure than sharp ones at the same currents [80, 81];

therefore, the welding speed limit of the former should be higher than of the latter. This effect was experimentally observed by Savage [49]. A method for improving productivity by modifying the arc with magnetic fields was proposed by Grigorenko *et al.* [82].

Stainless steel with lower sulfur showed to have a welding speed limit higher than that with high sulfur. Switching to low sulfur steels (of the order of 6 ppm) could dramatically improve the welding conditions. One important difference observed in the welding of steels with different amounts of sulfur is that the "contact angle" of the trailing region was more "non-wetting" for high sulfur than for low sulfur. This affects the capillary forces shifting the balance towards larger gouging regions, thus generating humping. The effect of additives in the metal or in the shielding gas aiming at correcting this defect is and unexplored area that could yield important results.

8.2 Future Work on Order of Magnitude Scaling

The systematic approach of the Order of Magnitude Scaling methodology makes it suitable for its implementation in computers. An automatic processing of the repetitive tasks would free an engineer to focus on the proper set-up of the problem under analysis and the results obtained. It would contribute to dissipate the "mistique" commonly associated with dimensional analysis and differential equations.

In this work it was assumed that the results of the dominant balance are unique, or that different results would yield unimportant differences. Although for all of the cases studied this was true, further study is recommended in order to evaluate the possibilities of safely incorporating the dominant balance into a computer algorithm, and preventing the occurrence of pathological cases.

Some aspects of the methodology presented here would benefit from further study. One of such aspects is that in many cases a lower bond is necessary when determining the order of magnitude of an unknown term; however, only an upper bound can be guaranteed in the general case. Another aspect would be the expansion of the range of

this methodology, to including higher order derivatives. Also, problems that involve functions with large second derivatives (such as stability problems) are currently beyond the capabilities of this method. A deeper understanding of these issues would be helpful towards a more general Order of Magnitude Scaling method.

Appendix A

Definitions of Concepts for Order of Magnitude Scaling

The order of magnitude scaling methodology involves the simultaneous use of dimensional analysis and differential equations, disciplines that do not have a fully compatible lexicon. The following set of definitions states the meaning given in this work of some fundamental terms and concepts.

Physical quantity: concept such as time, mass, temperature, velocity etc. which can be expressed in terms of one or more standards [29].

Magnitude: numerical value of a *physical quantity*.

Unit: selected *magnitude* of a *physical quantity* in terms of which other magnitudes of the same quantity may be expressed as multiples, for example the meter, Joule, etc. [12]

Reference units: *units* which are not to be defined in terms of simpler ones, for example the meter, kilogram, etc. in the International System of Units (SI) [12]. These units are also called "Primary" or "Fundamental" in some other texts.

Derived units: *units* that are defined in terms of simpler ones, for example the Newton or Joule in the SI. These units are also called "Secondary" in some other texts.

Combination of units, parameters or groups: multiplication of *units*, *parameters* or *groups* raised to a power.

Group: combination of *units* or *parameters*.

Dimensions: exponents of the *reference units* in a *unit*. It defines how the magnitude of a quantity changes when the reference units change [32].

Parameters: *physical quantities* that define properties of a system, such as viscosity, density, etc. In the literature of similitude and dimensional analysis these quantities are sometimes called "independent variables". In this work the term "independent variables" with respect to physical quantities will be avoided, in order to prevent confusion with the meaning of the term "variable" used in the literature of differential equations.

Independent arguments: set of arguments of functions that can be changed freely, without affecting each other, for example the coordinates X or Y in a function $U(X, Y)$. The set of *parameters* of a problem are excluded from this definition.

Unknowns: *physical quantities* that depend on the *independent arguments* and *parameters* of the problem, such as velocity, pressure, etc. In the literature of similitude and dimensional analysis the characteristic values of the unknowns are sometimes called "dependent variables". In this work the term "dependent variables" to define physical quantities will be avoided, to prevent confusion with the nomenclature used in the literature of differential equations.

Characteristic value: maximum value of the absolute value of a function. The characteristic values can be negative in some of the literature; however, in this work the characteristic values must be positive because they might be raised to a non-integer power during dimensional analysis.

Independent set of parameters: set of *parameters* in which all elements can be changed independently without affecting the others.

Complete set of parameters $\{P\}$: *independent set of parameters* that completely define a problem.

Set of reference units $\{R\}$: set of *reference units* that generate all the *units* in the *complete set of parameters*.

Dimensionally independent set of parameters: set of *parameters* whose *units* cannot be reproduced by a *combination of units* of the other parameters in the set.

Dimensionally complete set of parameters: subset of *parameters* whose *units* can generate all the units of other parameters in a larger set.

Set of reference parameters $\{P_k\}$: *dimensionally complete* and *independent* subset of the *complete set of parameters*.

Dimensionless group: *group* for which all *dimensions* are zero.

Independent set of dimensionless groups: set of *dimensionless groups* in which no element can be obtained by a *combination* of the other elements.

Complete set of dimensionless groups: set of dimensionless groups that completely define a problem in its dimensionless form.

Set of governing dimensionless groups $\{\Pi\}$**:** Complete and independent set of dimensionless groups.

Order of one (O(1))**:** mathematical expression that means that the maximum of the absolute value of a function is approximately one or less. The function can have any order of magnitude at any point, as long as that order of magnitude is smaller than one.

Order of magnitude of one (OM(1))**:** expression used in dimensional analysis that means that the maximum of the absolute value of a function is approximately one, but not much less. The mathematical notation for this last definition is: $= \mathrm{O}(1), \neq \mathrm{o}(1)$, but in this thesis OM(1) will be used instead.

Approximately equal to one (≈ 1)**:** expression that means that both the maximum and the minimum of a function have the same sign and are approximately one in absolute value.

Appendix B

Derivations for the Order of Magnitude Scaling Method

B.1 Properties of the Dimensionless Functions

As discussed above, the dimensionless functions as defined as in equation 2.2 and its derivatives have special properties such as being of the order of magnitude of one. Many of these properties depend on particular cases, and it would be beyond the scope of this work to focus on all of them. Below is a brief derivation for the case when the dimensionless second derivatives are of the order of one, in which the first derivatives will also be of the same order.

Let the function g_i be defined as:

$$g_i = \frac{\partial f}{\partial x_i} \tag{B.1}$$

then:

$$g_i(\mathbf{x}) - g_i(\mathbf{m}) = \int_S \nabla g_i(\mathbf{s}) \cdot \mathbf{e}_S ds \tag{B.2}$$

where $\mathbf{x}$ and $\mathbf{m}$ are arbitrary points inside the non-dimensional domain of a function of v independent arguments. An upper bound for this integral can be estimated from the upper bound for the gradient of the function and for the length of the straight

line S between $\mathbf{m}$ and $\mathbf{p}$.

$$|\nabla g_i|^2 = \sum_{j=1}^{v} \left(\frac{\partial g_i}{\partial x_j} \right)^2 \leq v[\mathrm{O}(1)]^2 \tag{B.3}$$

$$\int_S ds \leq \sqrt{v} \tag{B.4}$$

Using the mean value theorem, $\mathbf{m}$ can be defined as the point where $|g_i(\mathbf{m})| = \mathrm{O}(1)$. Finally, the upper bound for the first derivatives is:

$$\frac{\partial f}{\partial x_i} \leq (v+1)\mathrm{O}(1) \tag{B.5}$$

The first derivatives of the dimensionless functions are guaranteed to be of the order of one only for functions with few independent arguments (of the order of four or less).

With an upper bound defined for the first derivatives, it is possible to determine a lower bound for the distance between the points $\mathbf{A}$ and $\mathbf{B}$ defined in Section 2.2.2.

$$f(\mathbf{B}) - f(\mathbf{A}) = \int_{\mathbf{A}}^{\mathbf{B}} \nabla f \cdot \mathbf{e}_S ds \tag{B.6}$$

By definition (equation 2.2) the values of $f(\mathbf{A})$ and $f(\mathbf{B})$ are 0 and 1 respectively. Using the upper bounds determined above, the lower bound for the distance between points $\mathbf{A}$ and $\mathbf{B}$ is:

$$|\mathbf{B} - \mathbf{A}| \geq \left[\sqrt{v}(v+1)\mathrm{O}(1) \right]^{-1} \tag{B.7}$$

This lower bound is of the order of one for functions with few independent arguments.

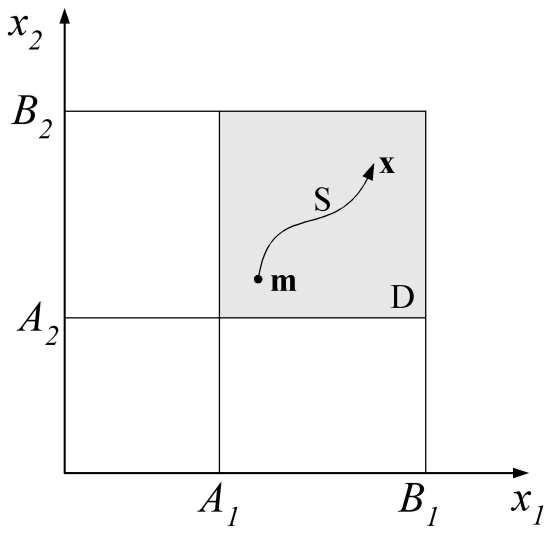

Figure B-1: Domain and integration path for a two dimensional case

B.2 Derivation of the Matrix Relationships

B.2.1 Derivation of Matrix $[A_S]$

When all elements of the set $\{N_1 \ldots = N_q\}$ have the value of one, their logarithms will be zero, and using the definition of the matrix $[A]$ (equation 2.1) it is possible to write:

$$(N_q)_S = [A_{11}](P) + [A_{12}](S) = 0 \tag{B.8}$$

therefore:

$$(S) = -[A_{12}]^{-1}[A_{11}](P) \tag{B.9}$$

B.2.2 Derivation of Matrix $[B]$

Combining the expression for matrix $[A_S]$ (equation 2.2) with the definition of matrix $[A]$ (equation 2.1), it is possible to write:

$$\left\{ \begin{array}{c} (\Pi) \\ (N_r) \end{array} \right\} = [A_1](P) + [A_2][A_S](P) = [B](P) \tag{B.10}$$

B.2.3 Derivation of Matrix $[B_N]$

From the definition of matrix $[B]$ it is possible to write

$$(\Pi) = [B_{11}](P_k) + [B_{12}](P_m) \tag{B.11}$$

$$(N_u) = [B_{21}](P_k) + [B_{22}](P_m) \tag{B.12}$$

therefore, from equation B.11:

$$(Pm) = [B_{12}]^{-1}(\Pi) - [B_{12}]^{-1}[B_{11}](P_k) \tag{B.13}$$

replacing equation B.13 into equation B.12:

$$(N_u)_\Pi = [B_{22}][B_{12}]^{-1}(\Pi) + \left([B_{21}] - [B_{22}][B_{12}]^{-1}[B_{11}]\right)(P_k) \tag{B.14}$$

where the second term on the right hand side is zero, because $\{P_k\}$ is a complete and independent set, and no combination of its elements can result in a dimensionless number.

B.3 Order of Magnitude Scaling of the Exponential Function

Let $Y(X)$ be a dimensional exponential function in the domain $D : 0 \leq X \leq L$, covering the range $Y_0 \leq Y \leq Y_L$:

$$Y = Y_0 e^{AX} \tag{B.15}$$

The domain D can be subdivided into smaller subdomains $D_i : X_i \leq X \leq X_{i+1}$ where the dimensionless variable x_i covers the range $0 \leq x_i \leq 1$ (see Figure B-2).

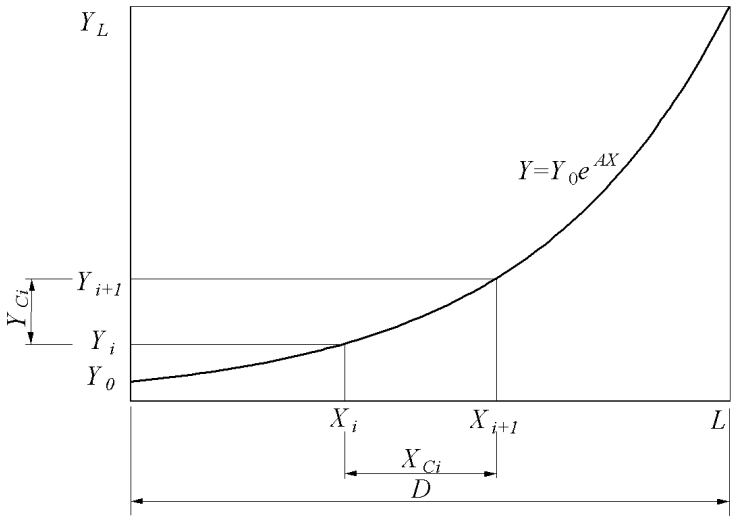

Figure B-2: Subdivided domain for an exponential function

The scaling relationships for X and Y in D_i are:

$$X = X_i + X_{C_i} x_i \tag{B.16}$$

$$Y = Y_i + Y_{C_i} y_i \tag{B.17}$$

Therefore:

$$Y''(X) = \frac{Y_{C_i}}{X_{C_i}^2} y_i''(x_i) = Y_0 A^2 e^{AX} \tag{B.18}$$

The maximum value of the dimensionless second derivative occurs at $x_i = 1$

$$y_i''(1) = \frac{A^2 X_{C_i}^2}{1 - e^{-AX_{C_i}}} \tag{B.19}$$

When $AL \lesssim 1$ the dimensionless second derivatives will be of the order of one over the original domain D. When $AL \gtrsim 1$ it is necessary to create subdomains where the dimensionless second derivative is of the order of one. This condition is satisfied for $AX_{C_i} = \mathrm{O}(1)$, therefore the size of the subdomains should be $X_{C_i} = \mathrm{O}(1/A)$, and their number approximately AL. A larger number of subdomains makes the order of magnitude scaling of the problem more complicated. When that number is too

high, it might be more appropriate to use other techniques to solve or approximate the solutions.

Appendix C

List of Symbols Used in Chapter 6

b	dimensionless magnetic flux
B^*	characteristic magnetic flux
B_y	magnetic flux
C_1	mass conservation constant
D	weld penetration
g	gravity
J^*	characteristic current density
j_a	dimensionless current density at the surface
J_a	current density at the surface
J_{max}	maximum current density at the surface
j_x	dimensionless current density in x
J_x	current density in X
j_z	dimensionless current density in z
J_z	current density in Z
k	liquid heat conductivity
L	characteristic length in X
L'	characteristic length in X'
p	dimensionless pressure
P	pressure

P^*	characteristic pressure
p_a	dimensionless pressure at the surface
P_a	pressure at the surface
P_{max}	maximum pressure at the surface
q_a	dimensionless heat flux at the surface
Q_a	heat flux at the surface
Q_{max}	maximum heat flux at the surface
T	temperature
T^*	characteristic temperature
T_l	liquidus temperature
T_s	solidus temperature
t_a	dimensionless gas shear stress at the surface
T_m	melting temperature
u	dimensionless velocity in x
U	velocity in X
U^*	characteristic velocity in X
u_m	dimensionless base material in x
U_m	base material velocity in X
U_∞	welding velocity
w	dimensionless velocity in z
W	velocity in Z
W^*	characteristic velocity in Z
w_m	dimensionless base material velocity in z
W_m	base material velocity in Z
${z_f}'$	dimensionless free surface position
${Z_f}'$	free surface position
${z_m}'$	dimensionless melting interface position
${Z_m}'$	melting interface position

Greek Symbols

α	liquid heat diffusivity
β	volumetric thermal expansion
δ^*	characteristic thickness of liquid film
Φ	electric potential
Φ^*	characteristic electric potential
ϕ	dimensionless electric potential
μ	viscosity
μ_0	magnetic permeability of vacuum
ν	kinematic viscosity
Π_i	governing dimensionless groups
θ	dimensionless temperature
ρ	liquid density
σ	surface tension
σ_e	electrical conductivity
σ_T	surface tension temperature coefficient
τ_a	gas shear stress at the surface
τ_{max}	maximum gas shear stress at the surface
ω	angle between tangent of melting front and horizontal
ω_0	angle between secant of melting front and horizontal

Subscript

$_{flat}$	corresponds to an arc on a flat surface

Superscript

*	estimation

Bibliography

[1] K. Ishizaki. Interfacial Tension Theory of the Phenomena of Arc Welding - Mechanism of Penetration. In *Physics of the Welding Arc*, pages 195–209, London, UK, 1962. The Institute of Welding.

[2] K. Ishizaki. A New Approach to the Mechanism of Penetration. In N. Bailey, editor, *Weld Pool Chemistry and Metallurgy*, volume 1, pages 65–76, London, UK, 1980. The Welding Institute.

[3] B. J. Bradstreet. Effect of Surface Tension and Metal Flow on Weld Bead Formation. *Weld. J.*, pages 314s–322s, 1968.

[4] V. P. Demyantsevich and V. D. Matyukhin. Characteristics of the Movement of Molten Metal in the Weld Pool During Welding with a Non-Consumable Electrode. *Svar. Proiz.*, (10):1–3, 1972.

[5] T. Yamamoto and W. Shimada. A Study on Bead Formation in High Speed TIG Arc Welding. In *International Symposium in Welding*, Osaka, Japan, 1975.

[6] W. Shimada and S. Hoshinouchi. A Study on Bead Formation by Low Pressure TIG Arc and Prevention of Under-Cut Bead. *Quart. J. Japan Weld. Soc.*, 51(3):280–286, 1982.

[7] A. Matsunawa and K. Nishiguchi. Arc Behaviour, Plate Melting, and Pressure Balance of the Molten Pool in Narrow Grooves. In W. Lucas, editor, *Arc Physics and Weld Pool Behaviour*, volume 1, pages 301–310, London, UK, 1979. The Welding Institute.

[8] M. M. Chen. Scales, Similitude, and Asymptotic Considerations in Convective Heat Transfer. In C. L. Tien, editor, *Annual Review of Heat Transfer*, volume 3, pages 233–291. Hemisphere Pub. Corp., New York, 1990.

[9] D. Rivas and S. Ostrach. Scaling of Low-Prandtl-Number Thermocapillary Flows. *Int. J. Heat Mass Transfer*, 35(6):1469–1479, 1992.

[10] C. I. Staicu. General Dimensional Analysis. *Journal of the Franklin Institute*, 292(6):433–439, 1971.

[11] W.-K. Chen. Algebraic Theory of Dimensional Analysis. *Journal of the Franklin Institute*, 292(6):403–422, 1971.

[12] E. d. S. Q. Isaacson and M. d. S. Q. Isaacson. *Dimensional Methods in Engineering and Physics.* John Wiley & Sons, New York, NY, first edition, 1975.

[13] F. W. David and H. Nolle. *Experimental Modelling in Engineering.* Butterworths, first edition, 1982.

[14] D. I. H. Barr. Consolidation of Basics of Dimensional Analysis. *J. Eng. Mech.*, 110(9):1357–1376, 1987.

[15] W. E. Baker, P. S. Westine, and F. T. Dodge. *Similarity Methods in Engineering Dynamics.* Fundamental Studies in Engineering. Elsevier, revised edition, 1991.

[16] T. Szirtes and P. Rzsa. *Applied Dimensional Analysis and Modeling.* McGraw Hill, New York, 1997.

[17] C. R. Heiple and J. R. Roper. Mechanism for Minor Element Effect on GTA Fusion Zone Geometry. *Weld. J.*, pages 97s–102s, 1982.

[18] G. M. Oreper, T. W. Eagar, and J. Szekely. Convection in Arc Weld Pools. *Weld. J.*, pages 307s–312s, 1983.

[19] T. Zacharia, A. H. Eraslan, and D. K. Aidun. Modeling of Non-Autogenous Welding. *Weld. J.*, pages 18s–27s, 1988.

[20] R. T. C. Choo and J. Szekely. The Effect of Gas Shear stress on Marangoni Flows in Arc Welding. *Weld. J.*, pages 223s–233s, 1991.

[21] S.-D. Kim and S.-J. Na. Effect of Weld Pool Deformation on Weld Penetration in Stationary Gas Tungsten Arc Welding. *Weld. J.*, pages 179s–193s, 1992.

[22] P. W. Bridgman. *Dimensional Analysis.* Yale University Press, New Haven, first edition, 1922.

[23] G. Murphy. *Similitude in Engineering.* The Ronald Press Company,, New York, first edition, 1950.

[24] H. L. Langhaar. *Dimensional Analysis and Theory of Models.* John Wiley & Sons, New York, NY, first edition, 1951.

[25] W. J. Duncan. *Physical Similarity and Dimensional Analysis.* Edward Arnold & Co,, London, UK, first edition, 1953.

[26] L. I. Sedov. *Similarity and Dimensional Methods in Mechanics.* Academic Press, New York, fourth edition, 1959.

[27] D. C. Ipsen. *Units, Dimensions, and Dimensionless Numbers.* McGraw-Hill, first edition, 1960.

[28] A. A. Gukhman. *Introduction to the Theory of Similarity.* Academic Press, first edition, 1965.

[29] E. S. Taylor. *Dimensional Analysis for Engineers.* Oxford University Press, Oxford, UK, first edition, 1974.

[30] D. J. Schuring. *Scale models in engineering : fundamentals and applications.* Pergamon Press, first edition, 1977.

[31] G. I. Barenblatt. *Scaling, self-similarity, and intermediate asymptotics.* Cambridge texts in applied mathematics ; 14. Cambridge University Press, New York, 1996.

[32] A. A. Sonin. *The Physical Basis of Dimensional Analysis.* Massachusetts Institute of Technology, Cambridge, MA, 1997.

[33] G. Astarita. Dimensional Analysis, Scaling, and Orders of Magnitude. *Chem. Eng. Sci.*, 52(24):4681–4698, 1997.

[34] C. M. Bender and S. A. Orszag. *Advanced Mathematical Methods for Scientists and Engineers.* International series in pure and applied mathematics. McGraw-Hill, New York, 1978.

[35] J. M. Supplee. Systems of Equations Versus Extended Reference Sets in Dimensional Analysis. *Am. J. Phys.*, 53(6):549–552, 1985.

[36] M. M. Denn. *Process Fluid Mechanics.* Prentice-Hall International Series in the Physical and Chemical Engineering Series. Prentice-Hall, Englewood Cliffs, NJ, first edition, 1980.

[37] E. Buckingham. On Physically Similar Systems; Illustrations of the Use of Dimensional Equations. *Phys. Rev.*, 4(4):345–376, 1914.

[38] I. S. Sokolnikoff and E. S. Sokolnikoff. *Matemática Superior para Ingenieros y Físicos.* Librería y Editorial Nigar, Buenos Aires, third edition, 1956.

[39] H. Schlichting. *Boundary-layer theory.* McGraw-Hill classic textbook reissue series. McGraw-Hill, New York, seventh edition, 1987.

[40] B. R. Bird, W. E. Stewart, and E. N. Lightfoot. *Transport Phenomena.* John Wiley & Sons, first edition, 1960.

[41] J. Grantham. How to Estimate Direct Arc Welding Costs. *Pract. Weld. Today*, pages 84–85, 1998.

[42] Hobart Institute of Welding. How to Calculate the Cost of Gas Metal Arc Welding. *Weld. J.*, pages 53–55, 1997.

[43] The Lincoln Electric Company. Welding Costs. In T. L. E. Company, editor, *The Procedure Handbook of Arc Welding*, pages 12.1–1,12.1–34. The Lincoln Electric Company, Cleveland, OH, thirteenth edition, 1994.

[44] The American Welding Society. Welding and Cutting Costs: Estimates and Controls. In L. P. Connor, editor, *Welding Handbook*, volume 1, pages 266–286. The American Welding Society, Miami, FL, eighth edition, 1987.

[45] D. van der Torre. Choice of Welding Process. *Weld. in the World*, 21(9/10):242–254, 1983.

[46] A. K. Pandjiris, C. N. Cooper, and W. J. Davies. Know Costs, Then Weld. *Weld. J.*, pages 561–568, 1968.

[47] A. Jain. *An Analysis of Automotive Body Assembly Technologies and their Implications in Lightweight Vehicle Development.* Master of Science, Massachusetts Institute of Technology, 1997.

[48] T. W. Eagar. Personal communication, 1998.

[49] W. F. Savage, E. F. Nippes, and K. Agusa. Effect of Arc Force on Defect Formation in GTA Welding. *Weld. J.*, pages 212s–224s, 1979.

[50] F. Gao and A. A. Sonin. Precise Deposition of Molten Microdrops: The Physics of Digital Microfabrication. *Proc. R. Soc. Lond. A*, 444:533–554, 1994.

[51] U. Gratzke, P. D. Kapadia, J. Dowden, J. Kroos, and G. Simon. Theoretical Approach to the Humping Phenomenon in Welding Processes. *J. Phys. D: Appl. Phys.*, 25:1640–1647, 1992.

[52] K. C. Mills and B. J. Keene. Factors Affecting Variable Weld Penetration. *Int. Materials Rev.*, 35(4):185–216, 1990.

[53] P. F. Mendez and T. W. Eagar. Magnitude Scaling of Free Surface Depression during High Current Arc Welding. In *Trends in Welding Research*, Pine Mountain, GA, 1998. ASM International.

[54] R. T. C. Choo, J. Szekely, and R. C. Westhoff. Modelling of High Current Arcs in Welding with Emphasis on Free Surface Phenomena in Weldpool. *Weld. J.*, 69(9):346s–361s, 1990.

[55] M. L. Lin and T. W. Eagar. Influence of Surface Depression and Convection on Arc Weld Pool Geometry. In *Transport Phenomena in Materials Processing*, volume 10, pages 63–69. ASME, 1983.

[56] M. L. Lin and T. W. Eagar. Influence of Arc Pressure on Weld Pool Geometry. *Weld. J.*, pages 163s–169s, 1985.

[57] M. L. Lin. *Transport Process Affecting the Shape of Arc Welds.* Doctor of Philosophy, Massachusetts Institute of Technology, 1985.

[58] M. L. Lin and T. W. Eagar. Effects of Surface Depression and Convection in GTA Welding. In S. A. David, editor, *International Conference on Trends in Welding Research*, Advances in Welding Science and Technology, pages 47–51, Gatlinburg, TN, 1986. ASM International.

[59] S. I. Rokhlin and A. C. Guu. A Study of Arc Force, Pool Depression, and Weld Penetration During Gas Tungsten Arc Welding. *Weld. J.*, pages 381s–390s, 1993.

[60] D. Weiss, U. Franz, and J. Schmidt. Simulation of Weld Pool Formation During Vertical Arc Welding with Emphasis on the Influence of Groove Preparation. In *Computer Technology in Welding*, page Paper 36, Lanaken, Belgium, 1996. The Welding Institute.

[61] E. Friedman. Analysis of Weld Puddle Distortion and Its Effect on Penetration. *Weld. J.*, pages 161s–166s, 1978.

[62] M. C. Tsai and S. Kou. Marangoni Convection in Weld Pools with a Free Surface. *Int. J. Num. Meth. Fluids*, 9:1503–1516, 1989.

[63] M. E. Thompson and J. Szekely. The Transient Behaviour of Weldpools with a Deformed Free Surface. *Int. J. Heat Mass Transfer*, 32(6):1007–1019, 1989.

[64] R. T. C. Choo. *Mathematical Modelling of Heat and Fluid Flow Phenomena in a Mutually Coupled Welding Arc and Weld Pool.* Doctor of Science, Massachusetts Institute of Technology, 1991.

[65] T. Zacharia, S. A. David, J. M. Vitek, and H. G. Kraus. Computational Modeling of Stationary Gas-Tungsten-Arc Weld Pools and Comparison to Stainles Steel 304 Experimental Results. *Met. Trans. B*, 22B:243–257, 1991.

[66] T. Zacharia and S. A. David. Heat and Fluid Flow in Welding. In *Mathematical Modelling of Weld Phenomena*, pages 3–23. 1992.

[67] W.-H. Kim, H. G. Fan, and S.-J. Na. A Mathematical Model of Gas Tungsten Arc Welding Considering the Cathode and the Free Surface of the Weld Pool. *Met. Mat. Trans. B*, 28B:679–686, 1997.

[68] S.-Y. Lee and S.-J. Na. A Numerical Analysis of Molten Pool Convection Considering Geometric Parameters of Cathode and Anode. *Weld. J.*, pages 484s–497s, 1997.

[69] T. Zacharia, A. H. Eraslan, and D. K. Aidun. Modeling of Autogenous Welding. *Weld. J.*, pages 53s–62s, 1988.

[70] J.-W. Kim and S.-J. Na. A Study on the Effect of Contact Tube-to-Workpiece Distance on Weld Pool Shape in Gas Metal Arc Welding. *Weld. J.*, pages 141s–151s, 1995.

[71] M. Ushio and C. S. Wu. Matematical Modeling of Three-Dimensional Heat and Fluid Flow in a Moving Gas Metal Arc Weld Pool. *Met. Mat. Trans. B*, 28B:509–516, 1997.

[72] P. S. Wei and W. H. Giedt. Surface Tension Gradient-Driven Flow Around an Electron Beam Welding Cavity. *Weld. J.*, pages 251s–259s, 1985.

[73] N.-S. Tsai. *Heat Distribution and Weld Bead Geometry in Arc Welding*. Doctor of Philosophy, Massachusetts Institute of Technology, 1983.

[74] Omega Engineering Inc. Chart of Dimensionless Numbers, 1995.

[75] Y. Chen Personal communication, 1997.

[76] R. T. C. Choo, J. Szekely, and S. A. David. On the Calculation of the Free Surface Temperature of Gas-Tungsten-Arc Weld Pools from First Principles: Part II. Modeling the Weld Pool and Comparison with Experiments. *Met. Trans. B*, 23B:371–384, 1992.

[77] P. Sahoo, T. DebRoy, and M. J. McNallan. Surface Tension of Binary Metal-Surface Active solute Systems under Conditions Relevant to Welding Metallurgy. *Met. Trans. B*, 19B:483–491, 1988.

[78] K. W. Mahin, A. B. Shapiro, and J. Hallquist. Assessment of boundary Condition Limitations on the Development of a General Computer Model for Fusion Welding. In S. A. David, editor, *International Conference on Trends in Welding Research*, Advances in Welding Science and Technology, pages 215–223, Gatlinburg, TN, 1986. ASM International.

[79] Y. Adonyi, R. W. Richardson, and W. A. Baeslack III. Investigation of Arc Effects in Subsurface GTA Welding. *Weld. J.*, pages 321s–330s, 1992.

[80] R. A. Chihoski. The Effects of Varying Electrode Shape on Arc, Operations, and Quality of Welds in 2014-T6 Aluminum. *Weld. J.*, pages 210–222s, 1968.

[81] S.-Y. Lee and S.-J. Na. A Numerical Analysis of a Stationary Gas Tungsten Arc Considering Various Electrode Angles. *Weld. J.*, pages 269s–279s, 1996.

[82] V. V. Grigorenko, O. N. Kiselev, G. G. Chernyshov, E. A. Gladkov, A. M. Rybachuk, Y. N. Bobylev, N. V. Zhulidov, and G. G. Poklonov. Formation of Defect-Free Welded Joints at Higher Speeds in Automatic Argon TIG Welding Thin-Wall Pipes. 11(1):58–60, 1997.